THE KINEMATICS AND DYNAMICS OF RIFTING IN SOUTH-CENTRAL TIBET

by

Elizabeth Aislin Nicole Reynolds

A dissertation submitted in partial fulfillment
of the requirements for the degree

of

Doctor of Philosophy

in

Earth Sciences

MONTANA STATE UNIVERSITY
Bozeman, Montana

May 2023

DEDICATION

I dedicate this dissertation to my family, friends, and everyone I've met in Bozeman, across the U.S., and around the world who've supported me over the past five years. You have each been an immeasurable part of my success in more ways than you could know. The pursuit of my PhD has provided a long list of experiences that have changed my life, teaching me lessons I could never have anticipated, and has helped me find a deeper sense of connection and purpose in this world. I am grateful for all the love and support I've received over the years which has helped me accomplish this goal.

ACKNOWLEDGEMENTS

I would like to express my sincere gratitude to my advisor Dr. Andrew Laskowski, whose continual guidance has been instrumental to my success. Thank you for teaching me to see the big picture, for supporting me through the times I struggled, and most of all, for your friendship. I am grateful to Dr. Devon Orme for being an unwavering mentor, role model, and friend. Thank you for your constant encouragement, kindness, and for teaching me not only about complex scientific ideas but also about the person I aspire to be. Thank you to Dr. David Lageson for sharing his extensive knowledge of structural geology and his willingness to go above and beyond to help me succeed in intellectual pursuits. Thank you to Dr. Mike Taylor for being the first to inspire my interest in graduate studies and for his continued support and encouragement.

Thank you to my field partner, office mate, and lifelong friend Caden Howlett, whose passion for learning and ability to find beauty and joy in the world is a constant inspiration to me. Thank you for being my first friend in Montana, for your camaraderie through eight weeks of fieldwork in the Anaconda Range, and for your companionship during our month of fieldwork on the high rugged terrain of the Tibetan Plateau. I thank Dr. Kurt Sundell for his assistance and uplifting energy in the field, for our many stimulating discussions of Tibetan tectonics, and for his continued support and friendship. I thank my family for their never-ending support, encouragement, and for helping me believe I can accomplish anything I set my mind on.

I thank Dr. Peter Reiners, the ARHDL, and staff of the Arizona LaserChron Center for assistance with sample analyses, and finally, this project would not have been possible without support from the MSU Department of Earth Sciences, the National Science Foundation, and the Geological Society of America.

TABLE OF CONTENTS

TABLE OF CONTENTS CONTINUED

LIST OF FIGURES

Figure Page

LIST OF FIGURES CONTINUED

Figure Page

ABSTRACT

Southern Tibet is a unique location to study complex interactions between continental collision and extension, or stretching, of the Earth's crust which forms linear structures called rifts. The study of rifts is important because the rocks they expose can record thermal changes in the Earth's crust related to large-scale processes such as shifts in tectonic plates which occur over long timescales and are difficult to observe. Rifts also interact with topography, can influence river systems, and cause changes in rainfall distribution across a landscape by forming topographic drainage divides. Despite their importance, the kinematics and dynamics of rifting, or processes that occur during rift formation and evolution, are not well understood. This study uses field and radiometric dating techniques to investigate the shape, orientation, and timing of extension in southern Tibet by testing kinematic models for two classes of rifts: (1) Tibetan rifts which are defined as rifts that are >150 km in length and crosscut the Lhasa Terrane, and (2) Gangdese rifts that are defined as rifts <50 km long that are isolated within the high topography of the Gangdese Range. Evaluation of rift age across the Tangra Yumco rift and three Gangdese rifts suggests the TYC rift formed through the linkage of smaller normal fault segments into larger and longer structures over time, while Gangdese rifts may have relatively constant lengths. Additionally, interactions between rifts and contractional structures have likely influenced the evolution of topography and drainage patterns in southern Tibet for at least the past sixteen million years. To further investigate structural interactions, a broader compilation of thermochronology ages expands results to include another Tibetan rift, the Lunggar rift. Trends in the data reveal all samples from Gangdese rifts and Tibetan rifts that spatially overlap the Gangdese Range yield ages between ~28-16 Ma, whereas samples north of the Gangdese Range yield ages between ~12-4 Ma. I interpret these results to reflect Gangdese rift initiation at ~28 Ma in conjunction with, and perhaps balancing, uplift driven by the India-Asia collision, while young ages North of the Gangdese Range (~12-4 Ma) reflect extension along Tibetan rifts.

CHAPTER ONE

INTRODUCTION

Southern Tibet is a unique location to study complex interactions between continental collision and extension through normal faulting or rifting of the Earth's crust. During rifting, rocks are brought to the Earth's surface in the footwalls of rift-bounding normal faults, and as these rocks are exhumed from depth, they can record the timing and rates of exhumation reflected by their thermal history. Thus, footwall rocks can collect information regarding thermal changes in the Earth's crust or related to large-scale processes like shifts in tectonic plates that occur over very long timescales and are otherwise difficult to observe. The study of rifts is important to develop our understanding of such large scale processes, and because rifts also interact with topography, can influence river systems, and even cause changes in rainfall distribution across a landscape by forming topographic drainage divides. The occurrence of rifting coeval with plate convergence has been documented in mountain belts around the world, including the Himalayan-Tibetan orogenic system (Burchfiel et al., 1992; England & Houseman, 1989; McCaffrey & Nabelek, 1998; DeCelles et al., 2002; Kapp & Guynn, 2004), the North American Cordillera (Wells & Hoisch 2008; Wells et al., 2012; Long et al., 2015; Platt & England, 1994), and the South American Cordillera (Allmendinger, 1986; Kay & Kay, 1993; Marrett & Strecker, 2000; Hughes et al., 2019). Despite their recognition and significance, the kinematics and dynamics of rifting, or the processes that occur during rift formation and evolution, are still not well understood (Wells et al., 2012). In this dissertation, I aim to investigate these questions through two manuscripts; the first focuses on the Tangra Yumco rift in south-central Tibet, while the second focuses on expanding this work to a regional synthesis, comparing thermochronologic data on the timing and rates of other Tibetan rifts to investigate tectonic models proposed to explain the mechanisms driving E-W extension synchronous with N-S plate convergence.

The first manuscript presented here (chapter two) is a detailed study of the kinematics of the Tangra Yumco (TYC) rift in south-central Tibet. We utilize field observation, U-Pb geochronology, and zircon (U-Th)/He (ZHe) thermochronology dating techniques to investigate the morphology and timing of extension onset in TYC. We then evaluate the patterns of normal faulting and spatial distribution of ZHe ages to determine a best-fit kinematic model (e.g., Curry et al., 2016) for the TYC rift. Our results suggest the TYC rift evolved through the linkage of smaller normal fault segments into a longer, inter-connected fault network over time. This evolution was likely influenced by ongoing collision and underthrusting of India beneath Asia (e.g., Styron et al., 2015), with rift processes influencing the evolution of topography and river systems in southern Tibet since at least Miocene time.

The second manuscript (chapter three) provides a regional synthesis for this work and examines a decades-long debate regarding the driving mechanisms or dynamics of rifting in southern Tibet. There are also persisting questions regarding the role that deep tectonic processes (e.g., slab rollback, continental underthrusting) may play in rift initiation and evolution (e.g., Kapp and DeCelles, 2019). To contribute to this debate, we use a compilation of ZHe thermochronology data to evaluate the timing of extension in southern Tibet for two classes of rifts: (1) Tibetan rifts which we define as rifts that are >150 km in length and crosscut the Lhasa Terrane, and (2) Gangdese rifts that we define as rifts that are <50 km long and are isolated within the high topography of the Gangdese Range. We investigate the spatial trends in thermochronologic data across three major rifts of the Tibetan plateau to compare with tectonic model predictions and determine a best-fit tectonic model for observed age trends.

Further, we investigate the relationships between rift timing and the timing of activity along contractional structures in southern Tibet and expand our analysis from the first chapter to include published data from another Tibetan rift, the Lunggar rift (Styron et al., 2013; 2015; Sundell et al., 2013), and assess the potential for variabilities in rift dynamics across a broader scale. Results show all samples from Gangdese rifts and samples from Tibetan rifts which overlap the Gangdese Range produce estimates for rift timing between ~28-16 Ma, whereas samples north of the Gangdese Range reflecting rifting produce ages between ~8-4 Ma. We interpret Gangdese rifts initiated in conjunction with, and perhaps balancing, uplift driven by the India-Asia collision, while young ages North of the Gangdese Range (~8-4 Ma) reflect extension timing along Tibetan rifts. These results contribute new details to interpret alongside other recent studies of Tibetan rifts (e.g., Bian et al., 2022; Wolff et al., 2023) as well as studies of rift processes in other settings (e.g., Brune et al., 2023). We suggest differing kinematics and dynamics for Tibetan rifts and Gangdese rifts, providing new insights into rift development at different scales in collisional tectonic settings. We encourage continued research on this topic as described in the conclusions of this dissertation.

References Cited

Allmendinger, R.W. (1986). Tectonic development, southeastern border of the Puna Plateau, northwestern Argentine Andes. GSA Bulletin 1986;; 97 (9): 1070–1082. doi: https://doi.org/10.1130/0016-7606(1986)97<1070:TDSBOT>2.0.CO;2

Bian, S., Gong, J., Zuza, A.V., Yang, R., Chen, L., Ji, J., et al. (2022). Along-strike variation in the initiation timing of the north-trending rifts in southern Tibet as revealed from the Yadong-Gulu rift. Tectonics, 41, e2021TC007091. https://doi.org/10.1029/2021TC007091

Brune, S., Kolawole, F., Olive, JA. *et al.* Geodynamics of continental rift initiation and evolution. *Nat Rev Earth Environ* (2023). https://doi.org/10.1038/s43017-023-00391-3

Burchfiel, B.C., Chen, Z., Hodges, K.V., Liu, Y., Royden, L.H., Deng, C., & Jiene, X. (1992). The South Tibetan detachment system, Himalayan orogen: Extension contemporaneous with and parallel to shortening in a collisional mountain belt. Geological Society of America, Special Papers, 269, 1–41. https://doi.org/10.1130/SPE269-p1

Curry, M. A. E., Barnes, J. B., and Colgan, J. P. (2016). Testing fault growth models with low-temperature thermochronology in the northwest Basin and Range, USA, Tectonics, 35, 2467– 2492, doi:10.1002/2016TC004211.

DeCelles, P.G., Robinson, D.M., & Zandt, G. (2002). Implications of shortening in the Himalayan fold-thrust belt for uplift of the Tibetan Plateau, Tectonics, 21, 1062, doi:10.1029/2001TC001322.

England P.C. & Houseman G.A., (1989). Extension during continental convergence, with application to the Tibetan Plateau: Journal of Geophysical Research, v. 94, p. 17,561–17,579, doi:10.1029/JB094iB12p17561.

Hughes, C.A., Jessup, M.J., Shaw, C.A., & Newell, D.L. (2019). Deformation conditions during syn-convergent extension along the Cordillera Blanca shear zone, Peru. Geosphere, 15(4), 1342-1367. Doi: https://doi.org/10.1130/GES02040.1

Kapp, P., & DeCelles, P.G. (2019). Mesozoic–Cenozoic geological evolution of the Himalayan-Tibetan orogen and working tectonic hypotheses. Am. J. Sci., 319, 159–254. DOI: 10.2475/03.2019.01

Kapp, P., & Guynn J.H. (2004). Indian punch rifts Tibet. Geology (2004); 32 (11): 993–996. doi:/10.1130/G20689.1

Kay, R.W., & Kay, S.M. (1993). Delamination and delamination magmatism. Tectonophysics, 219(1-3), 177-189. Doi: https://doi.org/10.1016/0040-1951(93)90295-U

Long, S.P., Thomson, S.N. Reiners, P.W., & V. Di Fiori, R. (2015). Synorogenic extension localized by upper-crustal thickening: An example from the Late Cretaceous Nevadaplano. Geology; 43 (4): 351–354. doi:10.1130/G36431.1

Marrett, R., & Strecker, M.R. (2000). Response of intracontinental deformation in the central Andes to late Cenozoic reorganization of South American Plate motions, Tectonics, 19(3), 452– 467, doi:10.1029/1999TC001102.

McCaffrey, R., & Nabelek J. (1998). Role of oblique convergence in the active deformation of the Himalayas and southern Tibet plateau. Geology; 26 (8): 691–694. doi: https://doi.org/10.1130/0091-7613(1998)026<0691:ROOCIT>2.3.CO;2

Platt, J.P., & England, P.C. (1994). Convective removal of lithosphere beneath mountain belts; thermal and mechanical consequences. American Journal of Science, 294(3), 307-336.

Styron, R. H., Taylor, M. H., Sundell, K. E., Stockli, D. F., Oalmann, J. A. G., Möller, A., McCallister, A. T., Liu, D., & Ding, L. (2013). Miocene initiation and acceleration of extension in the South Lunggar rift, western Tibet: Evolution of an active detachment system from structural mapping and (U-Th)/He thermochronology, Tectonics, 32, 880– 907, Doi:10.1002/tect.20053.

Styron, R., Taylor, M. & Sundell, K. (2015). Accelerated extension of Tibet linked to the northward underthrusting of Indian crust. Nature Geosci 8, 131–134. Doi:10.1038/ngeo2336

Sundell, K. E., Taylor, M. H., Styron, R. H., Stockli, D. F., Kapp, P., Hager, C., Liu, D., & Ding, L. (2013). Evidence for constriction and Pliocene acceleration of east-west extension in the North Lunggar rift region of west central Tibet, Tectonics, 32, 1454– 1479, Doi:10.1002/tect.20086.

Wells, M.L., & Hoisch, T.D. (2008). The role of mantle delamination in widespread Late Cretaceous extension and magmatism in the Cordilleran orogen, western United States. Geological Society of America Bulletin, 120(5-6), 515-530. Doi: https://doi.org/10.1130/B26006.1

Wells, M.L., Hoisch, T.D., Cruz-Uribe, A.M., & Vervoort, J.D. (2012). Geodynamics of synconvergent extension and tectonic mode switching: Constraints from the Sevier-Laramide orogen. Tectonics, 31(1). Doi: https://doi.org/10.1029/2011TC002913

Wolff, R., Hetzel, R., Dunkl, I., Xu Q., Bröcker, M., & Anczkiewicz A.A., (2019). High-Angle Normal Faulting at the Tangra Yumco Graben (Southern Tibet) since ∼15 Ma. The Journal of Geology 2019 127:1, 15-36. Doi:10.1086/700406

Wolff, R., Hetzel, R., Hölzer, K., Dunkl, I., Xu, Q., Anczkiewicz, A.A., & Li, Z. (2023). Rift propagation in south Tibet controlled by under-thrusting of India: a case study of the Tangra Yumco graben (south Tibet). Journal of the Geological Society, jgs2022-090. Doi: https://doi.org/10.1144/jgs2022-090

CHAPTER TWO

KINEMATIC EVOLUTION OF THE TANGRA YUMCO RIFT, SOUTH-CENTRAL TIBET

Contribution of Authors and Co-Authors

Manuscript in Chapter 2

Author: Aislin N. Reynolds

Contributions: Conception of study, funding acquisition, field investigation, performed analyses, interpreted results, created figures, and wrote the manuscript.

Co-Author: Andrew K. Laskowski

Contributions: Conception of study, funding acquisition, field investigation, supervision, discussed implications, and writing review.

Co-Author: Caden J. Howlett

Contributions: Field investigation and writing review.

Co-Author: Devon A. Orme

Contributions: Supervision of analyses and writing review.

Co-Author: Kurt E. Sundell

Contributions: Field investigation and writing review.

Co-Author: Michael H. Taylor

Contributions: Conception of study, funding acquisition, and writing review.

Co-Author: Adam M. Forte

Contributions: Conception of study, funding acquisition, and writing review.

Contribution of Authors and Co-Authors Continued

Co-Author: Fulong Cai

Contributions: Obtained permits for field investigation.

Co-Author: Xudong Guo

Contributions: Field investigation and aided in sample preparation.

Co-Author: Lin Ding

Contributions: Obtained permits for field investigation.

Manuscript Information

Aislin N. Reynolds[1], Andrew K. Laskowski[1], Caden J. Howlett[1,2], Devon A. Orme[1], Kurt E. Sundell[3], Michael H. Taylor[4], Adam M. Forte[5], Fulong Cai[6], Xudong Guo[6,7], Lin Ding[6]

[1]Department of Earth Sciences, Montana State University, Bozeman, MT, USA

[2]Now at Department of Geosciences, University of Arizona, Tucson, AZ, USA

[3]Department of Geosciences, Idaho State University, Pocatello, ID, USA

[4]Department of Geology, University of Kansas, Lawrence, KS, USA

[5]Department of Geology & Geophysics, Louisiana State University, Baton Rouge, LA, USA

[6]Institute of Tibetan Plateau Research, Chinese Academy of Sciences, Beijing, China

[7]Now at National Disaster Reduction Center of China (NDRCC), Beijing, China

Tektonika

Status of Manuscript:

____ Prepared for submission to a peer-reviewed journal

_x__ Officially submitted to a peer-reviewed journal *(submitted March 14, 2023)*

____ Accepted by a peer-reviewed journal

____ Published in a peer-reviewed journal

Abstract

We investigate rifting during continental collision in southern Tibet by testing kinematic models for two classes of rifts: Tibetan rifts are defined as >150 km in length and crosscut the Lhasa Terrane, and Gangdese rifts are <50 km long and isolated within the high topography of the Gangdese Range. Discerning rift kinematics is a crucial step towards understanding rift behavior and evolution that has been historically limited. We evaluate spatiotemporal trends in fault displacement and extension onset in the Tangra Yumco (TYC) rift and several nearby Gangdese rifts, and examine how contraction, surface uplift, and rift exhumation relate to evolution of the Gangdese drainage divide. Igneous U-Pb and zircon (U-Th)/He (ZHe) results indicate rift footwall crystallization between ~59-49 Ma and cooling between ~60-4 Ma, respectively, with ZHe ages correlating strongly with sample latitude. Samples from Gangdese latitudes (~29.4-29.8°N) yield predominantly Oligocene-early Miocene ages, whereas samples north of ~29.8°N yield both late Miocene-Pliocene ages and Paleocene-Eocene ages. Thermal history models indicate two-stage cooling, with initially slow cooling followed by accelerated cooling during late Miocene-Pliocene time. From spatial distributions of ZHe ages we interpret: (1) ~28-16 Ma ages from Gangdese latitudes reflect exhumation along contractional structures, (2) ~8-4 Ma ages reflect rift-related exhumation, and (3) ~60-48 Ma ages indicate these samples experienced lesser rift exhumation. Our data are consistent with a segment linkage evolution model for the TYC rift, with interactions between rifts and contractional structures likely influencing the evolution of topography and location of the Gangdese drainage divide since Miocene time.

Plain Language Summary

Tibet is a unique location where we can study the complex interactions between continental collision and stretching of the Earth's crust. The linear structures and valleys that form due to crustal extension and normal faulting are called rifts. The study of rifts is important because the rocks they expose can record thermal changes due to movement of the Earth's crust that are otherwise inaccessible to study. Additionally, rift behavior can be related to large-scale processes like shifts in tectonic plates, which make up the rigid outer shell of the Earth, that occur over long timescales and can be difficult to observe. Rifts also interact with topography, can influence river systems, and cause changes in rainfall distribution across a landscape by forming drainage divides. Despite their importance, the processes that occur during rift formation and evolution are not well understood. In this study we use field and radiometric dating techniques to investigate what the shape, orientation, and timing of activity along the Tangra Yumco rift can tell us about rift behavior. We look at the spatial distributions of these ages to investigate changes over time and better understand rift behavior in south-central Tibet. Our results suggest rifts form through the linkage of smaller normal fault segments into larger and longer structures over time, with their evolution likely related to continued collision between India and Asia. Interactions between rifts and contractional structures has also likely influenced the evolution of topography and drainage patterns in southern Tibet since at least sixteen million years ago.

Introduction

Mountain belts and continental plateaus that owe their high elevations to crustal shortening frequently undergo extension coeval with plate convergence (Burchfiel & Royden, 1985). Synconvergent extension has been documented in orogenic belts around the world, including the Himalayan-Tibetan orogenic system (Fig. 1; Burchfiel et al., 1992; England & Houseman, 1989; McCaffrey & Nabelek, 1998; Kapp & Guynn, 2004) the North American Cordillera (Wells & Hoisch 2008; Wells et al., 2012; Long et al., 2015; Platt & England, 1994), and the Andes (Allmendinger, 1986; Kay & Kay, 1993; Marrett & Strecker, 2000; Giovanni et al., 2010; Hughes et al., 2019). Despite this widespread recognition, uncertainties remain in our understanding of rifting during plate convergence: the conditions under which rifts initiate, normal fault growth and evolution patterns, and the influence of deep versus shallow crustal processes are several critical questions that are unresolved (e.g., Wells et al., 2012; Huntington & Klepeis, 2018; Brune et al., 2023).

Innovation and advancements in geo- and thermochronology techniques create new opportunities to develop spatially robust datasets that facilitate investigation of uncertainties in rift behavior through testing of kinematic models (e.g., Curry et al., 2016). We consider two classes of rifts in Tibet: (1) Tibetan rifts, which we define as rifts that are >150 km in length and crosscut the Lhasa Terrane, and (2) Gangdese rifts, which we define as rifts generally <50 km in length that are isolated within the high topography of the Gangdese Range of southern Tibet (Fig. 2; Burke et al., 2021). Collection of low-temperature thermochronology data and structural observations along strike of the southern TYC rift allows evaluation of spatial patterns of fault displacement and extension onset to determine a best fit kinematic model.

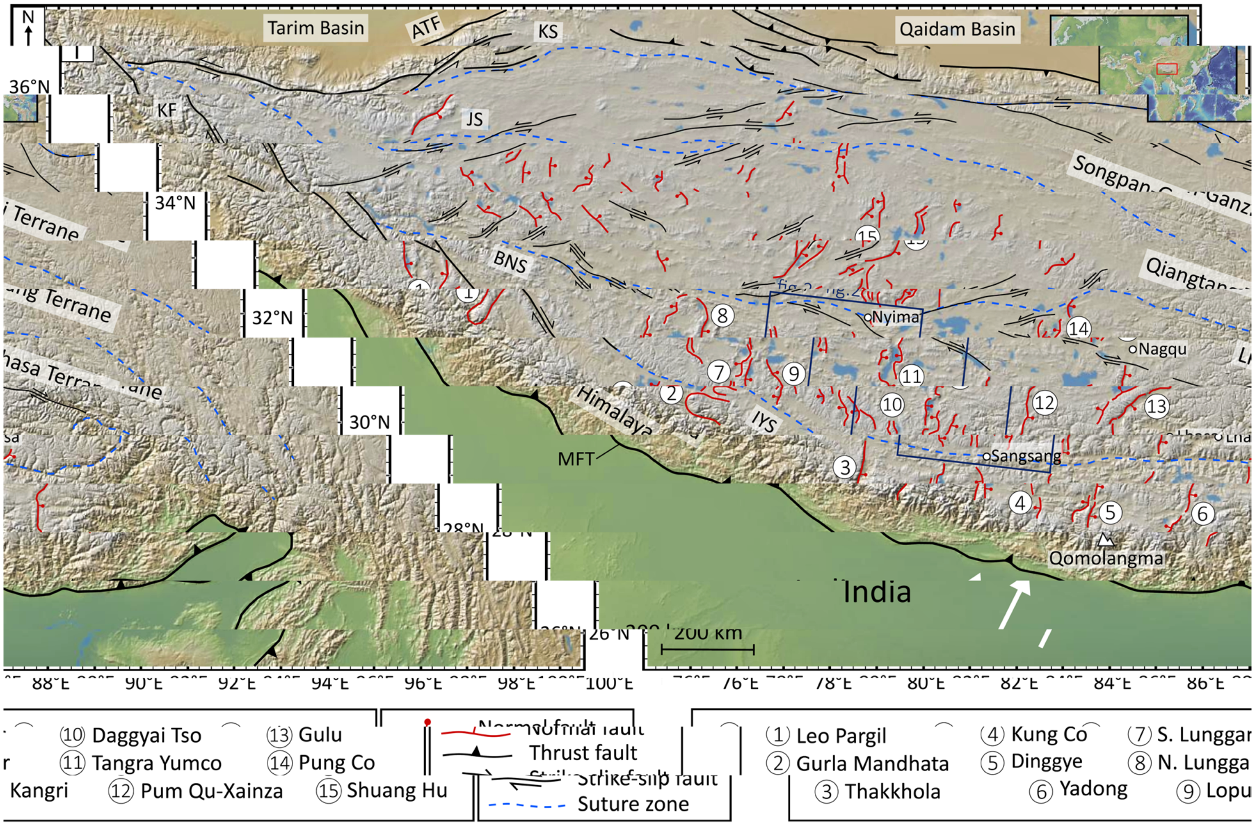

Figure 1: Digital elevation model of the Tibetan Plateau highlighting major structures and tectonic features adapted from Taylor and Yin (2009) with fault traces from HimaTibet database (Styron et al. 2010). 1 = Leo Pargil (Thiede et al. 2006); 2 = Gurla Mandhata dome (Murphy et al. 2002; McCallister et al. 2014); 3 = Thakkhola graben (Coleman & Hodges 1995; Garzione et al. 2003); 4 = Kung Co graben (Mahéo et al. 2007; Lee et al. 2011); 5 = Dinggye rift (Arma Drime massif; Jessup et al. 2008; Kali et al. 2010); 6 = Yadong rift (Ratschbacher et al. 2011); 7 = South Lunggar rift (Styron et al. 2013); 8 = North Lunggar rift (Kapp et al. 2008; Sundell et al. 2013); 9 = Lopu Kangri rift (Yin & Harrison, 2000; Sanchez et al. 2013, Laskowski et al. 2017); 10 = Daggyai Tso graben (Yin & Harrison, 2000; Williams et al., 2001); 11 = Tangra Yumco rift (this study, Wolff et al. 2019, 2023); 12 = Pum Qu-Xainza rift (Armijo et al. 1986; Hager et al., 2019); 13 = Gulu rift (Harrison et al. 1995; J. Kapp et al. 2005; Ratschbacher et al. 2011); 14 = Pung Co rift (Kapp et al., 2008); 15 = Shuang Hu rift (Blisniuk et al., 2001). White arrow indicates convergence vector of India relative to Asia. Suture zones shown as dashed blue lines. BNS = Bangong- Nujiang suture; IYS = Indus-Yarlung suture; JS = Jinsha suture; KS = Kunlun suture; KF = Karakorum fault; ATF = Altyn Tagh fault; MFT = Main Frontal Thrust. Topography from GeoMapApp.

We investigate the Tangra Yumco (TYC) rift and nearby Gangdese rifts in south-central Tibet to address the following research questions: (1) when did the TYC rift initiate?; (2) what are the kinematics of the TYC rift and how did TYC evolve through time?; (3) how does TYC compare to other rifts in Tibet?; (4) what can the timing and rates of extension in TYC reveal about interactions between contractional and extensional structures and the regional tectonics of southern Tibet?; and (5) how might rift processes relate to and interact with the Gangdese drainage divide? We investigate these questions and provide a review of the geologic history and prior research related to rifting in southern Tibet. We introduce key hypotheses related to the kinematics of east-west extension in Tibet and development of the Gangdese drainage divide, which separates the internally and externally drained portions of the Tibetan Plateau.

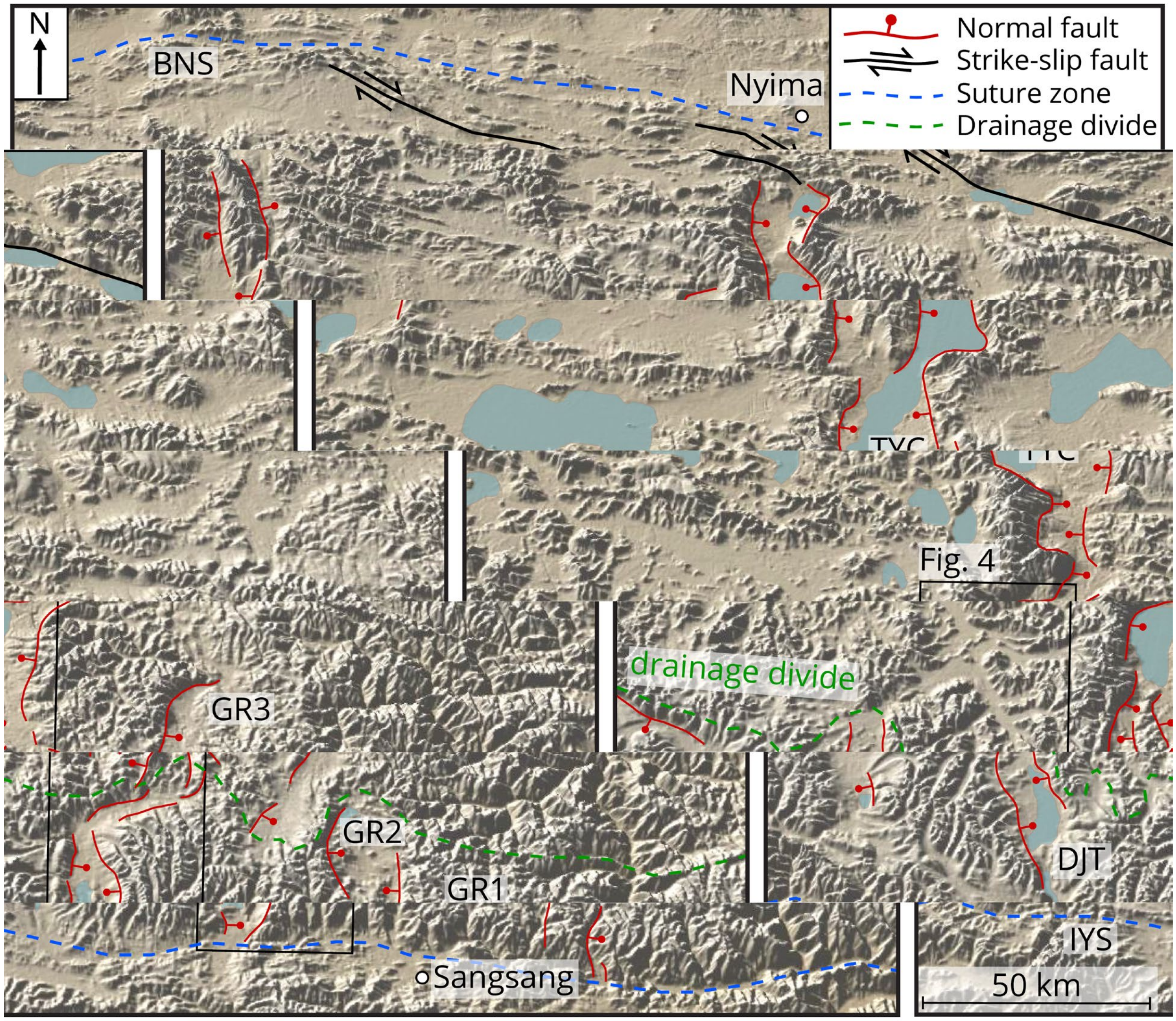

Figure 2. Digital elevation model of the south-central Tibetan Plateau, showing locations of the drainage divide along the approximate crest of the Gangdese Range (green), Tangra Yumco Rift (TYC; Wolff et al., 2019, 2023; this study), Gangdese rifts cutting high topography of the Gangdese Range including the Dajiamang Tso rift (DJT; Burke et al., 2021) and other previously unnamed Gangdese rifts (e.g., GR1, GR2, GR3; this study). The black box shows the extent of geologic mapping in the southern TYC rift (Fig. 4). Dashed blue lines = suture zones; BNS = Bangong-Nujiang suture; IYS = Indus-Yarlung suture. Fault traces from HimaTibet database (Styron et al. 2010). Topography from GeoMapApp, vertical exaggeration (VE) = 4.

Rift Kinematics

Characterizing rift kinematics is an essential step towards understanding the geologic and tectonic variables impacting rift initiation and growth and can advance our understanding of the forces which drive continental rifting in contractional settings (e.g., Yin, 2000; Sundell et al., 2013; Curry et al., 2016). Researchers have hypothesized that the orientation, structural style, timing of onset, magnitudes, and rates of extension of rifts in Tibet are spatially variable, with differences in rift evolution and behavior influenced by the following factors: (a) rift position relative to the India-Asia convergence vector (Fig. 1; Kapp & Guynn, 2004), (b) variations in the mechanical and/or thermal conditions of the lithosphere (England & Houseman, 1989; Molnar & Tapponnier, 1978; Molnar et al., 1993; Buck, 1991, 1993; Bischoff & Flesch, 2018), (c) strength contrasts or decoupling between the upper and lower crust (e.g., Copley et al., 2011), (d) the orientation and location of subducting Indian lithosphere (e.g., Yin, 2000; Styron et al., 2015; Klemperer 2022), (e) interactions with pre-existing and coevally formed structures (Taylor et al., 2003; Taylor & Yin, 2009; Ratschbacher et al., 2011; Sundell et al., 2013), or a combination of these and other factors (e.g., Labrousse et al. 2016; Wolff et al., 2019).

A model proposed by Kapp et al. (2008) details Tibetan rift geometry and kinematics based on observations from the Lunggar and Yadong-Gulu rifts (Fig. 1; section 2.2.4.) and provides a baseline for comparison and evaluation of TYC rift kinematics. In this model, rifts initiate as graben or half-graben basins bounded by a dominant high-angle normal fault which soles into a sub-horizontal shear zone at depth. As magnitudes of extension increase, tectonic unloading drives isostatic rebound and back-rotation of the footwall, allowing slip at lower angles but favoring slip along progressively younger basin-stepping high-angle faults. Enhanced isostatic rebound driving exhumation in areas of maximum horizontal extension (low-angle) or accommodation zones between overlapping fault segments (high-angle) may form intra-basin topographic highs capable of establishing new drainage divides (Anders & Schlische, 1994; Faulds & Varga, 1998; Kapp et al., 2008). This model is similar to rolling-hinge models proposed for the North American Cordillera (Buck, 1988; Wernicke, 1992) where high-angle basin-stepping fault segments may progressively link to form larger fault structures and preferentially reorganize to a simpler configuration through time.

We consider four possible models for fault growth and rift evolution: (A) tip propagation, (B) tectonically influenced tip propagation, (C) segment linkage, or (D) constant fault length. Each kinematic model predicts a specific map pattern of fault displacement and spatial distribution for the timing of extension onset. Assessing along strike trends in thermochronologic data can provide valuable information towards predicting how faults accumulate displacement and lengthen through time, furthering our understanding of how natural fault systems evolve (e.g., Curry et al., 2016). The tip propagation model (A) suggests extension initiation near Central TYC and rift propagation to the north and south through time, predicting a symmetric map pattern of fault displacement and age of extension onset to be oldest in Central TYC and younger towards the north and south. Tectonically influenced tip propagation (B) predicts an older age of extension onset at one end of the TYC rift (e.g., southern TYC) with rift propagation and progressively younger ages of extension onset focused in one direction (e.g., northward) driven by tectonic controls. Segment linkage (C) suggests rift initiation as individual, segmented normal faults along the TYC rift which link to form one larger fault system through time, predicting variable magnitudes of extension and a complexity of extension onset timing along strike due to the irregular behavior of individual fault segments. Finally, the constant fault length model (D) suggests TYC initiated at near present-day length (~250 km) and has remained relatively constant through time, predicting uniform fault distribution and timing of extension onset along strike.

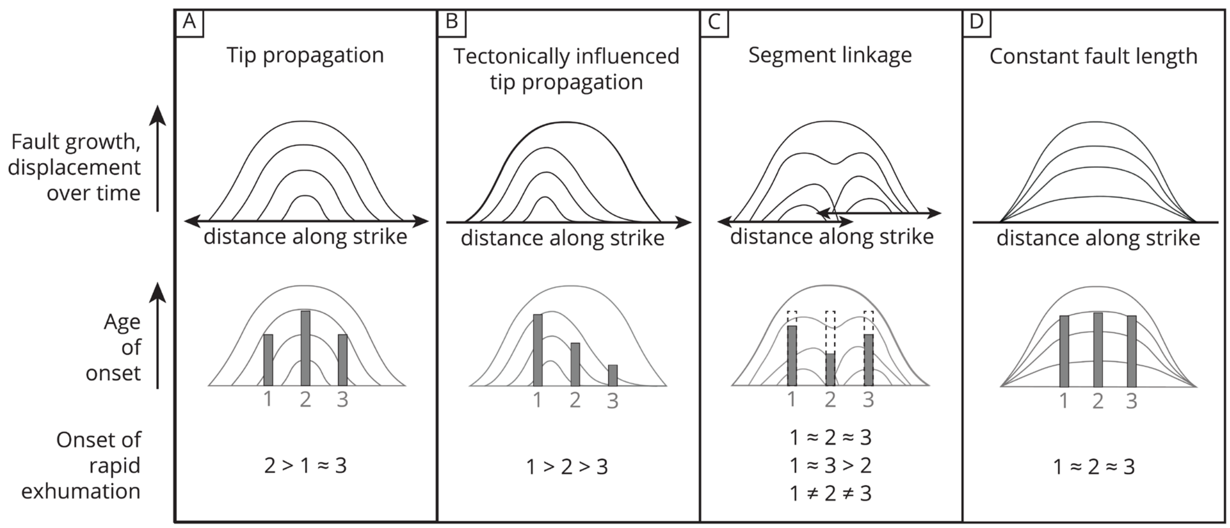

Figure 3. Proposed kinematic models for normal fault growth; (A) Tip propagation, (B) Tectonically influenced tip propagation, (C) Segment Linkage, and (D) Constant fault length. Each model predicts specific map patterns of fault displacement over time (top row) and relationships for age of extension onset (bottom row). Onset of rapid exhumation is determined from age-elevation profiles of samples at different locations along-strike. Thick horizontal lines indicate fault traces and fault propagation through time (arrows), thin black and gray lines illustrate evolving lateral displacement profiles, vertical gray bars represent age of onset (greater bar height = older age of onset) for hypothetical along-strike sample transects (1, 2, 3). Dashed bars (C) represent variability in onset age due to fault segment initiation at variable times. Figure modified from Curry et al., 2016.

Rift Timing

Early studies suggest rift initiation occurred synchronously across Tibet during Miocene time (ca. 14-8 Ma, Molnar et al., 1993; Turner et al., 1993; Harrison et al., 1995; Coleman & Hodges, 1995), but recent studies have shown rifting may have begun earlier and was diachronous across Tibet, with most graben systems initiating between 16 and 8 Ma (e.g., Laskowski et al. 2017; Wolff et al. 2019, 2023; Burke et al. 2021; Bian et al. 2022). The Tangra Yumco rift is one of the longest (~250 km) and most centrally located rifts in Tibet, spanning the entire N-S length of the Lhasa terrane (Fig. 1; Armijo et al. 1986; Taylor et al. 2003; Wolff et al., 2019, 2023). Active faulting in TYC is evidenced by well-developed triangular facets in fault footwalls and offset Quaternary alluvial fan deposits in the rift hanging wall (Wolff et al., 2019, 2023). Wolff et al. (2019) published data for three samples from a footwall granite intrusion in northern TYC, two of which yielded concordant igneous U-Pb ages of 86.6 ± 0.6 and 87.2 ± 0.6 Ma and average zircon (U-Th)/He (ZHe) ages of 12.5 ± 1.1 and 9.7 ± 0.7 Ma. Wolff et al., (2023) published four additional footwall samples from the southern end of TYC yielding mean ZHe ages between 16.7 ± 1.0 Ma and 13.3 ± 0.6 Ma. Thermo-kinematic modeling in Pecube (Braun, 2003; Braun et al., 2012) indicated initiation of normal faulting in northern TYC at 14.5 ± 1.8 Ma at a rate of ~0.2-0.3 km/Myr, which accelerated to ~0.6-0.8 km/Myr after ca. 3 Ma (Wolff et al., 2019, 2023). Both studies interpret a two-phase cooling history for northern TYC, with an initial phase of slow cooling in the mid-Miocene followed by rapid cooling during Pliocene time (Wolff et al., 2019, 2023), with the latter responsible for the modern topography of the TYC rift. A northward-younging trend in the timing of rift acceleration has also been proposed for other Tibetan rifts where along-strike fault timing is well constrained (section 2.2.4 Tibetan Rifts; Styron et al., 2013, 2015; Sundell et al., 2013; Bian et al., 2022).

Development of the Gangdese Drainage Divide

Tectonically driven spatial and temporal variations in rates of rock uplift within active mountain belts has the potential to drive dynamic reorganization of fluvial networks and the drainage divides that bound individual network component (Willett et al., 2014). The internally drained portion of the Tibetan Plateau forms a long wavelength depression that is ~600,000 km^2 in size (Fielding et al., 1994), with its southern boundary and the modern-day drainage divide marked by the crest of the Gangdese Range (Fig. 2). East-West extension in central and southern Tibet is proposed to have initiated in the mid-Miocene (ca. 18 Ma, e.g., Li et al., 2015) or coeval with N-S shortening during Eocene time (ca. 47 Ma, Wang et al., 2010). East-West extension and strike-slip faulting have been suggested as likely contributors to the diversion of river networks and relocation of lake centers in central Tibet since Miocene time (e.g., Han et al., 2019). Delamination, lithospheric dripping, and other deep crustal or mantle processes may enhance basin subsidence in central Tibet (Gao et al., 2013; Yin & Taylor, 2011; Bischoff & Flesch, 2018; Han et al., 2019; Kapp & DeCelles, 2019), acting simultaneously to the already complex interplay between uplift, erosion, sedimentation, and climate to drive topographic change (e.g., Sobel et al., 2003). We examine the tectonic development of the Gangdese drainage divide by evaluating low-temperature thermochronology results from north-trending rifts that crosscut or are localized within the high crest of the Gangdese Range. We investigate how contraction beneath the Gangdese Range, surface uplift, and rift exhumation relate to the timing of formation or potential change in location of the Gangdese drainage divide.

Regional Geologic Background

Rock Units

Rocks exposed in the southern TYC geologic map area (Fig. 2) include Permian sedimentary units of the Lhasa terrane, Late Cretaceous-Paleogene calc-alkaline intrusive rocks of the Gangdese (Trans-Himalaya) magmatic arc (herein referred to as the Gangdese Range) and nonmarine sedimentary, volcanic, and volcaniclastic rocks of the Linzizong Volcanic Group

(LVG), Cretaceous marine and Paleogene marine and nonmarine strata of the Xigaze forearc basin, and Oligocene-Miocene nonmarine Kailas (Gangrinboche) Formation conglomerates. Permian sedimentary rocks include the Angjie and Luobadui Formations. The Angjie Formation is exposed in the central and northern map area, and consists of dark gray sandy sericite slate, fine grained quartz sandstone, siltstone, mudstone, and limestone (e.g., Geng et al., 2009). The Luobadui Formation is composed of shallow-marine fossiliferous limestones, terrigenous sediments, and intercalated volcanic rocks (Wang et al., 2022). Fossils including abundant brachiopods, bryozoans, fusulinids, and corals indicate middle Permian deposition, likely related to southward subduction of the Paleotethys (Geng et al., 2009; Kapp & DeCelles 2019). Dating of volcanic rocks further constrain the Luobadui Formation to between ca. 275-260 Ma (Wang et al., 2022).

Gangdese Range rocks are composed of calc-alkaline intrusive granites and granodiorites (e.g., He et al., 2007; Ji et al., 2009; Zhu et al., 2011). Episodic magmatic activity in the Gangdese Range occurred between ca. 200 Ma and ca. 40 Ma, with a highest magmatic flux occurring at ca. 52 Ma (e.g., Zhu et al., 2011; Leary et al., 2016) and relatively low-volume magmatism continuing as late as ca. 8 Ma (Zhu et al., 2011; Zhang et al., 2014; Leary et al., 2016). Rocks of the Gangdese batholith and LVG are interpreted to be genetically linked (e.g., Leary et al., 2016) with their formation likely driven by continental arc magmatism related to northward subduction and/or breakoff of Neo-Tethyan lithosphere in the Late Cretaceous-Paleogene (Schärer et al., 1984; Pan et al., 2004; Lee et al., 2007, 2009; Liu et al.,2018; Kapp & Decelles, 2019). The LVG is subdivided into the lower Dianzhong (60.2-58.3 Ma), middle Nianbo (55.4-52.6 Ma), and upper Pana (52.6-52.3 Ma) Formations (Zhu et al. 2015). The

Paleocene Dianzhong Formation contains mainly porphyritic andesite with minor basaltic and rhyolitic clasts and tuffaceous lavas (Mo et al., 2008; Lee et al., 2012; Zhang et al., 2023). The Eocene Nianbo formation consists of sandstone and siltstone, rhyolitic tuff, and thin limestones interbedded with andesitic rocks (Huang et al., 2013; Zhu et al., 2015). The Eocene Pana Formation consists mainly of basalt, andesite, dacite, and coarse andesitic breccias with intercalated rhyolitic volcanic clasts (e.g., Mo et al., 2008; Liu et al., 2018). The middle Nianbo Formation is spatially variable in deposition in central Tibet, thus the Pana Formation may unconformably overly the Dianzhong Formation or Angjie Formation in this region. At the southernmost end of the TYC rift, the Cretaceous Ngamring Formation (Wu et al., 1977) of the Xigaze Forearc Group is observed in fault contact with the Dazhuka Formation of the Oligocene-Miocene Kailas Group along a steeply south-dipping reverse fault (Wang et al., 2012; An et al., 2014; Orme et al., 2015; Orme & Laskowski, 2016; Orme, 2019). The Ngamring Formation has been dated to ca. 107-84 Ma (Wu et al., 2010), is between 1000-4100 meters thick, and contains a series of fining-upward deep-marine turbidite sequences interbedded with thick channelized graded-bed conglomerates, gray feldspathic lithic sandstone, argillaceous siltstone and shale, calcareous mudstone, and minor fossiliferous limestone facies (Einsele et al., 1994; Dürr, 1996; Wang et al., 2012; An et al. 2014; Orme & Laskowski, 2016).

The Kailas Formation is spatially variable in depositional age and thickness and is additionally referred to by different names across the IYS, including the Kailas, Qiuwu, Dazhuka and Luobusa Formations (Heim & Gansser, 1939; Gansser, 1964; Aitchison et al., 2002; DeCelles et al., 2011; Li et al., 2017; Zhang et al., 2017; Laskowski et al., 2018). A west-to-east trend in depositional age for the Kailas Formation was recognized by Leary et al. (2016), varying from 26–24 Ma near Mt. Kailash (~81.3 °E) to 23–22 Ma near Dazhuka (~89.6 °E). The Dazhuka Formation is equivalent to the geographically central portion of the Kailas Formation and is comprised of dark gray to gray-green conglomerate with clasts of granite, gneiss, ultra-mafic and mafic rocks, lithic sandstone and siltstone, and minor rhyolite (Aitchison et al., 2002; Wang et al., 2013; Huang et al., 2019), with interpreted sediment sourcing from the Gangdese Range and Himalayan orogen (Decelles et al., 2011; Wang et al., 2013). The Dazhuka Formation typically overlaps, forms an angular unconformity, or is faulted onto rocks of the LVG or Gangdese batholith (Gansser, 1964; Leary et al., 2016; Laskowski et al., 2018).

It is proposed that anchoring or rollback of the Indian slab at ca. 26 Ma may have reactivated the IYS as a north-dipping normal fault to accommodate N-S extension and deposition in the Kailas basin until ca. 21 Ma (DeCelles et al., 2011, 2016; Wang et al., 2013; Leary et al., 2016; Laskowski et al., 2017, 2018; Kapp & Decelles, 2019). Finally, Paleocene-Eocene porphyritic rhyolite intrusions (Eqλ) related to the Chagele deposits of the Gangdese Metallogenic Belt (~63-32 Ma, Hou et al., 2004; Gao et al., 2021) and outcrop scale N-S trending dikes consistent with E-W extension observably crosscut rock units of the southern TYC map area. North trending dikes from the Daggyai Tso graben (recently referred to as the Dajiamang Tso rift; Burke et al., 2021) are located ~50 km west of TYC and yield U-Pb ages of ca. 18-13 Ma implying a minimum age of ~18 Ma for the onset of east-west extension in southern Tibet (Williams et al., 2001; McCallister et al., 2014; Burke et al., 2021).

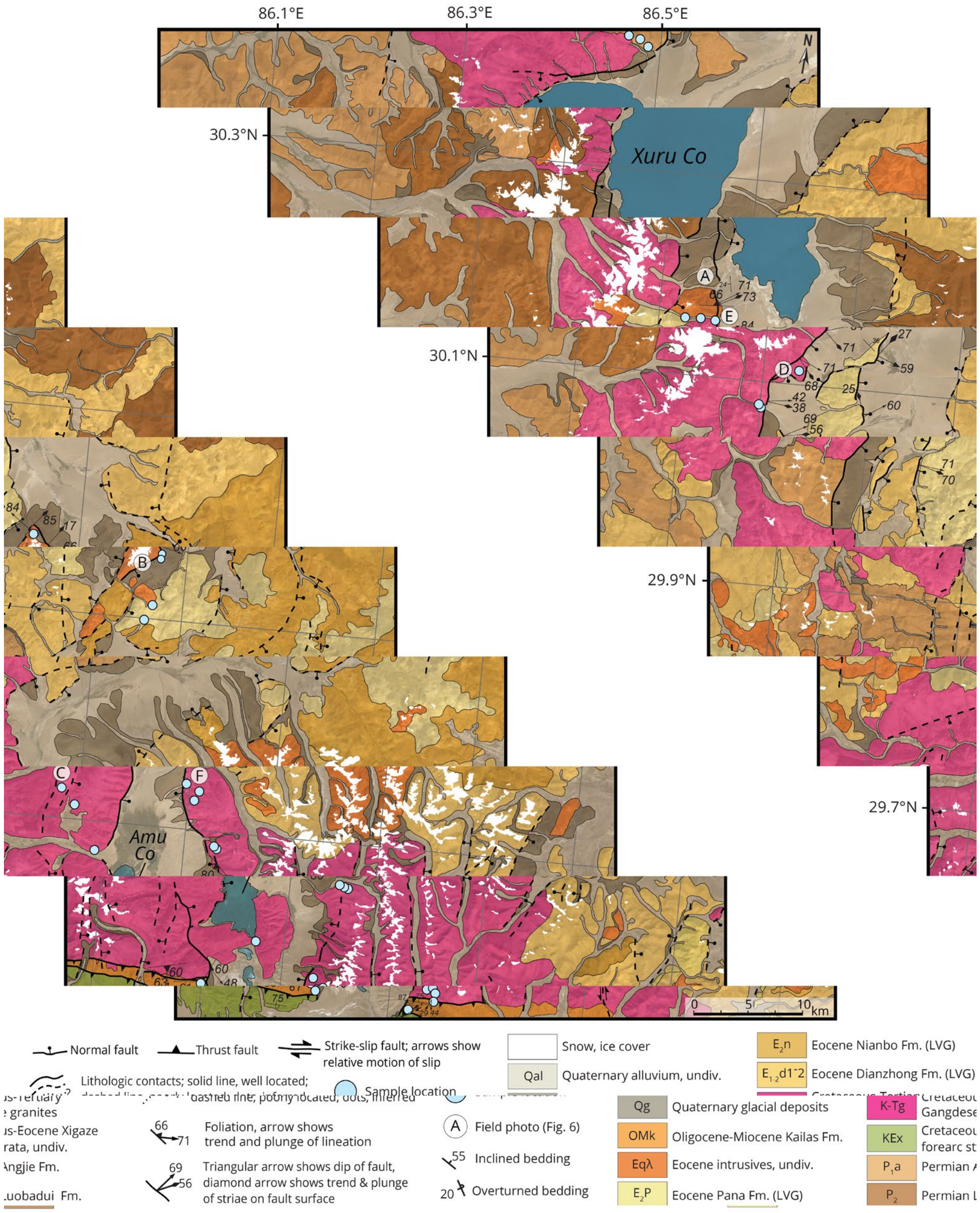

Figure 4. Geologic map of the southern Tangra Yumco rift. Mapping was conducted at ~1:100,000 scale including field observations supplemented by digital mapping from satellite imagery and previous geologic mapping at 1:250,000 scale (Pan et al., 2004). Geologic contacts were interpolated in difficult to access areas and between field traverses using Google Earth and Landsat imagery, as extreme elevations (>6000 m), snow and ice cover, and limited roads prohibited complete access to the map area. Mapped features were drafted over hill shade and slope maps with topography derived from Shuttle Radar Topography Mission (SRTM) 1 Arc-Second Global Digital Elevation data (DOI:/10.5066/F7PR7TFT) and draped Landsat Legacy Global Land Survey (GLS) imagery (DOI:/10.5066/F7M32TQB).

Fault Systems

Gangdese Retroarc Fold-Thrust Belt A contractional Cordilleran-style retroarc thrust belt north of the Gangdese Range in the Lhasa terrane has been proposed based on the presence of an angular unconformity separating highly shortened Permian-Cretaceous strata from overlying weakly deformed Cretaceous-Tertiary rocks of the LVG (e.g., Burg et al., 1983; England & Searle, 1986; Ratschbacher et al., 1992; Kapp et al., 2007; Leier et al., 2007) and portions of a potentially associated foreland basin system. To the west near the city of Lhasa, contractional structures potentially related to the GRTB are thought to have accommodated >230 km of N-S shortening between 105 and 53 Ma. (Kapp et al., 2007). The GRTB could be responsible for rapid shortening (>8 mm/yr) and southward underthrusting of lithosphere beneath the Gangdese Range concurrent with south-directed thrusting in the northern Lhasa terrane thrust belt (Murphy et al., 1997; Kapp et al., 2003, 2005, 2007; Kapp & DeCelles, 2019). Retroarc shortening ceased at ca. 50–55 Ma, roughly coeval with the initiation of India-Asia collision in southern Tibet and a southward sweep of magmatism across the Lhasa terrane, possibly reflecting a decrease in India-Asia convergence rates and rollback of the Neotethyan slab (e.g., Patriat & Achache, 1984; Zhu et al., 2005; Kapp et al., 2007; Kapp & DeCelles, 2019).

Gangdese Thrust The south-vergent, north-dipping Gangdese Thrust (GT) system was first interpreted by Yin et al. (1994) to place Cretaceous Xigaze Group forearc basin strata over Tethyan sedimentary rocks near the town of Xigaze (~250 km east of southern TYC), and Gangdese batholith rocks over Tethyan rocks to the east of Lhasa city near Zedong. Since then, many of the contacts near Xigaze have been revisited and determined to be predominantly related to the Great Counter Thrust system (e.g., Murphy et al., 2010; Leary et al., 2016; Laskowski et al., 2018). Exposure of the GT near Zedong is more viable, marked by a >200-m-thick mylonite shear zone that dips 25°-35° north, with abundant kinematic indicators suggesting top-to-the-south shear (Yin et al., 1994). In some places, a major south-dipping back thrust is present in the hanging wall of the GT, placing Xigaze forearc strata over Tertiary conglomerates or the Gangdese batholith (Yin et al., 1994). An absence of Xigaze forearc rocks in either the hanging wall or footwall of the GT near Zedong, and more broadly between the towns of Gongga and Milin of the eastern IYS (e.g., Wei et al., 2021) could be related to thrusting of Xigaze strata beneath the Gangdese batholith (Yin et al., 1994) or lateral variations in the depth of exhumation, with a marked absence of Xigaze forearc strata in the east (Wei et al., 2021). Minimum displacement and slip rate estimates along the GT are 46 ± 9 km and 12 ± 6 km/Myr, respectively (Yin et al., 1994); in broad agreement with present-day rates of India-Asia convergence (Molnar & Deng, 1984; Avouac & Tapponnier, 1993). Timing of GT activity was originally interpreted as late Oligocene-early Miocene (27-23 Ma), based on 40Ar/39Ar thermochronology results indicating the onset of crustal thickening and thrust-related cooling at ca. 23 Ma and rapid exhumation of the Gangdese batholith at ca. 20 Ma (Copeland et al., 1987, 1995; Richter et al., 1991; Harrison et al., 1992; Yin et al., 1994). However, these constraints overlap timing estimates for Kailas basin deposition in south-central Tibet (25-23 Ma ± 3 Myr along strike; Leary et al., 2016) which likely requires a period of N-S extension (DeCelles et al., 2011), and therefore GT initiation is unlikely to have occurred until after 23 Ma in this region (Laskowski et al., 2018). Evidence of the GT has not yet been observed in this region of south-central Tibet, but if the GT or equivalent structure were present at the surface or at depth, it would likely have been active between ca. 23-13 Ma, overlapping the estimated timing of Great

Counter thrust system activity and exhumation in southern Tibet (Tremblay et al., 2015; Laskowski et al., 2018).

The Great Counter Thrust System The IYS and Xigaze forearc are cut by a series of north-vergent, generally south-dipping (locally overturned) thrust faults known as the Great Counter Thrust System (GCT, e.g., Heim & Gansser, 1939; Yin et al., 1994, 1999; Murphy et al., 2010). The GCT is the northernmost fault system of the broader Tethyan Himalayan thrust belt, representing the northernmost extent of Himalayan fold-thrust belt deformation (Leary et al., 2016; Laskowski et al., 2018). The GCT places Tethyan Himalaya rocks over IYS rocks, and Xigaze forearc rocks over Kailas Formation conglomerates (Leary et al., 2016; Laskowski et al., 2017, 2018). The GCT could hypothetically be correlated with the Gangdese Thrust to the east (Yin et al., 1994), but a north-dipping fault contact placing Gangdese batholith rocks onto Xigaze forearc or Tethyan Himalayan rocks has not been observed in this region (Laskowski et al., 2018). Rollback of the Indian slab at ca. 26 Ma is interpreted to have initiated N-S oriented extension and deposition in the Kailas basin for ~5 Myr (Kapp & DeCelles, 2019), but this interpretation remains controversial (see discussion section 5.2). Following rollback, break off or delamination of Indian mantle lithosphere at ca. 21 Ma may have caused N-S extension and Kailas deposition to cease, triggering a return to N-S contraction, exhumation and uplift of the Kailas basin to ~4-6 km elevations between 20-16 Ma, and initiation of motion along the GCT (Laskowski et al., 2018). Movement on the GCT initiated as early as 23 Ma based on provenance changes in the Kailas Formation with continued activity until ca. 18-13 Ma (Laskowski et al., 2018; Kapp & DeCelles, 2019). The lower limit on GCT activity is constrained by the shift from N-S contraction to E-W extension in southern Tibet and is recorded by the initiation of Tibetan rifts which crosscut the GCT, requiring inactivity along the GCT by this time (Ratschbacher et al., 1994; Harrison et al., 2000; Yin et al., 1994, 1999; Yin, 2006; Murphy et al., 2010; Sanchez et al., 2013; Styron et al., 2013; Leary et al., 2016; Laskowski et al., 2017, 2018).

Tibetan Rifts Tibetan rifts are predominantly located in the Lhasa Terrane and are commonly > 150 km in N-S length, facilitating east-west extension that crosscuts the pre-Cenozoic structural grain of the Tibetan Plateau (Fig. 1; Burke et al., 2021; Armijo et al., 1986; Yin, 2000). In this section we review relevant field observations and timing constraints from studies of two major Tibetan rift systems, the Lunggar and Yadong-Gulu rifts located in western and eastern Tibet (Fig. 1) and compare these results to observations and timing constraints for the Tangra Yumco rift (described in section 1.1. Rift Initiation).

The Lunggar rift system is located ~300 km west of TYC (Fig. 1) and has been studied extensively in the south (Styron et al., 2013) and north (Kapp et al., 2008; Sundell et al., 2013). Unlike many of the high-angle rift systems in south-central Tibet and the Himalaya, motion along the Lunggar rift is dominated by two low-angle normal faults, the east-dipping North Lunggar Detachment (NLD) and west-dipping South Lunggar Detachment (SLD), which exhume Miocene leucogranites (ca. 15-9 Ma; Kapp et al., 2008) and mylonitic shear zones in their footwalls. Structural measurements of foliation, stretching lineations, and shear fabrics suggest top-to-the-east normal sense shear (Kapp et al., 2008; Styron et al., 2013, 2015; Sundell et al., 2013). Normal faulting in the South Lunggar Rift initiated during the mid-Miocene with relatively slow exhumation rates (~1m/Myr) which accelerated at ca. 8 Ma (~2.5-3.0m/Myr) as motion initiated along the SLD (Styron et al., 2013). Thermal history modeling of ZHe and AHe data yielded a minimum timing for North Lunggar Rift initiation of >10 Ma with initially slow rates of cooling (<50°C/Myr) and exhumation (<1m/Myr), followed by rapid footwall cooling (>400°C/Myr) and exhumation (4-10m/Myr) between 5-2 Ma (Sundell et al., 2013), suggesting synchronous rift initiation during the mid-Miocene followed by a northward sweep of rift acceleration in the late Miocene to Pliocene (Styron et al.,2015). An intra-basin high forms a drainage divide separating the North and South Lunggar Rifts, causing rivers to flow into lake basins in the northern and southern portions of the rift, respectively, and likely constitutes a region of maximum extension (Kapp et al., 2008).

The Yadong-Gulu rift (YGR) system is located ~360 km east of TYC (Fig. 1) and has also been studied extensively in its south (Yadong) and north (Gulu) segments (Armijo et al., 1986; Pan & Kidd, 1992; Cogan et al., 1998; Wu et al., 1998; Stockli et al., 2002; Kapp et al., 2005; Wu et al., 2015; Ha et al., 2019; Chevalier et al., 2020; Bian et al., 2022). Like the Lunggar rift, the YGR exposes a mylonitic shear zone and Miocene granites in its southern footwall, documenting significant and rapid exhumation during Pliocene time (Kapp et al., 2008). The YGR detachment is inactive at the surface with active extension occurring along higher angle faults within the rift basin that cut Quaternary deposits and likely sole into the detachment at depth. The YGR contains an intra-basin topographic high which likely corresponds to a region of maximum extension and forms a regional drainage divide (Cogan et al., 1998; Kapp et al., 2008). Recent geo- and thermochronology from YGR indicate a northward younging trend in the timing of rift initiation, from ca. 13-11 Ma in southern Tibet to ca. 7-5 Ma in the northern rift, suggesting a northward propagation of rift initiation (Bian et al., 2022) which could be consistent with both the segment linkage or tectonically influenced tip propagation models for fault growth. The YGR's variable along-strike timing of rift initiation could perhaps be attributed to its more oblique orientation and farther eastward location (Bian et al., 2022) or variations in the shape, angle, and extent of the subducting Indian plate, an idea which was also recently considered for the TYC rift (Wolff et al., 2023).

Observations from the Lunggar and Yadong-Gulu rifts reveal key similarities with the Tangra Yumco rift. The suggested timing of rift initiation in the mid-Miocene and subsequent northward sweep of rift acceleration in the late Miocene to Pliocene has been proposed for all three rift systems, suggesting they have at least in some part a common mechanism of origin and evolution (DeCelles et al., 2002; Kapp & Guynn, 2005; Styron et al., 2015; Wolff et al., 2019, 2023; Bian et al., 2022). Each rift is kinematically linked to a dextral strike slip fault to the north near its intersection with the Bangong-Nujiang Suture Zone (BNS), which further suggests a common evolution (Armijo et al. 1986; Taylor et al. 2003; Wolff et al., 2019, 2023). Though TYC is dominated by active high-angle normal faults rather than low-angle fault systems observed in Lunggar and YGR, active extension in all three systems occurs along stepped high angle faults within the rift basins that cut Quaternary deposits, exhume Miocene leucogranites and shear zones in their footwalls, and likely sole into a detachment fault at depth. Finally, the presence of an intra-basin high in central TYC forms a drainage divide, causing river systems to flow into one of three distinct lakes within the rift basin; Tangra Yum Co in the north, Xuru Co in the center, and Dajia Co in the south (Wolff et al., 2023). Tangra Yum Co and Xuru Co lakes are situated within the internally drained portion of the plateau (i.e., north of the drainage divide), whereas Dajia Co is located south of the divide and drains into the Dogxung-Tsangpo river, a tributary of the Yarlung-Tsangpo river (e.g., Wolff et al., 2023), which is similar to the drainage systems observed in the other rift systems.

Gangdese Rifts Gangdese rifts are usually shorter (< 150 km) than Tibetan rifts and are concentrated within the high topography of the Gangdese Range along the southern margin of the Lhasa terrane (Burke et al., 2021). Gangdese rifts are typically horst-and- graben structures, with the high relief horsts bounded by high-angle active east-dipping and west-dipping normal faults. Recently published geo- and thermochronology results from the Dajiamang Tso rift constrain the age of extension onset to between 16-8 Ma for south-central Tibet (Burke et al., 2021). A minimum age of ca. 16 Ma for extension onset is consistent (within ± 2 Ma) with results from other Gangdese rifts (Yin & Harrison, 2000; Williams et al., 2001; McCallister et al., 2014; Sanchez et al., 2013; Laskowski et al., 2017). U-Pb dating of north trending extensional dikes of the Daggyai Tso graben (the northern portion of the Dajiamang Tso rift) yielded ages between 18-13 Ma (Williams et al., 2001; McCallister et al., 2014). 40Ar/39Ar results dating movement along the Lopu Kangri rift (Sanchez et al., 2013; Laskowski et al., 2017) and north striking mineralized fractures near the Thakkhola graben (Murphy et al., 2010) yielded ages of ~15 and ~14 Ma, respectively. Furthermore, active extension and exhumation along the high-angle normal faults that border Gangdese rift grabens are evidenced by young ZHe cooling ages (Laskowski et al., 2017), seismogenic activity, and well-formed triangular facets and quaternary alluvial deposits cut by fault scarps (Zhang et al., 2004, Gan et al., 2007).

Methods

Geologic Mapping

Geologic mapping was conducted in the southern Tangra Yumco rift, ~40 km northwest of the city of Sangsang, Tibetan Autonomous Region, China (Fig. 2). Sangsang is located ~430 km west of Lhasa and ~160 km north of Mt. Qomolangma (Everest) (Fig. 1). Geologic mapping followed a ‘mapping mode’ workflow in the StraboSpot digital geologic data system application for iOS; geologic features were recorded by direct observation in the field at scales locatable by GPS (Walker et al., 2019). Mapping was conducted at ~1:100,000 scale across the study area within the southern TYC rift (Fig. 4). Field mapping was supplemented with digital mapping from satellite imagery and previous geologic mapping at 1:500,000 scale (Pan et al., 2004). Mapped features were drafted over hill shade and slope maps derived from Shuttle Radar Topography Mission (SRTM) 1 Arc-Second Global Digital Elevation data (DOI:/10.5066/F7PR7TFT) and draped Landsat Legacy Global Land Survey (GLS) imagery (DOI:/10.5066/F7M32TQB). Geologic contacts were interpolated in difficult to access areas and between field traverses using Google Earth and Landsat imagery, as extreme elevations (>6000 m), snow and ice cover, and limited roads prohibited complete access to the map area. Digitally mapped features were interpreted based on tonal variations in satellite imagery, presence of triangular facets, mountain front sinuosity, linearity of features (e.g., fault scarps), and deflected streams, rivers, and drainages.

Zircon U-Pb Geochronology

Eighteen of fifty samples collected from rift footwall transects were selected for zircon U-Pb geochronology to constrain the crystallization age for footwall rocks along strike of the TYC rift (location and lithology data for each sample are provided in supplementary Table S1). Zircons were extracted from bulk samples using standard crushing, sieving, electro-magnetic, and heavy liquid mineral separation techniques. Zircon grains for each sample (n = 75) were mounted in 1 inch epoxy ring forms alongside Sri Lanka (SLmix), R33, and FC zircon standards (Paces et al., 1993; Schmitz et al., 2003; Black et al., 2004; Gehrels et al., 2008), then polished to a depth of ~20 μm at the Tectonic Sedimentology and Thermochronology (TeST) laboratory at Montana State University. Backscattered electron (BSE) and cathodoluminescence (CL) imagery was obtained for each sample prior to analysis at the University of Arizona LaserChron Center (ALC) to provide generalized maps for isotopic analysis and targeting of specific age domains. Zircon U-Pb geochronology was conducted at ALC following the detailed analytical procedures and data reduction methods of Gehrels et al. (2006, 2008) and Pullen et al. (2018). A Photon Machines Analyte G2 Excimer laser attached to a Thermo Element2 HR single-collector ICP-MS was used to measure U, Th, and Pb isotopes. Analytical uncertainties related to determination of 206Pb/238U and 206Pb/204Pb are between 1-2% (2σ) for individual reported ages. Standard sample bracketing with SLmix, R33, and FC zircon reference materials of known age were used to correct for inter-element fractionation of U and Pb isotopes (Gehrels et al., 2008). U-Pb weighted mean age determinations reject and exclude from visual representation all U-Pb analyses with >20% discordance or >5% reverse discordance. The AgePick Excel Tool available online from ALC (Gehrels, 2009) was utilized to calculate the reported weighted mean age, uncertainty, and MSWD for each sample. An MSWD = 1 indicates the degree of scatter is consistent with analytical precision. Weighted mean plots were generated using the AgeCalcML Weighted Mean Plotter (Sundell et al., 2020; Figure S2). Analyses for spots recording >1000 ppm U or ages exceeding 2σ error on weighted mean plots are considered outliers based on Chauvenet's criterion (e.g., Vermeesch, 2018), and therefore these analyses were systematically excluded from AgePick calculations, data visualizations, and subsequent interpretation. Reported ages reflect systematic error including standard calibration, age of the calibration standard, composition of common Pb, and the 238U decay constant, and is generally ~1%–2% at the 2σ level (Gehrels et al., 2009). Full analytical details and U-Pb results for each sample are provided in supplementary data Table S2. Weighted mean plots for all samples are included in supplementary Figure S2

Zircon (U-Th)/He Thermochronology

Fifty igneous samples were collected for zircon (U-Th)/He (ZHe) dating. We utilize ZHe dating because it generally records cooling over a closure temperature range of ~140-220 °C (Guenthner, 2013), well suited to investigate tectonic questions within the upper ~2-10 km of the Earth's crust, with the closure temperature dependent on additional parameters including the geothermal gradient and rates of exhumation (e.g., Dodson, 1973; Reiners et al., 2002; Ault et al., 2019). Sample transects were collected perpendicular to the strike of normal faults bounding the TYC and Gangdese rifts (Figs. 2, 4). Bulk samples underwent standard crushing, sieving, electro-magnetic, and heavy liquid mineral separation techniques at the Chinese Academy of Sciences in Beijing, China. All but one sample (19AL14) yielded sufficient zircon separates suitable for ZHe analysis. Five zircon grains from each sample (245 total grains) were handpicked for analysis at the Montana State University Tectonic Sedimentology and Thermochronology (TeST) laboratory. Grains were selected based on morphology (subhedral to euhedral), size (diameter >60µm), and clarity (minimal inclusions or fractures) to reduce grain size effects on intrasample age variation (Reiners & Farley, 2001). Long and short axis grain dimensions were measured from photomicrographs for α-ejection correction calculations (Farley et al., 1996) following procedures outlined in Hourigan et al. (2005). Grains were individually sealed into 1mm Nb foil packets to ensure even heating and prevent volitization of parent nuclides during helium extraction. Collection and measurement of 4He and isotopic dissolution to determine U-Th-Sm content was completed at the Arizona Radiogenic Helium Dating Laboratory (ARHDL) following the detailed procedures of Reiners et al. (2004) and Reiners (2005).

During analysis, individual packets were loaded into a vacuum laser cell and individually heated for 15 min using a focused beam from a 1-2W laser to extract 4He gas from the grain. A minimum of one re-extraction was completed for each zircon by reheating for 15-20 minutes, repeated until 4He extractions were 2% or less of the compounded total. 4He/3He ratios were measured using a quadrupole mass spectrometer equipped with a Channeltron electron multiplier. Fish Canyon Tuff (FCT) zircon standards with accepted ZHe age of 28.48 ± 0.06 (2σ) Ma (Schmitz & Bowring, 2001) were analyzed between every 5–7 unknowns to account for changes in isotopic fractionation or sensitivity bias (Reiners, 2005). Parent concentrations (U, Th, and Sm) were measured by isotope dissolution and inductively coupled plasma mass spectrometry (ICP-MS) using appropriate acids (Reiners, 2005). Analytical uncertainties include systematic and measurement errors for ZHe ages typically on the order of 1–3% at 2σ (Reiners et al., 2004). Analytical error includes the propagation of uncertainties from measurements such as grain size, 4He, U, Th, and Sm, but does not include errors associated with the alpha ejection correction which assumes homogenous parent nuclide distributions for individual grains (Hourigan et al., 2005). Detailed sample information and single grain ZHe analytical data are provided in supporting information Table S3. Reported mean ages were determined by averaging 3-5 grains per sample to allow exclusion of outliers beyond acceptable error. We note intra-sample variability of effective uranium (eU = [U] + 0.28[Th] + 0.0012[Sm]; Cooperdock et al., 2019), a proxy for radiation damage within individual crystals, as well as noting minor variations in grain size and 4He content. Intra-sample variabilities are examined for potential structural context during interpretation of cooling ages.

HeFTy Thermal Modeling

Inverse modeling was conducted using HeFTy thermal modeling software program version 1.9.3 (Ketcham, 2005). HeFTy inverse models use measured cooling ages as inputs and produce a suite of time-temperature (t-T) paths containing predicted ages that might provide good or acceptable fits to measured ages. This allows the user to test thousands of potential thermal histories based on measured data and additional imposed search constraints in the model's time-temperature space to determine a path which best fits the known thermochronology and geologic data. HeFTy is based on a Monte-Carlo algorithm that accounts for the diffusive loss and radiogenic ingrowth of 4He for individual grains as a function of thermal history, and utilizes a frequentist approach, meaning that formal statistical hypothesis tests can assess the goodness-of-fit between user input data and thermal model predictions (Vermeesch & Tian, 2014). Interpreting t-T paths for samples across a broad study area can expose spatial trends in the timing and rates of exhumation, which may provide broader tectonic implications. Conversely, HeFTy forward models generate predicted cooling ages for a specified t-T history that is input by the user. Predicted cooling ages can then be iteratively compared with measured data to test a variety of hypothesized thermal histories. Forward models are useful for ruling out thermal histories based on geologic scenarios that are inconsistent with field observations or measured values and can reveal how grain-specific parameters (e.g., grain size, radiation damage, diffusion kinetics) might affect intra-sample age variability. In this study we have developed a large dataset of measured ZHe cooling ages and are interested in generating potential thermal histories based on these results; therefore we utilize inverse HeFTy models rather than forward HeFTy models. Inputs for inverse models include grain-specific measurements (grain radius, U and Th concentration, and uncorrected cooling age) which force model paths to pass through a known t-T point based on these parameters. Models can include additional imposed t-T constraints based on measured results from other geochronology or thermochronology systems (e.g., U-Pb crystallization ages to constrain the higher temperature range of predicted thermal histories) or known geologic relationships from field observations. Results for preliminary HeFTy thermal models are detailed in section 4.4.

Results

Structural Results

We report field data collected from the Tangra Yumco rift (Fig. 4), the southernmost extent of which intersects the IYS ~40 km west of the town of Sangsang (Fig. 1). TYC is characterized by a series of approximately north-striking (~N30E-N35E) high-angle (~45-70°) active normal faults (Fig. 5D), exhuming ~1-2 vertical km of granodiorite in rift footwalls (Fig. 5F). In northern TYC (north of ~30.5°N) and southern TYC (south of ~29.5°N), west-dipping faults bounding the east flank of TYC rift constitute the dominant structures, whereas in the central TYC rift (between 29.5°N to 30.5°N) the dominant structures are east-dipping faults bounding the western rift flank. In both northern and southern TYC, hanging wall rocks consisting of Quaternary glacial and alluvial deposits are cut by a sequence of basin-stepping high-angle normal faults (Fig. 5E). In the central TYC rift, hanging wall rocks display synthetic graben structures and stepped fault scarps at the surface, suggesting the occurrence of low-angle detachment style faulting at shallow (~1-2 km) depths (e.g., Axen et al., 1999). Footwall granodiorites display pervasive northeast dipping foliation, with fault plane striations consistent with northeast directed oblique sinistral-normal slip (Fig. 4). The general trend of structures mapped from aerial imagery, field measurements, and modern GPS velocities support a preferential NNE-SSW trend of extensional structures at this longitude, suggesting a left-lateral strike-slip component of displacement within TYC and supporting interpretations of a general clockwise rotation of central Tibet (e.g., Zhang et al., 2004; Taylor & Yin, 2009). At the southern extent of the mapped area where TYC intersects the IYS, we observe Xigaze forearc strata faulted onto nonmarine strata of the Kailas Formation along a top-to-the north reverse fault that dips approximately ~75° to the south (Fig. 4). Approximately 1.5-2 km to the north, a second top-to-the north reverse fault that dips ~64° to the south places rocks of the Kailas Formation in the hanging wall atop Gangdese granites and exhibits fault plane striations consistent with a top-to-the-north-northwest oblique sense of motion. We interpret both structures as splays of the Great Counter thrust system based on their similar geometries and kinematics (Heim & Gansser, 1939; Yin et al., 1994, 1999; Murphy et al., 2010).

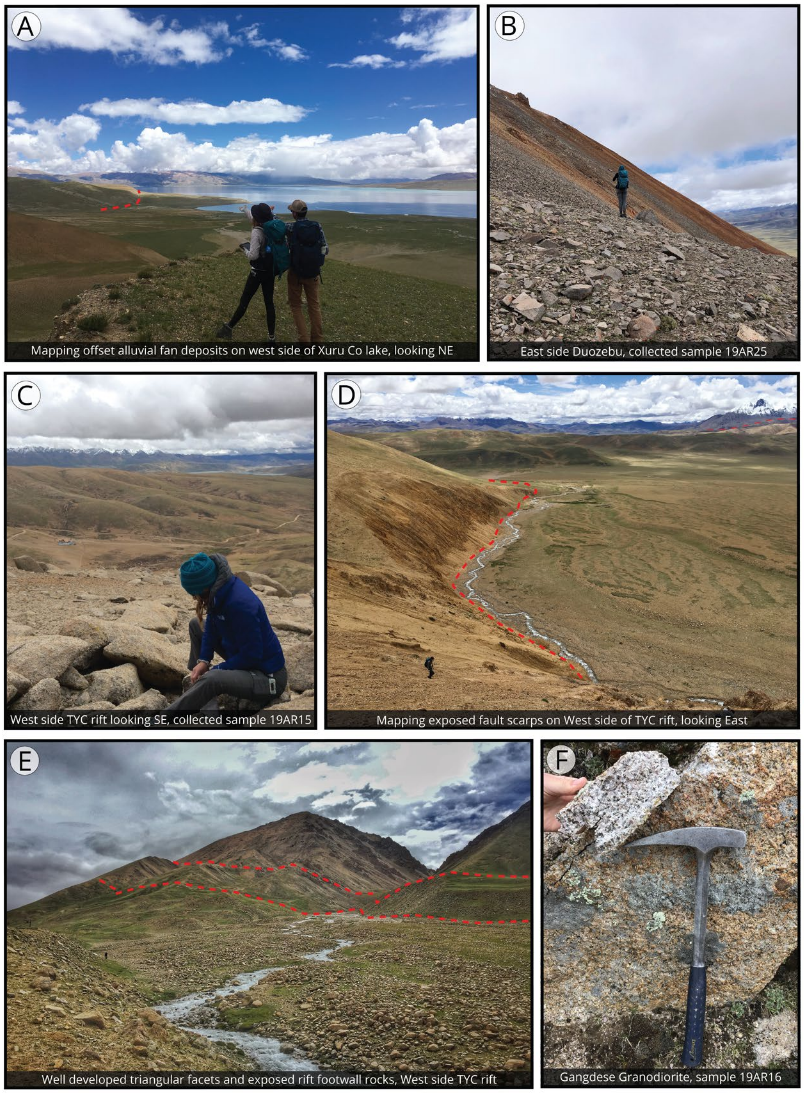

Figure 5: field photographs from the southern Tangra Yumco rift. (A) Mapping offset hanging wall alluvial fan deposits west of Xuru Co lake (photo looking NE). Red dashed lines show approximate fault trace. (B) Geologic mapping on the East face of Duozebu at ~5,600 m elevation (photo looking NE). (C) Collecting sample 19AR15 from the western footwall of the TYC rift (photo looking SE). (D) Mapping along exposed fault scarps, west side TYC. Height of fault scarp exposure is ~30 m (~98 ft). (E) Looking SW at the west side of the TYC rift; well-developed triangular facets exposing footwall rocks, sinistral-normal slip causes drainage to be offset towards the NNE. Relief in photo is ~777 m (~2,550 ft) (F) Gangdese granodiorite sample collected from rift footwall along East side of TYC.

Zircon U-Pb Geochronology

Igneous zircon U-Pb results for eighteen samples yield weighted mean ages between ~153 Ma and 11 Ma (Fig. 6, 7). Fourteen samples yield ages between 58.8 ± 0.2 Ma and 49.4 ± 0.2 Ma, consistent with previous results from this region (e.g., Lee et al., 2009; Zhu et al., 2011; Wang et al., 2015), whereas four samples yield ages outside of this range. Sample 19AR11 was collected from a N-S striking ~15m-wide porphyritic andesite dike and generated three distinct age domains at ~38 Ma (n =5), 24 Ma (n = 14), and 16 Ma (n = 17) likely due to inheritance, with the highest population of grains yielding a weighted mean age of 16.1 ± 0.1 Ma (Fig. 7; see section 5.1 for further discussion). Samples 19AR25 and 19AR26 are a dark gray porphyritic andesite-to-dacite which intrudes a heavily fractures cataclasite breccia zone along the east face of Duozebu mountain and generated weighted mean ages of 10.9 ± 0.1 Ma and 11.0 ± 0.1 Ma, respectively, with sample 19AR26 yielding two age populations at ~54 Ma (n = 5) and ~11 Ma (n = 17; Fig. 7). Finally, sample 19KS34 yields a significantly older weighted mean age of 152.9 ± 0.6 Ma (Fig. 7) and was collected from volcanic rocks just north of Xuru Co lake along a section of the rift where the dominantly N-S striking rift bounding fault curves abruptly to an E-W striking orientation.

Analyzed zircons from this study show oscillatory zonation with no obvious metamorphic rims in CL imagery, widely variable concentrations of U (~98–5551 ppm) and Th (1055–7438 ppm), and U/Th ratios between 0.33 to 3.49 (Table S2). These results are consistent with an igneous origin (e.g., Corfu et al., 2003; Hoskin & Schaltegger, 2003; Harley et al., 2007; Gehrels et al., 2009). Additionally, no inherited cores were identifiable in CL imagery for all samples other than 19KS34, which revealed oscillatory zoned cores with homogeneous metamorphic rims. Therefore, weighted mean ages for most samples are considered to represent the age of primary zircon crystallization, with the mean age for sample 19KS34 warranting further investigation (see section 5.1). High-U analyses which correlate to anomalously young ages may alternatively indicate Pb-loss (Gehrels et al., 2009), however, zircons in this study show no correlation of high-U concentrations with youngest ages, indicating no analytically significant Pb-loss has occurred. The AgePick tool for Excel (Gehrels, 2009) was utilized to evaluate individual sample analyses and determine outliers based on anomalous age or U concentrations. Analyses for spots recording >1000 ppm U or resulting in ages exceeding 2σ error were considered outliers and excluded from data visualizations and interpretation. Sample coordinates and complete data for all U-Pb analyses included in Table S2.

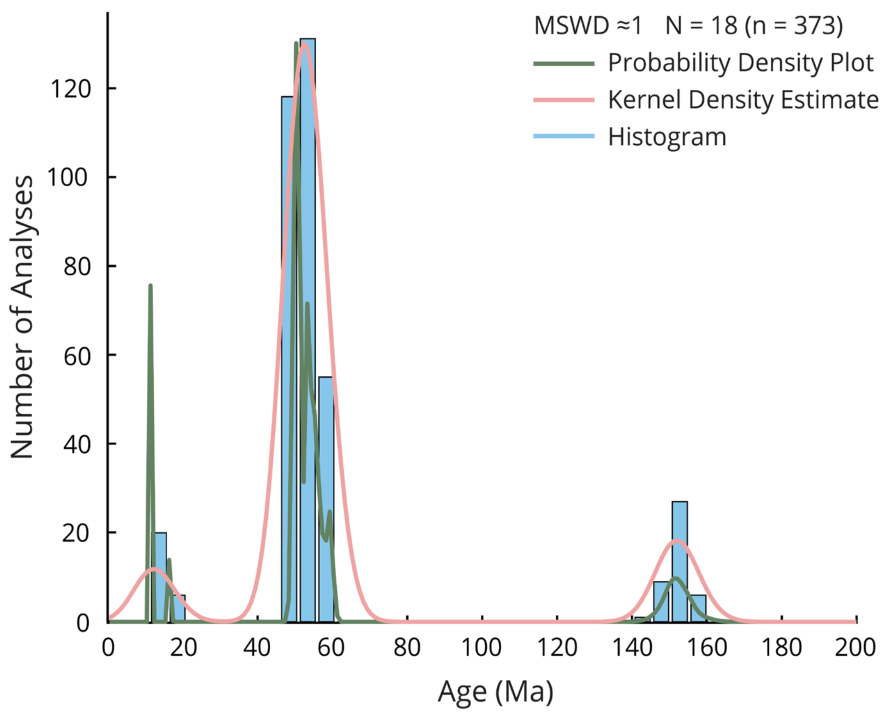

Figure 6. U-Pb probability density plot (PDP, green), kernel density estimate (KDE, pink), and histogram (blue) for analyses within MSWD ≈ 1 (n = 373/698). Grains with >1000 ppm Uranium and ages exceeding 2σ error are considered outliers and not plotted or included in MSWD calculation.

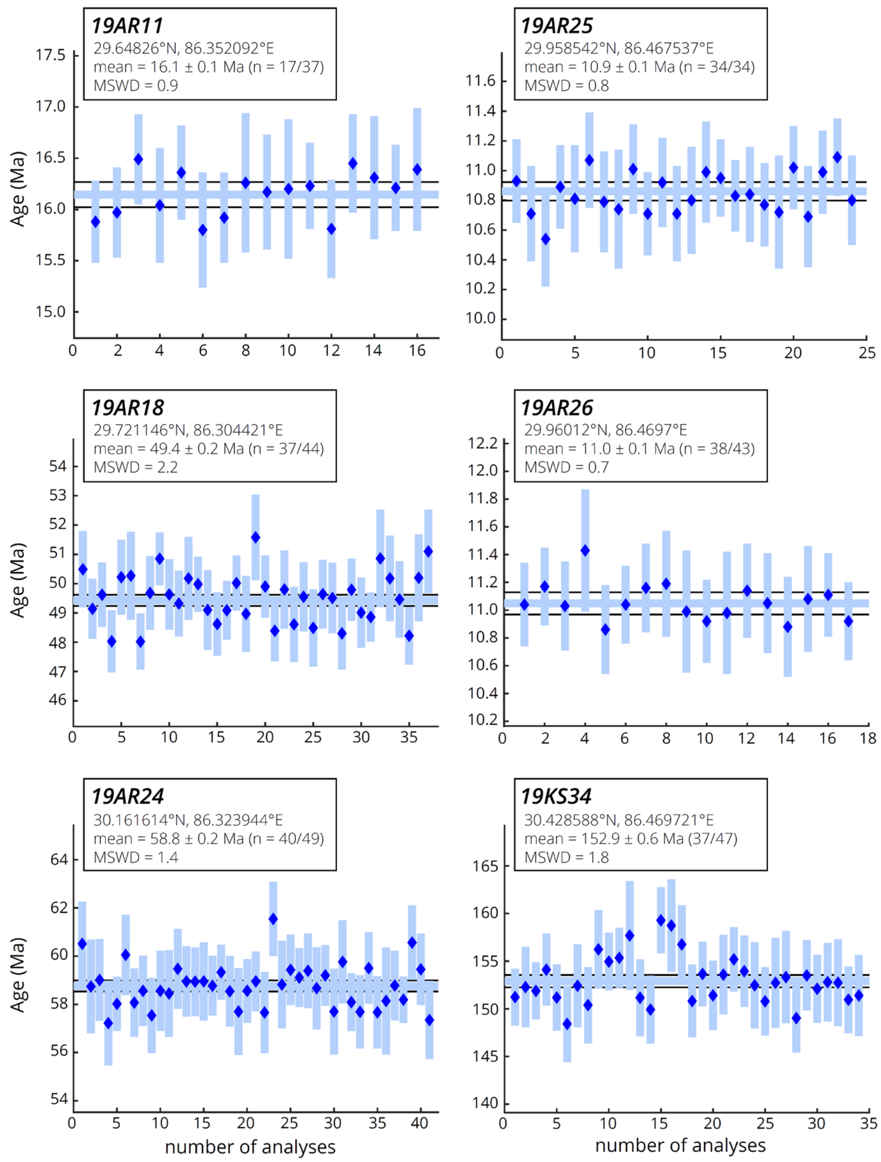

Figure 7. Igneous zircon U-Pb weighted mean age plots for samples collected from TYC and Gangdese (19AR04, 19AR07, 19AR08) rift footwalls. Ages reflect the timing of latest crystallization with plots for samples 19AR11, 19AR25, and 19AR26 representing youngest age populations (Fig. 6). Grains with >1000 ppm Uranium and ages outside of 2σ error were considered outliers and not plotted or included in MSWD calculations. Sample locations shown on geologic map (Fig. 4). Weighted mean plots for all samples are included in supplementary Figure S2.

Zircon (U-Th)/He Thermochronology

Here we report ZHe mean ages (Fig. 8, Fig. S3, Table S3) for forty-nine samples including thirty-two samples from the southern TYC rift and seventeen samples from three Gangdese rifts (GR) located ~90 km (GR1, five samples), ~75 km (GR2, ten samples), and ~40 km (GR3, two samples) east of TYC. Mean ages and errors were calculated by averaging five single-grain analyses per sample (245 total single grain ages), excluding eight grains that were considered outliers. Outliers were not plotted or included in calculations due to their anomalous results for age, Th/U ratio, or Zr content (Table S3). We note nine samples from TYC (19AR14, 19AR19, 19AR20, 19AR21, 19KS32, 19AL09, 19AL10, 19AL13, 19AL14) and two samples from Gangdese rifts (19AR01 and 19AR06) show poor intra-sample reproducibility (i.e., single-grain ages within each sample yield standard deviations >5 Ma). We report mean ages for these samples for completeness and consider causes of intra-sample variability in our discussion. Detailed sample data and ZHe results are included in Table S3.

Tangra Yumco Rift One hundred sixty single-grain ZHe analyses from southern TYC produced mean ages between 59.3 ± 0.8 Ma and 4.72 ± 0.06 Ma. Mean ages show no significant correlation with elevation (Fig. 8a), grain radius, or effective uranium (eU = 0.235 Th x U; supplementary Figure S3) but correlate strongly with sample latitude (Fig. 8b). Samples can be separated into three groups by mean age: Group one (red) includes samples collected from latitudes where the TYC rift crosscuts the Gangdese Range (~29.4°N-29.8°N) and is comprised of Oligocene to mid-Miocene ages (~28-15 Ma). Group two (orange) and group three (yellow) include samples from latitudes north of the Gangdese Range (~29.8°N-30.43°N) and yield Paleocene-Eocene (~59-41 Ma) and late Miocene-Pliocene (~9-4 Ma) ages, respectively.

Group one: the nineteen samples in group one yield mean ages between ca. 28-15 Ma, with all but three samples (19AR21, 19AR23, 19AL09) having mean ages falling within the narrower window of ~23-16 Ma. Sample 19AR21 was collected from the mid-rift pluton near the southern end of TYC and yields widespread single-grain ages between 38.74 ± 0.49 Ma and 22.57 ± 0.29 Ma (mean age of 28.04 ± 0.36 Ma). Sample 19AL09 was collected from the southeast flank of the TYC rift proximal to the mapped location of the great counter thrust system and Kailas Conglomerate, yielding widespread single-grain ages between 38.71 ± 0.51 Ma and 12.00 ± 0.17 Ma (mean age of 26.10 ± 0.34 Ma). Sample 19AR23 was the only sample falling into the group one age range that was collected north of Gangdese Range latitudes (~30.16°N) and yields single-grain ages between 28.11 ± 0.36 Ma and 20.85 ± 0.28 Ma with a mean age of 24.56 ± 0.31 Ma. Age-elevation relationships for sample transects suggest complex cooling histories, with some samples generating well constrained intra-sample age ranges spanning as little as ~1.98 Myr, whereas others span as much as ~26.7 Myr within a single sample.

Group two: eight samples include 19AR19, 19AR20, 19KS32, 19KS33, 19KS34, 19AL12, 13AL13, and 19AL14 with mean ages falling between ~59.3-45.5 Ma. Samples 19AR19 and 19AR20 were collected from two ~6 m tall east facing fault scarps located ~5-7 km southeast of Duozebu. Samples 19AL12-14 were collected ~15 km and ~10 km southwest of Xuru Co lake along the western flank of TYC. Finally, 19KS32-34 constitute the farthest north transect in this study and were collected ~5 km northeast of Xuru Co lake where the normal fault bounding the west flank of TYC bends abruptly from approximately N-S striking to E-W striking. Each of these samples produced significantly older mean ages than Group two samples and widespread intra-sample age variability. Age-elevation relationships for sample transects suggest prolonged cooling histories, with all samples producing broad intra-sample age ranges spanning more than 8 Myr and up to 28.5 Myr.

Group three: five samples include 19AR22, 19AR24, 19AR25, 19AR26, and 19AR27 with mean ages falling between ~8.98-4.72 Ma. Samples 19AR22 and 19AR24 were collected along a footwall transect from the west side of TYC just southwest of Xuru Co lake and yield mean ages of 4.72 ± 0.06 Ma and 8.98 ± 0.12 Ma. Sample 19AR22 which produced the youngest mean age of all samples was collected from exposed footwall granodiorite along an apparently active basin-bounding normal fault, with biotite chloritization within the sample potentially related to hydrothermal alteration. Samples 19AR25-27 were collected from the east and north faces of Duozebu and yield well-constrained single-grain ages between 10.62 ± 0.13 Ma and 7.58 ± 0.09 Ma and mean ages of 8.11 ± 0.10 Ma, 8.13 ± 0.10 Ma, and 8.83 ± 0.11 Ma, respectively. Age-elevation relationships for sample transects suggest rapid exhumation and cooling, with all samples producing well constrained intra-sample age ranges less than ~3.7 Myr.

Gangdese Rifts Eighty-five single-grain ZHe analyses were completed for seventeen samples from three Gangdese rifts located ~90 km (GR1, five samples), ~75 km (GR2, ten samples), and ~40 km (GR3, two samples) east of TYC. Gangdese rift samples yield mean ages between 27.98 ± 0.35 Ma and 15.65 ± 0.2 Ma (Fig. 8; Table S3). Mean ages show no clearly meaningful correlation with sample elevation, grain radius, or effective uranium (Table S3). One north-south oriented sample transect of five samples was collected along GR1 including 19AR04, 19AR05, 19AR06, 19AR07, and 19AR08 from south to north. Nine samples along three approximately east-west transects were collected from the east flank of GR2 including

19AR01, 19AR02, 19AR03, 19GR01, 19GR02, 19GR03, 19GR05, 19GR06, and 19GR07. One sample, 19AL20, was collected from the northwest flank of GR2. Finally, samples 19AL15 and 19AL18 were collected along a north-south transect in GR3.

Of the seventeen Gangdese rift samples, all except one sample (19AL20) yield Oligocene-early Miocene mean ages between ~28-15 Ma which align with group one samples from the TYC rift collected at latitudes where TYC crosscuts the Gangdese Range, and twelve of the Gangdese rift mean ages fall within the narrower age range of ~23-16 Ma (Fig. 8). Samples 19AR05 and 19AR06 were collected from granodiorites near the contact with the basal Kailas Formation and yield the oldest mean ages of 27.98 ± 0.35 and 24.87 ± 0.32, respectively. Sample 19AL20 was the farthest north Gangdese rift sample, collected nearest to the northern extent of the Gangdese Range, and yields an older Paleocene-Eocene mean age of 44.68 ± 0.53, aligning with group three age ranges for samples from the TYC rift. Age-elevation relationships for sample transects suggest monotonic cooling for some samples and complex cooling histories for others, with some Gangdese rift samples generating well constrained intra-sample age ranges spanning as little as ~1.23 Myr, whereas others span up to ~17.7 Myr within a single sample. Sample transects suggest average exhumation rates of ~0.1 km/Myr for GR1 and ~0.2 km/Myr for GR2.

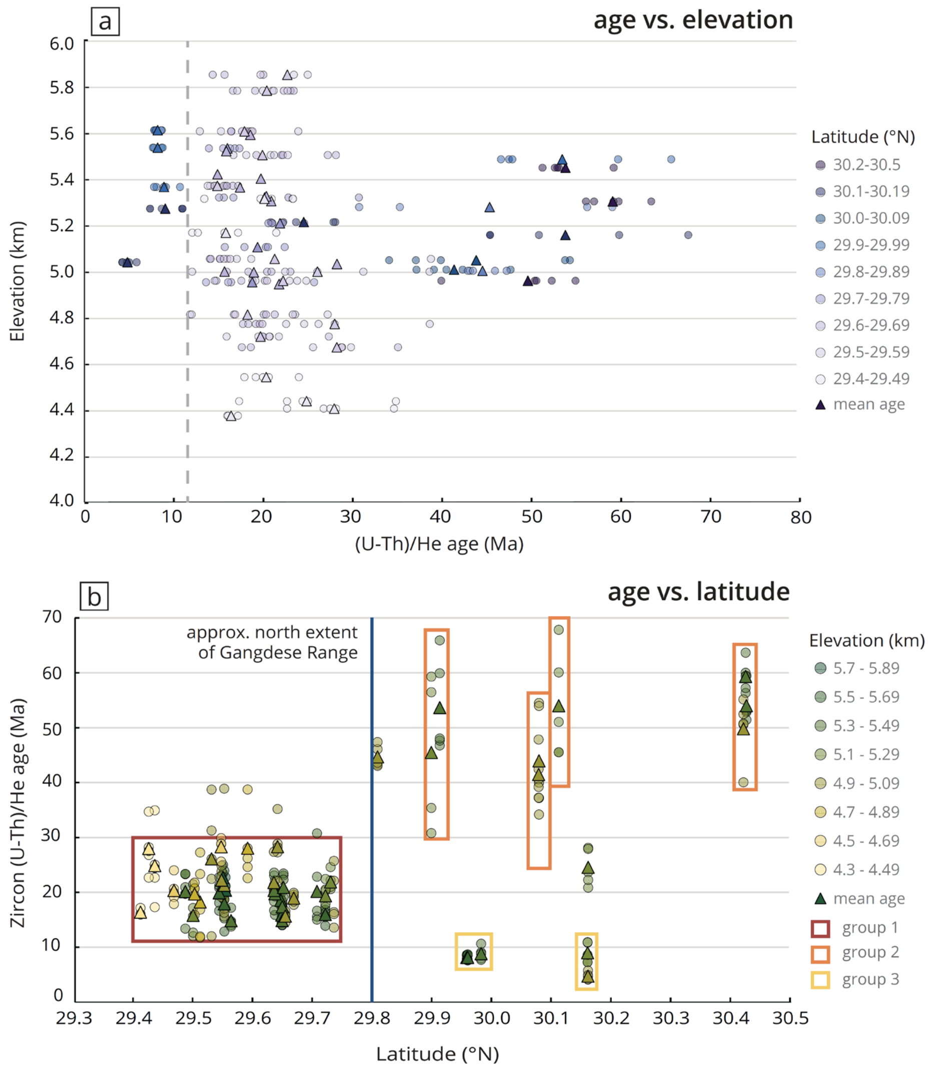

Figure 8. (a) ZHe age plotted against elevation; triangles are mean ages for each sample. Color gradient shows variation in sample latitude (darker colors = higher latitudes). Samples show no correlation between age and elevation. Note samples younger than ~12 Ma (gray dashed line) produce well constrained ages suggesting rapid exhumation, whereas samples older than ~12 Ma produce broader intra-sample age variability. (b) ZHe age as a function of sample latitude, with strong correlation. Color gradient shows variation in sample elevation (darker colors = higher elevations). Samples collected at Gangdese latitudes (group 1) exhibit mean ages clustered between ~22-15 Ma, whereas samples north of the northern extent of the Gangdese Range (~29.8°N) exhibit both older Paleocene to Eocene (~59-45 Ma) ages (group 2) and younger late Miocene to Pliocene (~9-4 Ma) ages (group 3). The wide intra-sample age variability for individual samples in group 2 may indicate a greater length of time spent at depth in the ZHe partial retention zone. Color Gradients for plots were selected using inclusive color guidelines (Crameri, 2018; Crameri et al., 2020).

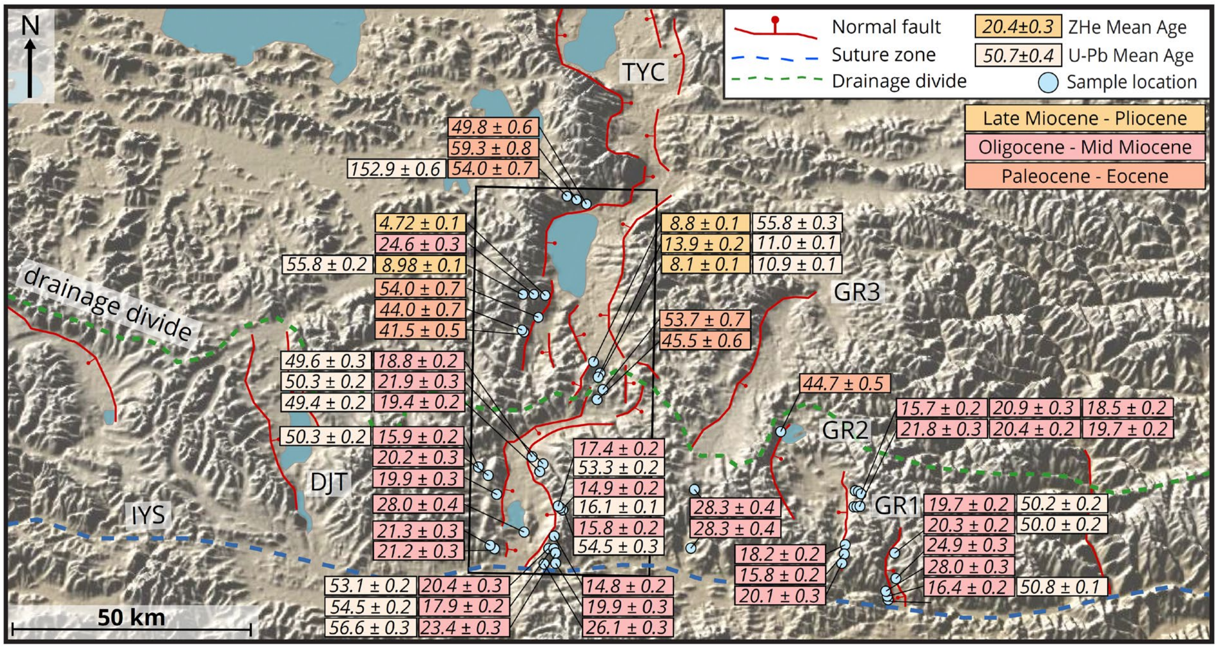

Figure 9. Digital elevation model of the southern TYC rift showing 49 ZHe mean ages and 18 U-Pb weighted mean ages for samples from the Tangra Yumco (TYC) rift and nearby Gangdese rifts (GR1, GR2, GR3) which crosscut the high topography of the Gangdese Range. ZHe ages are color coded: orange = Paleocene to Eocene; red = Oligocene to mid-Miocene; yellow = late Miocene to Pliocene. The black box shows the extent of the geologic map (Fig. 4). The green dashed line shows the location of the Gangdese drainage divide marking the high crest of the Gangdese Range. Blue dashed lines indicate suture zones; IYS = Indus-Yarlung suture. DJT = Daijaimang Tso rift (e.g., Burke et al., 2021). Normal fault traces from geologic mapping and HimaTibet database (Styron et al. 2010). Topography from GeoMapApp (VE = 4).

HeFTy Thermal Model Inputs and Results

HeFTy inverse modeling for each of eighteen samples from southern TYC was completed using input parameters for the median grain from each sample (i.e., single-grain models for each sample). Model inputs include the uncorrected age and corresponding error, grain radius, and measured concentrations of U and Th for each grain. Model calibrations from Guenthner (2013) for zircon and helium diffusion kinetics or stopping distances from Ketcham et al. (2011) were selected. The following criteria were used to define the searchable space for t-T paths during model runs:

1. Paths for samples with no U-Pb results began above ZHe closure temperature (>200°C) with initial timing left unconstrained (100-0 Ma) to allow broad exploration of the t-T space.
2. Zircon U-Pb weighted mean ages indicate temperatures >900°C from ~59-49 Ma.
3. ZHe ages reflect cooling through 200-140°C from ~60-4 Ma. Note that model inputs for individual grains force t-T paths to pass through a specified point as defined by the ZHe model.
4. Paths end at the model surface (20-0°C) at present day (0 Ma).

The t-T histories resolved by HeFTy are shown as a series of good (pink) and acceptable (green) t-T paths and a single best-fit path (black) from n = 50,000 model runs (Fig. 10). To determine spatial trends in HeFTy predicted thermal histories, it is easiest to compare the farthest south and farthest north samples that have been reset. Looking at trends and clusters within the t-T paths in Figure 10, each sample likely experienced a multi-phase cooling history, with a likely initial phase of slower cooling followed by one or more phases of rapid cooling. The onset of rapid cooling in the southern-most sample (19AL06) has the greatest density of paths between ~22 and 18 Ma, whereas in the northern-most sample (19AR24) the onset of rapid cooling is much younger, falling between ~12 and 8 Ma (Fig. 10). These results support observations that the onset of rapid cooling youngs to the north, which broadly agrees with the ZHe results from this and previous studies (e.g., Styron et al 2015).

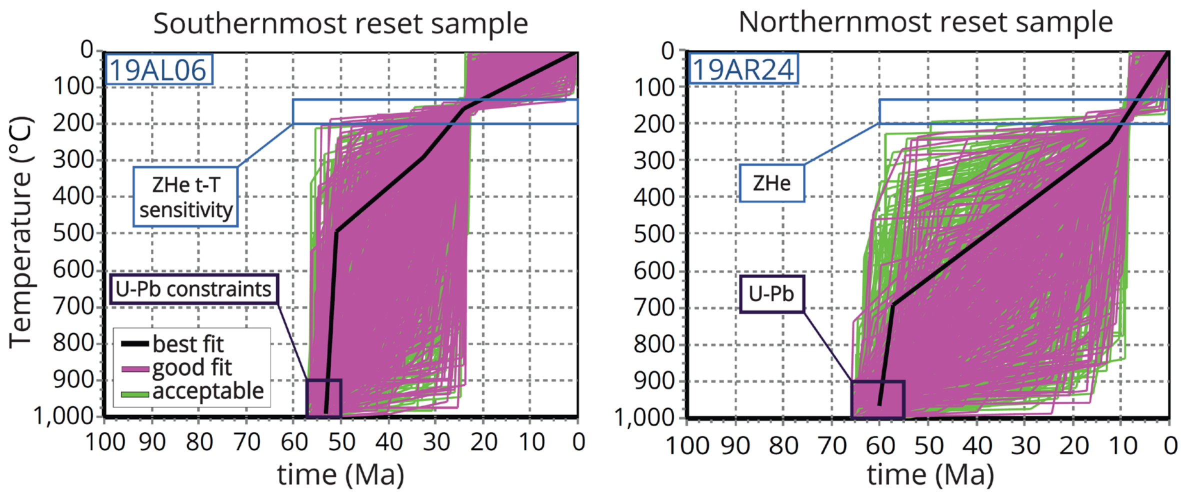

Figure 10. HeFTy models for the southern-most and northern-most reset samples from the TYC rift showing best fit (black), good fit (pink), and acceptable fit (green) paths. Model paths (n= 50,000) initiate within the dark blue boxes representing time-Temperature constraints from U-Pb dating of samples 19AL06 (>900°C between 58-50 Ma) and 19AR24 (>900°C between 65-55 Ma). Paths end at the surface (20–0°C) at present day (0 Ma) and are dominantly constrained by ZHe t-T sensitivities (light blue boxes) that are established through model inputs including the age and diffusion parameters (e.g., grain radius) specific to the median grain for each sample. Thus, the light blue boxes are a visual representation of model input parameters rather than an additional constraint box in the model space. ZHe HeFTy model results for all samples are available in supplementary material Figure S4.

Discussion

Kinematic History of the Tangra Yumco Rift

Structural results from TYC indicating north-northeast directed oblique sinistral normal slip are consistent with field observations from previous studies in the northern (Wolff et al., 2019) and southern (Wolff et al., 2023) TYC rift, and broader plateau-scale observations of Tibetan rift orientation and kinematics (e.g., Kapp & Guynn, 2004). Near the southern extent of the TYC rift, we observe Xigaze forearc strata faulted onto the Kailas Formation, and Kailas Formation strata faulted onto rocks of the Gangdese batholith along two moderately south-dipping, top-to-the north reverse faults (Fig. 4). The faults dip ~64° to the south and exhibit slickenlines consistent with top-to-the-northeast oblique sense of motion. We interpret these faults as splays of the GCT, as their geometry and kinematics are consistent with regional interpretations and recent work from the Dajiamang Tso rift which crosscuts the IYS just 50 km west of TYC (Burke et al., 2021). Although northern and southern TYC are bounded by dominantly high-angle normal faults with minimal field evidence for low-angle faulting (Wolff et al., 2019, 2023; this study), satellite imagery of unmapped and thus far inaccessible portions of central TYC appear to reveal footwall mylonite fabrics, hanging wall scarps, and synthetic graben structures which may indicate the presence of active low-angle faulting at depth. This observation may be consistent with fault models suggesting high angle normal faults are likely to sole into a master rift-bounding fault at depth (e.g., Kapp et al., 2008). Additional similarities of the southern TYC rift to the Lunggar and Yadong Gulu rifts include the abandonment of rift bounding structures in favor of slip along a basinward-stepping series of high-angle normal faults, and the apparent presence of a young (ca. 8 Ma) intra-basin topographic high (Duozebu, ~6,429m).

The oldest igneous U-Pb mean age in this study from sample 19KS34 (152.9 ± 0.6 Ma) comes from a hornblende- and biotite-poor, pink-white granite collected just north of Xuru Co lake where the main fault bounding the west side of the TYC rift curves sharply from a N-S strike orientation along the western shore of Xuru Co lake to a nearly E-W oriented fault strike along the north shore of the lake. We interpret this age to reflect rare but previously documented igneous rock crystallization at ~150 Ma within 0-150 km distances from the IYS, likely related to Gangdese Range magmatism which was active from at least ca. 150-40 Ma (Lee et al., 2009), though we note significantly higher abundances of ages between ca. 140-120 Ma are typically reported for the northern Lhasa terrane (e.g., Orme et al., 2015). The early-Miocene U-Pb weighted mean age for sample 19AR11 (16.1 ± 0.1 Ma), and middle to late-Miocene U-Pb weighted mean ages for samples 19AR25 and 19AR26 (10.9 ± 0.1 Ma and 11.0 ± 0.1 Ma) are likely related to their collection from syn-extensional igneous deposits. Sample 19AR11 is from a ~15-m-wide E-W opening porphyritic andesite dike yielding three age domains, potentially due to inheritance or incorporation of older zircon crystals from the host rock. Samples 19AR25 and 19AR26 were collected from the east face of Duozebu, a prominent intra-basin high (>6,500 m) within the central portion of the southern TYC rift. Sample 19AR25 was collected from a dark gray, porphyritic andesite to dacite intruding a cataclasite breccia, and sample 19AR26 was collected from a phaneritic diorite deposit just ~0.3 km northeast of sample 19AR25. U-Pb results for the E-W opening synextensional dike (19AR11, ~16.1 ± 0.1 Ma) are consistent (± 2 Ma) with dating of extensional dikes near the Daggyai Tso graben (~18 Ma, Williams et al., 2001) located ~75 km west of sample 19AR11, as well as biotite 40Ar/39Ar age estimates from the Lopu Kangri rift (~16 Ma, Sanchez et al., 2013; Laskowski et al., 2017) and Thakkhola graben (~14 Ma, Murphy et al., 2010) that have been used to infer a minimum age of east–west extension onset in southern Tibet (e.g., Yin & Harrison, 2000; Burke et al., 2021). Therefore, we interpret the age of 16.1 ± 0.1 Ma to reflect a minimum age of onset for E-W extension in southern TYC, with continued and likely rapid rift exhumation through ~11 Ma reflected by crystallization of syn-extensional intrusive igneous bodies in southern TYC.

Results from ZHe dating correlate strongly with sample latitude (Fig. 8b, Fig. 9). ZHe ages for samples from Gangdese latitudes in the southern map area fall between ~28 Ma-16 Ma and cluster strongly around ~21 Ma, whereas samples north of the Gangdese Range produced both younger (13-4 Ma) and older (66-45 Ma) ages. We interpret Oligocene to early-Miocene ZHe ages from Gangdese latitudes as reflecting a distinct exhumation event prior to TYC rift initiation, middle to late-Miocene ZHe ages to reflect samples that have been reset due to rift-related exhumation, and Paleocene-Eocene ZHe ages to reflect partially reset samples from portions of the TYC rift that have experienced insufficient rift exhumation for samples to be fully reset (Fig. 4, 9). Observed widespread intra-sample ages variability in the partially reset Paleocene-Eocene samples could be explained by structural controls related to sample location, with some samples collected along minor fault scarps or E-W striking portions of major fault scarps. Samples 19KS32-34 were collected in a portion of TYC where the main rift bounding fault curves from a N-S strike orientation to nearly E-W orientation and may be a region where slip is preferentially dominated by strike-slip rather than dip-slip motion. Samples 19AR19 and 19AR20 were collected form portions of the rift where fault segments are relatively young, small, and appear not be linked with one another, potentially causing greater partitioning of E-W extensional deformation across multiple fault segments leading to lesser magnitudes of extension than in areas of TYC where E-W extension is concentrated along more well-developed, longer, and more interconnected fault segments. Individual samples exhibiting a large spread or variability in ZHe age may indicate a longer time spent in the ZHe partial retention zone (PRZ) due to slower cooling and exhumation rates along these fault segments.

Based on kinematic observations from the field, normal fault patterns from geologic mapping, U-Pb weighted mean ages, and spatial trends in ZHe ages from this and previous studies, we interpret the best fit kinematic model to be the segment linkage model. This model predicts similar patterns of fault displacement to what is observed in the TYC rift, with complex distributions in the age of extension onset potentially related to variations in the timing and rates of exhumation along different fault segments. An earlier onset of extension, higher magnitudes of extension, and greater exhumation rates in the southern portion of the TYC rift could be attributed to most E-W extension being accommodated along a single larger fault segment consisting of linked fault segments rather than E-W extension being partitioned across several smaller or un-linked fault segments, which may be operating in the central and northern portions of the TYC rift. Additionally, the timing of onset for rapid exhumation due to faulting is variable across sample transects from southern TYC, which may also be best explained by the segment linkage fault growth model. An alternate explanation is that the faults bounding the TYC rift may have evolved due to some force causing the overall fault displacement to increase in rate and magnitude from south to north. However, this south to north sweep is not explicitly necessary to explain our results, as variability in the timing and rates of exhumation and partitioning of slip across multiple fault segments could explain this independently. Thermal history models reveal multi-stage cooling histories for footwall rocks in southern TYC, with the timing of rapid exhumation for each sample indicated by the break in slope. The t-T paths for the farthest south reset sample (19AL06) indicates rapid exhumation beginning at around ~13 Ma, whereas the model for the farthest north reset sample (19AR24) indicates rapid exhumation at around ~8 Ma. If models for samples between 19AL06 and 19AR24 indicate a smooth northward sweep in the onset of rapid exhumation, then perhaps there is a major tectonic influence on the northward propagation of accelerated rifting during late Miocene-Pliocene time. If the models indicate inconsistencies or irregularities in the onset of rapid exhumation from south to north, then it is likely the segment linkage model can better explain the spatial trend in the onset of rapid exhumation.

Exhumation History of South-Central Tibet

Post-Collisional Deformation Along the Gangdese Thrust and Great Counter Thrust

ZHe ages from latitudes where the TYC rift crosscuts the Gangdese Range (Group A) generated mean cooling ages between ca. 28-15 Ma, with all but one age clustering between ~22-15 Ma. These ages are older than reset rift footwall samples north of the Gangdese Range, suggesting a different structural mechanism for their cooling. The oldest mean age in this study (28.04 ± 0.36 Ma) from sample 19AR21 was calculated from relatively widespread single-grain ages from 22.57 ± 0.29 Ma to 38.74 ± 0.49 Ma. This age could reflect exhumation in the hanging wall of the north dipping Gangdese Thrust (GT) which we infer to be located at depth in this region, with previous timing estimates suggesting the southernmost splay of the GT became active by ~27 Ma (Yin et al., 1994; Laskowski et al., 2018). The widespread single-grain cooling ages within sample 19AR21 could potentially reflect progressive cooling via exhumation along the GT in this region, and potentially even an older splay of the GT, beginning as early as ca. 38 Ma and continuing to at least ca. 22 Ma. Sample 19AR21 was collected from the mid-rift pluton at the southern end of TYC (Fig. 4). With a mean age of ~28 Ma, it is likely the mid-rift pluton is a portion of the Gangdese Range which became isolated within the basin as the TYC rift crosscut and dissected the Gangdese Range during Miocene time. Conversely, the young late Miocene ages from the east and north faces of Duozebu likely reflect rift exhumation at ~11 Ma, suggesting Duozebu represents a rift-related intra-basin high rather than an isolated portion of the Gangdese Range, similar to documented intra-basin highs in other Tibetan rifts (e.g., central

Lunggar rift, Kapp et al., 2008). The southernmost sample transect from TYC (19AL06, 19AL07, 19AL08) also produced ZHe mean cooling ages between ca. 23-18 Ma, consistent with previous estimates for the timing of activity along the south-dipping Great Counter Thrust (GCT) beginning as early as 23 Ma and continuing until ca. 18-13 Ma (Laskowski et al., 2018; Kapp & DeCelles, 2019). This range of ZHe ages overlaps timing estimates for deposition of the Kailas Formation in south-central Tibet beginning at ca. 21 Ma (DeCelles et al., 2011; Leary et al., 2016) and subsequent exhumation of the IYS and Kailas Formation at ca. 19-15 Ma (Carrapa et al., 2014). The timing of exhumation of the Indus-Yarlung Suture zone and Kailas Formation could be related to focused erosion along the GCT, Yarlung River establishment, and drainage reorganizations documented in the early Miocene (Carrapa et al., 2014; Lang & Huntington, 2014). Therefore, we interpret that the Gangdese Range has experienced at least semi-continuous exhumation during the time in which it has been construed as located in the hanging wall of the GT (Yin et al., 1994), in the footwall of the GCT, and/or in the hanging wall of a north-dipping normal fault which possibly created accommodation space for deposition of the Kailas Formation (DeCelles et al., 2011; Wang et al., 2015; Leary et al., 2016; Laskowski et al., 2018).

Timing of Exhumation and Cooling Along Tibetan Rifts and Gangdese Rifts Potential differences in the structural style, timing, and rates of extension between Tibetan rifts and Gangdese rifts have been investigated by few studies (Yin, 2000; Burke et al., 2021). Here we compare kinematic interpretations based on field observations and thermochronologic data from the TYC rift with results from three nearby Gangdese rifts (GR1, GR2, and GR3). Through the comparison of a Tibetan rift and Gangdese rifts, we investigate the potential for a shared mechanism of origin as opposed to rift initiation related to discrete structural processes or tectonic events. Additionally, we establish potential links between rifting and the evolution of the Gangdese drainage divide. Samples from TYC which reflect rift-related exhumation and cooling rather than pre-extensional cooling include those from latitudes north of the northern extent of the Gangdese Range (~29.8°, Fig. 8b) consisting of ZHe cooling ages in Group two (~59-45 Ma, 8 samples) and Group three (~9-4 Ma, 5 samples). Group two is comprised of Paleocene-Eocene ages which likely reflect un-reset or partially reset samples collected from fault segments that have experienced lesser magnitudes of extension due to structural controls, whereas Group three contains late Miocene-Pliocene ages that are interpreted to reflect the timing of recent rift-related exhumation in the southern TYC rift between 9-4 Ma (see section 5.1, Fig. 4, 9). We interpret E-W extension in the southern TYC rift to have initiated by ~16 Ma continuing until at least 4 Ma, whereas E-W extension across the Gangdese rifts appears to have begun by ~28 Ma and continued until ~16 Ma.

Previous studies documented spatiotemporal trends of ZHe ages indicating an older in the south and younger in the north timing of extension onset, with thermal models indicating multi-stage cooling histories with a northward younging acceleration of extension rates along the TYC rift during late Miocene to Pliocene time (~13-5 Ma; Fig. 11; Wolff et al., 2019). This observed south to north acceleration of exhumation rates through time has been previously attributed to the northward propagation of underthrusting Indian lithosphere beneath south-central Tibet (DeCelles et al., 2002; Kapp & Guynn, 2004; Styron et al., 2015; Wolff et al., 2019, 2023). However, we document significantly more complex spatial relationships for the timing of exhumation in southern TYC (Fig. 11), which could alternatively reflect variable timing, rates, and magnitudes of extension along different fault segments. This may also relate to field observations and mapping results revealing greater horizontal displacement in the central TYC rift rather than northern or southern TYC, which may reflect a complex zone of interaction and linkage between fault segments. Furthermore, the presence of both high- and low-angle extensional structures across Tibet and their variabilities in fault length, magnitude, and strike orientation are suggestive of spatial variability in the mechanical and/or thermal properties of Tibetan lithosphere (e.g., Wolff et al., 2019; Bischoff & Flesch, 2018), or alternatively, that the stress field produced by oblique collision of India with Asia exerts a key control on Tibetan rift structure and kinematics (Kapp & Guynn, 2004). Advanced comparisons of rift kinematics across the Plateau and between Tibetan and Gangdese rifts may help discern which of these factors is likely to exert the most influence or control on the variable expression of continental rifting across the Plateau.

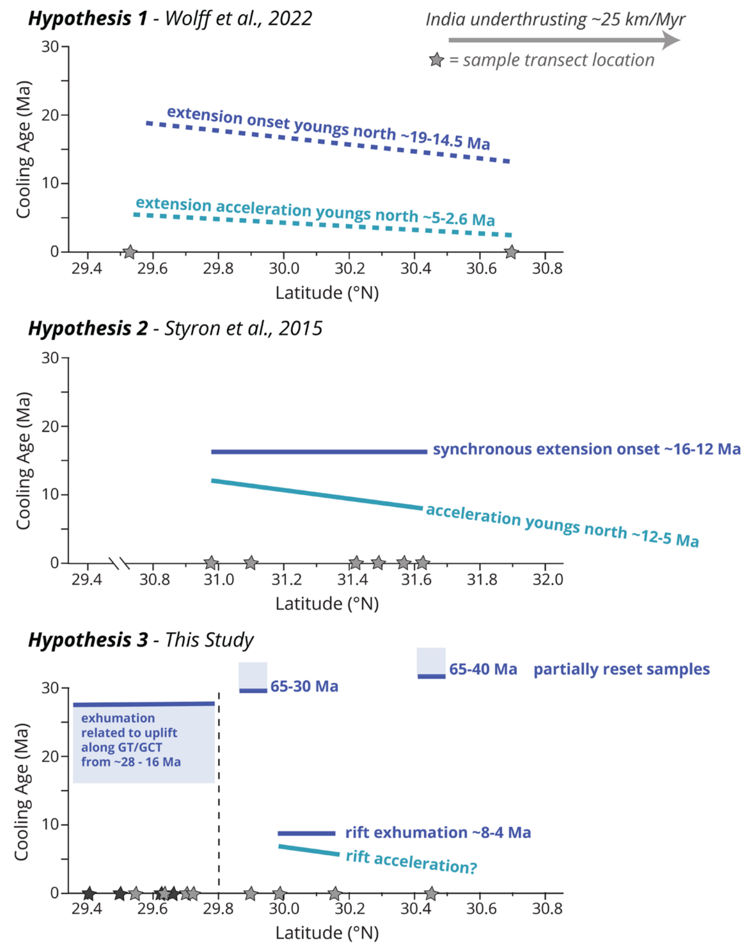

Figure 11. Tectonic hypotheses for extension in southern Tibet. Each hypothesis shows cooling age versus latitude to evaluate along-strike trends. Stars on x-axis represent sample transects. In hypothesis 1 after Wolff et al. (2023), both the timing of extension onset and rift acceleration in TYC young to the north at a rate which is consistent with underthrusting of the Indian plate (~25 km/Myr). Hypothesis 2 after the work of Styron et al. (2015) in the Lunggar rift presumes synchronous extension onset followed by a northward sweeping acceleration of extension rates. This study proposes hypothesis 3 as the best fit model based on ZHe results from this study, relating the timing of exhumation at Gangdese latitudes to contraction and uplift along the GT and/or GCT, whereas samples north of the Gangdese Range reflect the true rift exhumation signal and reveal the timing of extension onset in south TYC. Each tectonic model is consistent with India underthrusting as a driver of extension but reflective of different kinematic models. Hypothesis 1 is most consistent with model (b) tectonically influenced tip propagation, hypothesis 2 which predicts synchronous extension onset is most consistent with model (d) constant length. Based on our data for hypothesis 3, we interpret model (c) fault segment linkage as the best fit kinematic model for south TYC due to the observed variability in the age of extension onset along-strike, with this model also predicting similar map patterns of fault displacement to structural observations from South TYC.

Based on distinctions in the timing of rift initiation, rates and magnitudes of extension, and fault growth model interpretations, we suggest the Gangdese rifts and Tibetan rifts initiated and evolved through time in response to distinct tectonic events or structural controls. For sample transects from Gangdese rifts, the timing of exhumation is nearly coeval along all three sample transects from GR2 within the resolution of the thermochronology data (between ~21.8 ± 0.3 Ma to 15.7 ± 0.2 Ma for each transect). Our interpretation is that the Gangdese rift data are more closely aligned with the constant fault-length kinematic model. This model, although represented as a distinct end member, may be the most accurate within the spatial scale of this study as rifting in the Gangdese Range likely relates to the timing of exhumation during Gangdese Range uplift from around ~21-16 Ma, with continued exhumation along Gangdese rifts simply balancing continued uplift of the Gangdese Range (e.g., Sundell et al., 2021). The Gangdese rifts likely initiated at similar to present-day lengths due to a "block" uplift of the entire Gangdese Range and accumulated near present-day magnitudes of extension by ca. 16 Ma, in broad agreement with previous studies investigating the timing and structural morphology of Gangdese rifts (Burke et al., 2021). It is likely that minimal additional rift exhumation has occurred or is driven by subsequent tectonic processes like India underthrusting which conversely, has been interpreted as a driving force for northward sweeping accelerated extension in Tibetan rifts.

Implications for the Dynamics of East-West Extension in Southern Tibet Many models have been proposed to explain the dynamics or driving forces of extension in Tibet, with each model characterized by testable predictions for the spatial and temporal distributions of the age of extension onset, rates and magnitudes of extension, fault orientations, and relation to magmatism. Here we compare our data and observations from TYC and Gangdese rifts to the predictions of four dynamic models: (a) removal of dense lithosphere, (b) lithospheric weakening, (c) decreasing horizontal collisional stress, and (d) increasing crustal thickness by underthrusting India (Fig. 12).

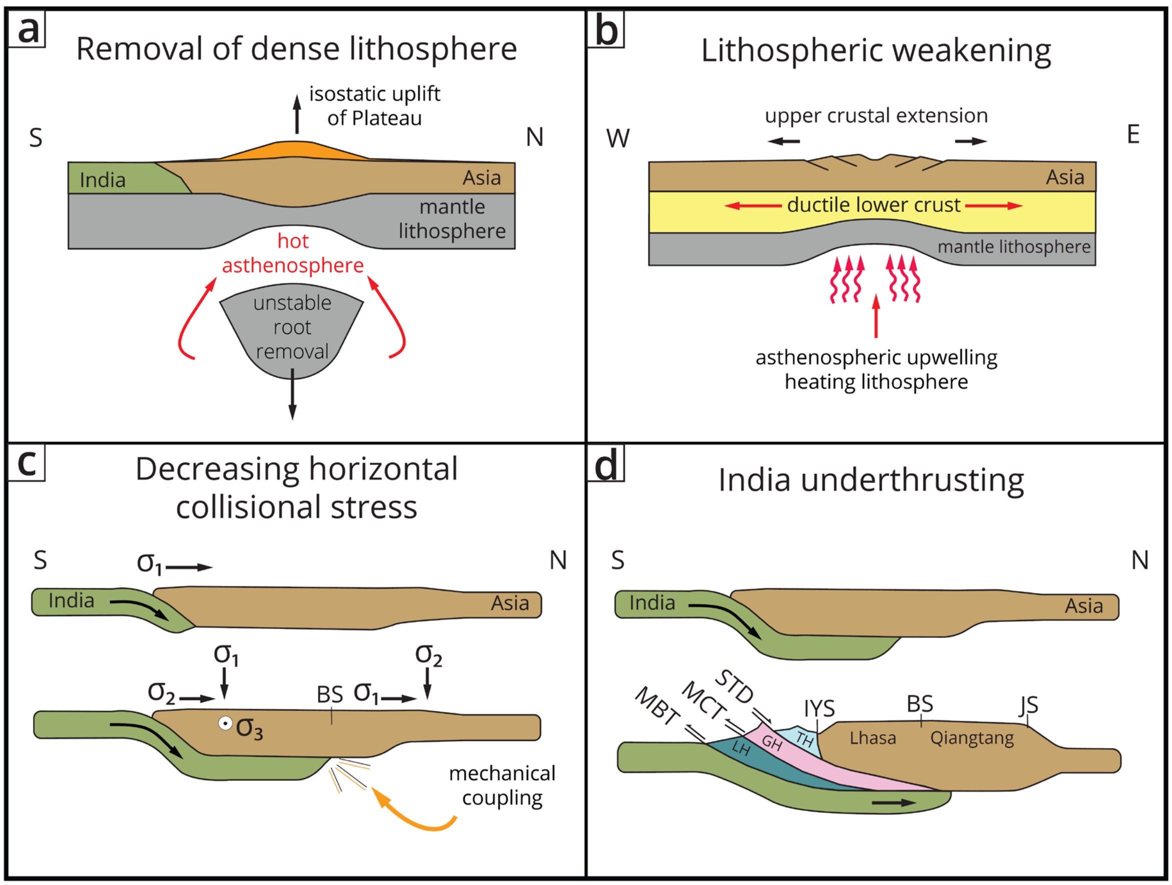

Figure 12. Dynamic models for extension of the Tibetan Plateau: (a) Removal of an unstable dense lithospheric root causing isostatic uplift followed by gravitational collapse, triggering synchronous extension across the plateau; (b) Thermal weakening of the lithosphere due to asthenospheric upwelling and heating; (c) Decreasing horizontal collisional stress through mechanical coupling of Asian and Indian lithosphere causing the maximum principal stress σ1 to rotate to vertical in southern Tibet; (d) Increasing crustal thickness by underthrusting Indian lithosphere beneath Asia to achieve a critical gravitational potential energy (GPE), leading to gravitational collapse of the plateau during Miocene time followed by a northward sweep in extension acceleration related to continued underthrusting of the Indian plate.

The results of this study suggest predictions of models (a), (b) and (c) cannot fully explain the observed spatial pattern and timing of rifting in southern Tibet, consistent with interpretations from previous studies which support the India underthrusting model as the best-fit dynamic model for Tangra Yumco and other rifts (Styron et al., 2015; Wolff et al., 2019, 2023). In this model, underthrusting of Indian lithosphere beneath Tibet thickens the crust to reach a critical gravitational potential energy (GPE), causing the maximum principal stress ($\sigma 1$) to rotate from horizontal to vertical and initiating E-W extension in southern Tibet (e.g., Yin, 2000; DeCelles et al., 2002; Kind et al., 2002; Tilmann et al., 2003; Kapp & Guynn, 2004; Styron et al., 2011, 2013, 2015; Sundell et al., 2013, 2021; Wolff et al., 2019, 2023). This model was initially suggested to follow synchronous extension onset across southern Tibet in middle to late-Miocene time due to a gravitational collapse of the thickened Plateau (Styron et al., 2015). However, this interpretation is inconsistent with later studies that show rifting began earlier and was diachronous across Tibet, with most graben systems initiating between 16 and 8 Ma (e.g., Laskowski et al. 2017; Wolff et al. 2019, 2023; Burke et al. 2021; Bian et al. 2022). Regardless of variabilities in the timing of extension onset, previous studies supporting the India underthrusting model find initially low rates and magnitudes of extension (~1mm/yr), followed by a northward sweeping acceleration of extension rates (~1.5-5mm/yr) during the late Miocene-Pliocene (~12-5 Ma) tracking the leading edge of underthrusting Indian lithosphere which also cannot be explained by the other models (e.g., Styron et al., 2015; Wolff et al., 2023). Active rifting can be explained by the continued insertion of Indian crust beneath Tibet which further increases Plateau crustal thickness, driving coeval rifting to balance the GPE of the plateau (e.g., Sundell et al., 2021). Rifts in southern Tibet would experience a longer period of accelerated extension than those in central Tibet and therefore have stronger morphological expressions and greater magnitudes of extension, with normal fault orientations in both southern and northern Tibet following a pattern suggesting their common mechanism of origin (Kapp & Guynn, 2004). Finally, documented bimodal volcanism (Williams et al., 2004; Zhu et al., 2012) and seismic studies (e.g., Owens & Zandt, 1997; Nábělek et al., 2009) provide additional supporting evidence for the India underthrusting model independent from reported thermochronologic data.

The 245 ZHe ages produced in this study allow us to further ground-truth dynamic model predictions for the TYC rift. Our results indicate rifting in southern TYC initiated in Miocene time by a minimum of ~16 Ma and has continued until at least ~4 Ma, with field observations suggesting rifting is active and ongoing. We document complex spatial relationships for the onset of exhumation, with ages at Gangdese Range latitudes likely reflecting a more protracted cooling history, and ages north of the Gangdese Range suggesting variable timing, rates, and magnitudes of extension across multiple fault segments along the TYC rift. It is unclear whether fault processes such as segment linkage or the stress field produced by oblique collision and underthrusting of India (e.g., Kapp & Guynn, 2004) exert a greater control on our results and thus on Tibetan rift structure, kinematics, and dynamics. Advanced comparisons of rift kinematics and dynamics across the Plateau and between Tibetan and Gangdese rifts through thermal and kinematic modeling may help discern which of these factors is likely to exert the most influence on the expression and evolution of continental rifts across the Plateau.

Development of the Gangdese Drainage Divide This study reveals ZHe ages between ca. 28 Ma and ca. 15 Ma for all samples collected at latitudes between ~29.4°N-29.8°N, which we interpret to reflect enhanced exhumation and surface uplift related to the growth of the Gangdese

Range. These ages overlap existing timing estimates for surface uplift and exhumation along the Gangdese Thrust at ca. 23 Ma continuing as late as 18-13 Ma in this region (Laskowski et al., 2018; Kapp & DeCelles, 2019; Taylor et al., 2021). The ZHe ages also overlap timing estimates for deposition of the Kailas Formation between ca. 26-24 Ma in the Mt. Kailas region to the west (~81°E), ca. 25–23 Ma north of Lazi (87.8°E) in south-central Tibet, ca. 23-22 Ma near Dazhuka (~90°E), and as late at 18 Ma near Lhasa City to the east (~92°E; Leary et al., 2016). The timing of Kailas Formation deposition is potentially linked to development of a short-lived extensional basin, fluvial drainage reorganization, and the establishment of the modern Yarlung River during early Miocene time (DeCelles et al. 2011; Wang et al. 2013; Carrapa et al. 2014; Lang & Huntington, 2014; Leary et al. 2016; Taylor et al., 2021; Ai et al., 2022).

ZHe results in this study reflecting timing of exhumation and surface uplift in the Gangdese Range concurrent with Kailas Formation deposition are consistent with previous work and may provide additional constraints on the timing of formation of the Gangdese drainage divide and modern day Yarlung River drainage networks. We interpret ZHe results as indicating formation of the drainage divide at or near its modern location along the crest of the Gangdese Range (Fig. 2) and onset of internal drainage of the Tibetan plateau as early as ca. 28 Ma. We further suggest the timing of flow reversal of the Yarlung River from paleo-westward flow to its present-day eastward course can be constrained to between ~28-18 Ma (e.g., Zhang et al., 2012; Carrapa et al. 2014; Taylor et al., 2021). Coeval formation of Gangdese rifts during uplift of the Gangdese Range likely exerted some influence on drainage network patterns, but we posit that the onset of rifting in the Gangdese Range is not required to explain the timing of development of the drainage divide. Initiation of upper crustal extension along Tibetan rifts which crosscut the Lhasa terrane has been constrained to ca. 18-15 Ma (e.g., Li et al., 2015; Laskowski et al., 2018), which is ~10-13 Myr after the potential earliest timing of drainage divide establishment. Thus, we infer that Tibetan rifting is also not a requirement or constraint for the initial formation of the drainage divide, with normal faults in southern TYC apparently crosscutting features related to uplift of the Gangdese Range such as the GT and GCT (e.g., Wolff et al., 2023). It is likely that rifting and strike slip faulting in central Tibet has contributed to subsequent fluvial reorganization through the diversion of river networks and relocation of lake centers, with a hypothetical southward migration of the boundary between internal and external drainage of the Plateau occurring since early Miocene time (Han et al., 2019; Taylor et al., 2021). It is possible that Gangdese rifting works to balance continued surface uplift and exhumation driven by duplexing beneath the Gangdese Range, which could in turn cause the location of the drainage divide along the Gangdese crest to migrate from a more northward location during Oligocene to early-Miocene time to a more southward location by late-Miocene time, or in other words, the crest of the Gangdese Range may have shifted southwards through time due to continued surface uplift and exhumation accommodated by Gangdese rifts. The Gangdese Culmination Model (Laskowski et al., 2018) hypothesizes continued uplift and exhumation of the Gangdese Range through kinematically linked motion along the GCT and GT and is consistent with our data and interpretations. The Gangdese Culmination Model may be required to explain the structural feasibility of continued uplift of Gangdese Range topography and existence of the drainage divide in relation to ongoing contraction due to India-Asia collision (Taylor et al., 2021). It is possible that mantle delamination, lithospheric dripping, and other deep crustal or mantle processes act concurrently to the already complex interplay between surface uplift, exhumation, erosion, sedimentation, and climate to drive topographic change and enhanced basin subsidence in southern and central Tibet (Sobel et al., 2003; Gao et al., 2013; Yin & Taylor, 2011; Bischoff & Flesch, 2018; Han et al., 2019; Kapp & DeCelles, 2019; Taylor et al., 2021).

Conclusions

Tibet offers a unique opportunity to study synconvergent extension related to continental collision and to better understand the mechanics of early-stage continental rift initiation and development through time, offering a detailed account of the behavior and morphological expression of young or "failed" continental rifts. The TYC rift is bounded by two NNE striking (~N10°E-N35°E) high-angle (~45-70°) active normal faults that alternate dominance along strike. Footwall granodiorites show pervasive northeast dipping foliation, with slip lineations and fault plane striations indicating northeast directed oblique sinistral-normal slip. Analysis of 32 samples collected across key structural relationships in the southern TYC rift yielded 14 weighted mean U-Pb ages between ~59-49 Ma and 245 single-grain ZHe ages, with mean ZHe ages falling between ~60-4 Ma. Analysis of 17 samples collected from Gangdese rifts located ~90 km (GR1, five samples), ~75 km (GR2, ten samples), and ~40 km (GR3, two samples) east of TYC yielded ~85 single-grain ZHe ages with mean ages between ~28-16 Ma. Spatial trends in ZHe data correlate strongly with sample latitude. Samples collected from Gangdese latitudes in southern TYC and Gangdese rifts show a concentration of Oligocene-early Miocene ages (~28-16 Ma), whereas TYC rift samples north of ~29.8° latitude generated both younger late Miocene-Pliocene ages (~8-4 Ma) and older Paleocene-Eocene ages (~60-48 Ma). We interpret the following: (1) Gangdese Range samples from TYC and Gangdese rifts likely reflect exhumation during contraction, uplift, and erosion along the GCT peaking at ~21-20 Ma, (2) ~8-4 Ma ages from TYC reflect extension timing along fault segments experiencing significant rift-related exhumation, and (3) ~60-48 Ma ages represent un-reset or partially reset samples from segments of the TYC rift that have experienced lesser magnitudes of rift exhumation. HeFTy thermal models indicate a two-stage cooling history with initial slow cooling followed by accelerated cooling rates in late Miocene-Pliocene time (~13-4 Ma), consistent with results from previous studies of TYC and other Tibetan rifts. We interpret the TYC rift evolved through fault segment linkage, with a northward sweeping acceleration of extension potentially related to underthrusting of the Indian plate beneath Tibet. This work contributes an unprecedented dataset for south-central Tibet including 18 U-Pb mean ages and ~240 single-grain ZHe ages from the southern TYC rift and neighboring Gangdese rifts and demonstrates the utility of low-temperature thermochronology methods to address major tectonic questions. Reported data and kinematic interpretations may be relevant to future studies investigating outstanding questions related to the early evolution of continental rifts. This study may also provide context for the investigation of extensional structures in other settings where synconvergent extension is documented, such as the North American Cordillera.

Acknowledgements

This work was funded by NSF Tectonics Awards to Dr. Andrew K. Laskowski (#1917685), Dr. Michael H. Taylor (#1917706), and Dr. Adam M. Forte (#1917695), and a GSA Graduate Student Research Grant award to PhD Candidate Aislin N. Reynolds. We thank Dr. Peter Reiners and Dr. Uttam Chowdhury at the ARHDL for ZHe sample analyses and staff of the Arizona LaserChron Center for U-Pb sample analyses and data interpretation.

Author Contributions

Aislin N. Reynolds: Conception of study, Investigation, Methodology, Funding acquisition, Writing-original draft. Andrew K. Laskowski: Conception of study, Investigation, Supervision, Funding acquisition, Writing-review and editing. Caden J. Howlett: Investigation, Writing-review and editing. Devon A. Orme: Methodology, Writing-review. Kurt E. Sundell: Investigation, Writing-review. Michael H. Taylor: Conception of study, Funding acquisition, Writing-review. Adam M. Forte: Conception of study, Funding acquisition, Writing-review. Fulong Cai: Permitting, Investigation. Guo Xudong: Investigation, Methodology. Ding Lin: Permitting, Methodology.

Data Availability

Data from this research are included in the supplementary material file as tables and figures. Data from this research will be posted on Zenodo upon manuscript acceptance. Provided spreadsheets to be published include location and lithology information for all samples (Table S1), igneous U-Pb data tables for all analyzed samples (Table S2), and zircon (U-Th)/He data tables for all analyzed samples (Table S3). Supplementary figures include a compilation of previous studies with published geo- and thermochronology data in the Tangra Yumco Rift region (Figure S1, data source: DOI:/10.1002/2017GC007217), weighted mean plots for all igneous zircon U-Pb analyses (Figure S2), plots of zircon (U-Th)/He data showing age as a function of grain size and age as a function of effective uranium (Figure S3), and HeFTy models (resulting thermal history paths and envelopes) for all samples (Figure S4). Geologic map was drafted over hill shade and slope maps generated in ArcGIS Pro, derived from Shuttle Radar

Topography Mission (SRTM) 1 Arc-Second Global Digital Elevation data (DOI:/10.5066/F7PR7TFT) and draped Landsat Legacy Global Land Survey (GLS) imagery (DOI:/10.5066/F7M32TQB).

References Cited

Ai, K., Zhang, K., Song, B., Shen, T., & Ji, J. (2022). Upper Oligocene–Lower Miocene Gangdese Conglomerate Along the Yarlung-Zangbo Suture Zone and its Implications for Palaeo-Yarlung-Zangbo Initiation. Front. Earth Sci. 10:808843. doi: 10.3389/feart.2022.808843

Aitchison, J.C., Davis, A.M., Zhu, B.D., & Luo, H. (2002). New constraints on the India-Asia collision: the Lower Miocene Gangrinboche conglomerates, Yarlung Tsangpo suture zone, SE Tibet. J. Asian Earth Sci., 21 (3), pp. 251-263. Doi:10.1016/S1367-9120(02)00037-8

Allmendinger, R.W. (1986). Tectonic development, southeastern border of the Puna Plateau, northwestern Argentine Andes. GSA Bulletin 1986;; 97 (9): 1070–1082. doi: https://doi.org/10.1130/0016-7606(1986)97<1070:TDSBOT>2.0.CO;2

An, W., Hu, X., Garzanti, E., BouDagher-Fadel, M.K., Wang, J., & Sun, G. (2014) Xigaze forearc basin revisited (South Tibet): Provenance changes and origin of the Xigaze Ophiolite. GSA Bulletin; 126 (11-12): 1595–1613. doi: https://doi.org/10.1130/B31020.1

Anders, M.H., & Schlische, R.W. (1994). Overlapping Faults, Intrabasin Highs, and the Growth of Normal Faults. The Journal of Geology, 102, 165 - 179. Doi:10.1086/629661

Armijo, R., Tapponnier, P., Mercier, J. L., & Han, T.L. (1986). Quaternary extension in southern Tibet: Field observations and tectonic implications, J. Geophys. Res., 91(B14), 13803–13872, doi:10.1029/JB091iB14p13803.

Ault, A.K., Gautheron, C., & King, G.E. (2019). Innovations in (U–Th)/He, fission track, and trapped charge thermochronometry with applications to earthquakes, weathering, surface-mantle connections, and the growth and decay of mountains. Tectonics, 38, 3705– 3739. https://doi.org/10.1029/2018TC005312

Avouac, J.P., & Tapponnier, P. (1993). Kinematic model of active deformation in central Asia. Geophysical Research Letters, 20(10), 895– 898. Doi:10.1029/93gl00128

Axen, G.J., Fletcher, J.M., Cowgill, E., Murphy, M., Kapp, P., MacMillan, I., Ramos-Velázquez, E., & Aranda-Gómez, J. (1999). Range-front fault scarps of the Sierra El Mayor, Baja California: Formed above an active low-angle normal fault?. Geology; 27 (3): 247–250. doi: https://doi.org/10.1130/0091-7613(1999)027<0247:RFFSOT>2.3.CO;2

Bian, S., Gong, J., Zuza, A.V., Yang, R., Chen, L., Ji, J., et al. (2022). Along-strike variation in the initiation timing of the north-trending rifts in southern Tibet as revealed from the Yadong-Gulu rift. Tectonics, 41, e2021TC007091. https://doi.org/10.1029/2021TC007091

Bischoff, S.H., & Flesch, L.M. (2018). Normal faulting and viscous buckling in the Tibetan Plateau induced by a weak lower crust. Nature Communications, 9, 4952. https://doi.org/10.1038/s41467-018-07312-9

Black, L.P., Kamo, S.L., Allen, C.M., Davis, D.W., Aleinikoff, J.N., Valley, J.W., & Foudoulis, C. (2004). Improved 206Pb/238U microprobe geochronology by the monitoring of a trace-element-related matrix effect; SHRIMP, ID–TIMS, ELA–ICP–MS and oxygen isotope documentation for a series of zircon standards. Chemical Geology, 205(1-2), 115-140. Doi: https://doi.org/10.1016/j.chemgeo.2004.01.003

Blisniuk, P., Hacker, B., Glodny, J. et al. Normal faulting in central Tibet since at least 13.5 Myr ago. Nature 412, 628–632 (2001). https://doi.org/10.1038/35088045

Braun, J. (2003). Pecube: A new finite-element code to solve the 3-D heat transport equation including the effects of a time-varying, finite amplitude surface topography. Computers and Geosciences, 29(6), 787–794. https://doi.org/10.1016/S0098-3004(03)00052-9

Braun, J., van der Beek, P., Valla, P., Robert, X., Herman, F., Glotzbach, C., et al. (2012). Quantifying rates of landscape evolution and tectonic processes by thermochronology and numerical modeling of crustal heat transport using PECUBE. Tectonophysics, 524–525(1), 1–28. https://doi.org/10.1016/j.tecto.2011.12.035

Brune, S., Kolawole, F., Olive, JA. *et al.* Geodynamics of continental rift initiation and evolution. *Nat Rev Earth Environ* (2023). https://doi.org/10.1038/s43017-023-00391-3

Buck, W.R. (1988). Flexural rotation of normal faults: Tectonics,v. 7, p. 959–973, doi:10.1029/TC007i005p00959.

Buck, W.R. (1991). Modes of continental lithospheric extension, J. Geophys. Res., 96, 20161, https://doi.org/10.1029/91JB01485.

Buck, W.R. (1993). Effect of lithospheric thickness on the formation of high- and low-angle normal faults. Geology; 21 (10): 933–936. doi: https://doi.org/10.1130/0091-7613(1993)021<0933:EOLTOT>2.3.CO;2

Burchfiel, B.C. & Royden, L.H. (1985). North-south extension within the convergent Himalayan region: Geology, v. 13, p. 679–682, doi:10.1130/0091-7613(1985)13<679:NEWTCH>2.0.CO;2.

Burchfiel, B.C., Chen, Z., Hodges, K.V., Liu, Y., Royden, L.H., Deng, C., & Jiene, X. (1992). The South Tibetan detachment system, Himalayan orogen: Extension contemporaneous with and parallel to shortening in a collisional mountain belt. Geological Society of America, Special Papers, 269, 1–41. https://doi.org/10.1130/SPE269-p1

Burg, J. P., Proust, F., Tapponnier, P., & Ming, C. G. (1983). Deformation phases and tectonic evolution of the Lhasa block (southern Tibet, China). Eclogae Geologicae Helvetiae, 76(3), 643-665.

Burke, W.B., Laskowski, A.K., Orme, D.A., Sundell, K.E., Taylor, M.H., Guo, X., & Ding, L. (2021). Record of Crustal Thickening and Synconvergent Extension from the Dajiamang Tso Rift, Southern Tibet. Geosciences, 11, 209. https://doi.org/10.3390/geosciences11050209

Carrapa, B., Orme, D.A., DeCelles, P.G., Kapp, P., Cosca, M.A., & Waldrip R. (2014). Miocene burial and exhumation of the India-Asia collision zone in southern Tibet: Response to slab dynamics and erosion. Geology; 42 (5): 443–446. doi: https://doi.org/10.1130/G35350.1

Chevalier, M.L., Tapponnier, P., van der Woerd, J., Leloup, P.H., Wang, S., Pan, J., et al. (2020). Late Quaternary extension rates across the northern half of the Yadong-Gulu rift: Implication for east-west extension in southern Tibet. Journal of Geophysical Research: Solid Earth, 125, e2019JB019106. https://doi.org/10.1029/2019JB019106

Cogan, M.J., Nelson, K.D., Kidd, W.S.F., & Wu, C., (1998), Shallow structure of the Yadong-Gulu rift, southern Tibet, from refraction analysis of Project INDEPTH common midpoint data, Tectonics, 17(1), 46– 61, doi:10.1029/97TC03025.

Coleman, M., & Hodges, K. (1995). Evidence for Tibetan plateau uplift before 14 Myr ago from a new minimum age for east-west extension. Nature, 374, 49–52. https://doi.org/10.1038/374049a0

Cooperdock, E. H. G., Ketcham, R. A., and Stockli, D. F.: Resolving the effects of 2-D versus 3-D grain measurements on apatite (U–Th)/He age data and reproducibility, Geochronology, 1, 17–41, https://doi.org/10.5194/gchron-1-17-2019, 2019.

Copeland, P., Harrison, T.M., Kidd, W.E.A., Ronghua, X., & Yuquan, Z. (1987). Rapid early Miocene acceleration of uplift in the Gangdese Belt, Xizang (southern Tibet), and its bearing on accommodation mechanisms of the India-Asia collision. Earth and Planetary Science Letters, 86(2-4), 240-252. Doi: https://doi.org/10.1016/0012-821X(87)90224-X

Copeland, P., Harrison, T.M., Pan, Y., Kidd, W. S.F., Roden, M., & Zhang, Y. (1995). Thermal evolution of the Gangdese batholith, southern Tibet: A history of episodic unroofing. Tectonics, 14(2), 223-236. Doi: https://doi.org/10.1029/94TC01676

Copley, A., Avouac, J.P., & Wernicke, B.P. (2011). Evidence for mechanical coupling and strong Indian lower crust beneath southern Tibet. Nature, 472(7341), 79–81. https://doi.org/10.1038/nature09926

Corfu, F., Hanchar, J. M., Hoskin, P., & Kinny P., (2003). Atlas of Zircon Textures. Reviews in Mineralogy and Geochemistry; 53 (1): 469–500. doi: https://doi.org/10.2113/0530469

Crameri, F., G.E. Shephard, and P.J. Heron (2020). The misuse of colour in science communication, Nature Communications, 11, 5444. https://doi.org/10.1038/s41467-020-19160-7

Crameri, F. (2018). Geodynamic diagnostics, scientific visualisation and StagLab 3.0, Geosci. Model Dev. Discuss. https://doi.org/10.5194/gmd-2017-328

Curry, M. A. E., Barnes, J. B., and Colgan, J. P. (2016). Testing fault growth models with low-temperature thermochronology in the northwest Basin and Range, USA, Tectonics, 35, 2467– 2492, doi:10.1002/2016TC004211.

DeCelles, P.G., Robinson, D.M., & Zandt, G. (2002). Implications of shortening in the Himalayan fold-thrust belt for uplift of the Tibetan Plateau, Tectonics, 21, 1062, doi:10.1029/2001TC001322.

DeCelles, P.G., Kapp, P., Quade, J., & Gehrels, G.E. (2011). Oligocene–Miocene Kailas basin, southwestern Tibet: Record of postcollisional upper-plate extension in the Indus-Yarlung suture zone. GSA Bulletin; 123 (7-8): 1337–1362. doi: https://doi.org/10.1130/B30258.1

DeCelles, P.G., Carrapa, B., Gehrels, G.E., Chakraborty, T., & Ghosh, P. (2016), Along-strike continuity of structure, stratigraphy, and kinematic history in the Himalayan thrust belt: The view from Northeastern India, Tectonics, 35, 2995– 3027, doi:10.1002/2016TC004298.

Dodson, M.H. (1973), Closure temperature in cooling geochronological and petrological systems, Contrib. Mineral. Petrol., 40(3), 259– 274, doi:10.1007/BF00373790.

Dürr, S.B. (1996). Provenance of Xigaze fore-arc basin clastic rocks (Cretaceous, south Tibet). Geological Society of America Bulletin, 108(6), 669-684. Doi: https://doi.org/10.1130/0016-7606(1996)108%3C0669:POXFAB%3E2.3.CO;2

Einsele, G., Liu, B., Dürr, S., Frisch, W., Liu, G., Luterbacher, H.P., Ratschbacher, L., Ricken. W., Wendt, J., Wetzel, A., Yu, G., & Zheng H. (1994). The Xigaze forearc basin: evolution and facies architecture (Cretaceous, Tibet) Sediment. Geol., 90 (1–2), pp. 1-32

England P.C. & Houseman G.A., (1989). Extension during continental convergence, with application to the Tibetan Plateau: Journal of Geophysical Research, v. 94, p. 17,561–17,579, doi:10.1029/JB094iB12p17561.

England, P., & Searle, M. (1986), The Cretaceous-tertiary deformation of the Lhasa Block and its implications for crustal thickening in Tibet, Tectonics, 5(1), 1– 14, doi:10.1029/TC005i001p00001.

Farley, K.A., Wolf, R.A., & Silver, L.T. (1996). The effects of long alpha-stopping distances on (U-Th)/He ages. Geochimica et cosmochimica acta, 60(21), 4223-4229. https://doi.org/10.1016/S0016-7037(96)00193-7

Faulds, J.E., & Varga, R.J. (1998). The role of accommodation zones and transfer zones in the regional segmentation of extended terranes. Geological Society of America Special Papers, 323, 1-45. https://doi.org/10.1130/0-8137-2323-X.1

Fielding, E., Isacks, B., Barazangi, M., & Duncan, C. (1994). How flat is Tibet? Geology, 22(2), 163– 167. https://doi.org/10.1130/0091-7613(1994)022<0163:HFIT>2.3.CO;2

Gan, W., Zhang, P. et al. (2007). Present-day crustal motion within the Tibetan Plateau inferred from GPS measurements. Journal of Geophysical Research, 112, B08416. https://doi.org/10.1029/2005JB004120

Gansser, A. (1964), Geology of the Himalayas, pp. 289, Wiley Interscience, London.

Gao, R., Chen, C., Lu, Z.W., Brown, L.D., Xiong, X.S., Li, W.H., & Deng, G. (2013). New constraints on crustal structure and Moho topography in Central Tibet revealed by SinoProbe deep seismic reflection profiling. Tectonophysics, 606, 160– 170. https://doi.org/10.1016/j.tecto.2013.08.006

Gao, T., Ding, Z., Wang, X., & Jiang, L. (2021). Joint inversion of receiver functions, Rayleigh wave dispersion and ZH ratio for crustal structure in Southeast Tibetan Plateau and its implications for dynamics. Chinese Journal of Geophysics, 64(6), 1885-1906. Doi: 10.6038/cjg2021O0282

Garzione, C.N., DeCelles, P.G., Hodkinson, D.G., Ojha, T.P., & Upreti, B.N. (2003). East–west extension and Miocene environmental change in the southern Tibetan Plateau: Thakkhola graben, central Nepal. Geological Society of American Bulletin , 115, 3–20. Doi: https://doi.org/10.1130/0016-7606(2003)115%3C0003:EWEAME%3E2.0.CO;2

Gehrels, G., Valencia, V., & Pullen, A. (2006). Detrital Zircon Geochronology by Laser-Ablation Multicollector ICPMS at the Arizona LaserChron Center. The Paleontological Society Papers, 12, 67-76. doi:10.1017/S1089332600001352

Gehrels, G.E., Valencia, V.A., & Ruiz, J. (2008), Enhanced precision, accuracy, efficiency, and spatial resolution of U-Pb ages by laser ablation–multicollector–inductively coupled plasma–mass spectrometry, Geochem. Geophys. Geosyst., 9, Q03017, doi:10.1029/2007GC001805.

Gehrels G.E., (2009), Arizona LaserChron Center analysis tools for U-Th-Pb geochronologic data: Homepage: https://sites.google.com/laserchron.org/arizonalaserchroncenter/home; Document:https://drive.google.com/file/d/1ju5B_h4kHvbK7PR2WHM9DJQELByqdJP_/view?pli=1 (accessed February 2023).

Gehrels, G., Rusmore, M., Woodsworth, G., Crawford, M., Andronicos, C., Hollister, L., ... & Girardi, J. (2009). U-Th-Pb geochronology of the Coast Mountains batholith in north-coastal British Columbia: Constraints on age and tectonic evolution. Geological Society of America Bulletin, 121(9-10), 1341-1361. doi: https://doi.org/10.1130/B26404.1

Geng, Q.R., Sun, Z.M., Pan, G.T., Zhu, D.C., & Wang, L.Q. (2009). Origin of the Gangdise (Transhimalaya) Permian arc in southern Tibet: Stratigraphic and volcanic geochemical constraints. Island Arc, 18(3), 467-487. Doi: https://doi.org/10.1111/j.1440-1738.2009.00664.x

Giovanni, M. K., Horton, B. K., Garzione, C. N., McNulty, B., & Grove, M. (2010). Extensional basin evolution in the Cordillera Blanca, Peru: Stratigraphic and isotopic records of detachment faulting and orogenic collapse in the Andean hinterland. Tectonics, 29(6).

Guenthner, W.R., Reiners, P.W., Ketcham, R.A., Nasdala, L., & Giester, G. (2013). Helium diffusion in natural zircon: Radiation damage, anisotropy, and the interpretation of zircon (U-Th)/He thermochronology. American Journal of Science, 313(3), 145-198. DOI: https://doi.org/10.2475/03.2013.01

Ha, G., Wu, Z., & Liu, F. (2019). Late quaternary vertical slip rates along the southern Yadong–Gulu rift, southern Tibetan plateau. Tectonophysics, 755, 75-90. Doi: https://doi.org/10.1016/j.tecto.2019.02.014

Han, Z., Sinclair, H.D., Li, Y., Wang, C., Tao, Z., Qian, X., et al (2019). Internal drainage has sustained low-relief Tibetan landscapes since the early Miocene. Geophysical Research Letters, 46, 8741– 8752. https://doi.org/10.1029/2019GL083019

Harrison, T.M., Copeland, P., Kidd, W.S.F., & Yin, A.N. (1992). Raising tibet. Science, 255(5052), 1663-1670. Doi: https://doi.org/10.1126/science.255.5052.1663

Harrison, T.M., Copeland, P., Kidd, W.S.F., & Lovera, O.M. (1995). Activation of the Nyainqentanghla Shear Zone: Implications for uplift of the southern Tibetan Plateau, Tectonics, 14(3), 658– 676, doi:10.1029/95TC00608.

Harrison, T.M., Yin, A., Grove, M., Lovera, O.M., Ryerson, F.J., & Zhou, X. (2000). The Zedong Window: A record of superposed Tertiary convergence in southeastern Tibet. Journal of Geophysical Research: Solid Earth, 105(B8), 19211-19230. Doi: https://doi.org/10.1029/2000JB900078

Harley, S.L., Kelly, N.M., & Mӧller, A. (2007). Zircon behaviour and the thermal histories of mountain chains. Elements, 3(1), 25-30. Doi: https://doi.org/10.2113/gselements.3.1.25

He, S., Kapp, P., DeCelles, P.G., Gehrels, G.E., & Heizler, M. (2007). Cretaceous–Tertiary geology of the Gangdese Arc in the Linzhou area, southern Tibet. Tectonophysics, 433(1-4), 15-37. Doi: https://doi.org/10.1016/j.tecto.2007.01.005

Heim, A., & Gansser, A., 1939, Central Himalaya, geological observations of the Swiss expeditions 1936: Memoires de la Société Helvetiques des Sciences Naturelles , 73. 1-245.

Hoskin, P.W., & Schaltegger, U. (2003). The composition of zircon and igneous and metamorphic petrogenesis. Reviews in mineralogy and geochemistry, 53(1), 27-62. Doi: https://doi.org/10.2113/0530027

Hou, Z.Q., Gao, Y.F., Qu, X.M., Rui, Z.Y., & Mo, X.X. (2004). Origin of adakitic intrusives generated during mid-Miocene east-west extension in southern Tibet. Earth Planet. Sci. Lett., 220, pp. 139-155. Doi: https://doi.org/10.1016/S0012-821X(04)00007-X

Hourigan, J.K., Reiners, P.W., & Brandon, M.T. (2005). U-Th zonation-dependent alpha-ejection in (U-Th)/He chronometry. Geochimica et Cosmochimica Acta, 69(13), 3349-3365. Doi: https://doi.org/10.1016/j.gca.2005.01.024

Houseman, G.A., McKenzie, D.P., & Molnar, P. (1981). Convective instability of a thickened boundary layer and its relevance for the thermal evolution of continental convergent belts. Journal of Geophysical Research: Solid Earth, 86(B7), 6115-6132. Doi: https://doi.org/10.1029/JB086iB07p06115

Huang, W., Dupont-Nivet, G., Lippert, P.C., van Hinsbergen, D.J., & Hallot, E. (2013). Inclination shallowing in Eocene Linzizong sedimentary rocks from Southern Tibet: correction, possible causes and implications for reconstructing the India–Asia collision. Geophysical Journal International, 194(3), 1390-1411. Doi: https://doi.org/10.1093/gji/ggt188

Huang, F., Li, M., Xu, J., Zeng, Y., Chen, J., Wang, B., ... & Zhang, Z. (2019). Geodynamic transition from subduction to extension: evidence from the geochronology and geochemistry of granitoids in the Sangsang area, southern Lhasa Terrane, Tibet. International Journal of Earth Sciences, 108, 1663-1681. Doi: https://doi.org/10.1007/s00531-019-01729-3

Hughes, C.A., Jessup, M.J., Shaw, C.A., & Newell, D.L. (2019). Deformation conditions during syn-convergent extension along the Cordillera Blanca shear zone, Peru. Geosphere, 15(4), 1342-1367. Doi: https://doi.org/10.1130/GES02040.1

Huntington, K.W., & Klepeis, K.A. (2018). Challenges and opportunities for research in tectonics: Understanding deformation and the processes that link Earth systems, from geologic time to human time. A community vision document submitted to the US National Science Foundation. URI: http://hdl.handle.net/1773/40754

Jessup, M.J., Newell, D.L., Cottle, J. M., Berger, A. L., & Spotila, J. A. (2008). Orogen-parallel extension and exhumation enhanced by denudation in the trans-Himalayan Arun River gorge, Ama Drime Massif, Tibet-Nepal. Geology; 36 (7): 587–590. doi: https://doi.org/10.1130/G24722A.1

Ji, W.Q., Wu, F.Y., Chung, S.L., Li, J.X., & Liu, C.Z. (2009). Zircon U–Pb geochronology and Hf isotopic constraints on petrogenesis of the Gangdese batholith, southern Tibet. Chemical Geology, 262(3-4), 229-245. Doi: https://doi.org/10.1016/j.chemgeo.2009.01.020

Kali, E., Leloup, P.H., Arnaud, N., Mahéo, G., Liu, D., Boutonnet, E., Van der Woerd, J., Liu, X., Liu-Zeng, J., & Li, H. (2010). Exhumation history of the deepest central Himalayan rocks, Ama Drime range: Key pressure-temperature-deformation-time constraints on orogenic models, Tectonics, 29, TC2014, doi:10.1029/2009TC002551.

Kapp, P., & DeCelles, P.G. (2019). Mesozoic–Cenozoic geological evolution of the Himalayan-Tibetan orogen and working tectonic hypotheses. Am. J. Sci., 319, 159–254. DOI: 10.2475/03.2019.01

Kapp, P., & Guynn J.H. (2004). Indian punch rifts Tibet. Geology 2004;; 32 (11): 993–996. doi:/10.1130/G20689.1

Kapp, P., Yin, A., Manning, C.E., Harrison, T.M., Taylor, M.H., & Ding, L. (2003). Tectonic evolution of the early Mesozoic blueschist-bearing Qiangtang metamorphic belt, central Tibet, Tectonics, 22, 1043, doi:10.1029/2002TC001383, 4.

Kapp, J. L.D., Harrison, T.M., Kapp, P., Grove, M., Lovera, O.M., & Lin, D. (2005), Nyainqentanglha Shan: A window into the tectonic, thermal, and geochemical evolution of the Lhasa block, southern Tibet, J. Geophys. Res., 110, B08413, doi:10.1029/2004JB003330.

Kapp, P., DeCelles, P.G., Leier, A., Fabijanic, J.M., He, S., Pullen, A., Gehrels G.E., & Ding, L. (2007). The Gangdese retroarc thrust belt revealed. GSA Today. 17. 4-9. doi: 10.1130/GSAT01707A.1.

Kapp, P., Taylor, M., Stockli, D., & Ding, L. (2008). Development of active low-angle normal fault systems during orogenic collapse. Geology 36, 7–10. doi: https://doi.org/10.1130/G24054A.1

Kay, R.W., & Kay, S.M. (1993). Delamination and delamination magmatism. Tectonophysics, 219(1-3), 177-189. Doi: https://doi.org/10.1016/0040-1951(93)90295-U

Ketcham, R.A. (2005). Forward and inverse modeling of low-temperature thermochronometry data. Reviews in mineralogy and geochemistry, 58(1), 275-314. Doi: https://doi.org/10.2138/rmg.2005.58.11

Ketcham, R.A., Gautheron, C., & Tassan-Got, L. (2011). Accounting for long alpha-particle stopping distances in (U–Th–Sm)/He geochronology: Refinement of the baseline case. Geochimica et Cosmochimica Acta, 75(24), 7779-7791. Doi: https://doi.org/10.1016/j.gca.2011.10.011

Kind, R., Yuan, X., Saul, J., Nelson, D., Sobolev, S., Mechie, J., & Achauer, U. (2002). Seismic images of crust and upper mantle beneath Tibet: Evidence for Eurasian plate subduction. Science, 298, 1219–1221. Doi: 10.1126/science.1078115

Klemperer, S.L., Zhao, P., Whyte, C.J., Darrah, T.H., Crossey, L.J., Karlstrom, K.E., ... & Ding, L. (2022). Limited underthrusting of India below Tibet: 3He/4He analysis of thermal springs locates the mantle suture in continental collision. Proceedings of the National Academy of Sciences, 119(12), e2113877119. Doi: https://doi.org/10.1073/pnas.2113877119

Labrousse, L., Huet, B., Le Pourhiet, L., Jolivet, L., & Burov, E. (2016). Rheological implications of extensional detachments: Mediterranean and numerical insights. Earth-Science Reviews, 161, 233-258. Doi: https://doi.org/10.1016/j.earscirev.2016.09.003

Lang, K.A., & Huntington, K.W. (2014). Antecedence of the Yarlung–Siang–Brahmaputra River, eastern Himalaya. Earth and Planetary Science Letters, 397, 145-158. Doi: https://doi.org/10.1016/j.epsl.2014.04.026

Laskowski, A.K., Kapp, P., Ding, L., Campbell, C., & Liu, X.H. (2017). Tectonic evolution of the Yarlung suture zone, Lopu Range region, southern Tibet, Tectonics, 36, 108– 136, doi:10.1002/2016TC004334.

Laskowski A.K., Kapp, P., & Cai, F. (2018). Gangdese culmination model: Oligocene–Miocene duplexing along the India-Asia suture zone, Lazi region, southern Tibet. GSA Bulletin; 130 (7-8): 1355–1376. doi: https://doi.org/10.1130/B31834.1

Leary, R., Orme, D.A., Laskowski, A.K., DeCelles, P.G., Kapp, P., Carrapa, B., & Dettinger, M. (2016). Along-strike diachroneity in deposition of the Kailas Formation in central southern Tibet: Implications for Indian slab dynamics. Geosphere; 12 (4): 1198–1223. doi: https://doi.org/10.1130/GES01325.1

Lee, H.Y., Chung, S.L., Lo, C.H., Ji, J., Wen, D.J., Qian, Q., ... & Zhang, Q. (2007). On the age and geodynamic significance of the Linzizong volcanic successions, southern Tibet: Neo-Tethyan slab breakoff in the early stage of the India-Asia collision.

Lee, H.Y., Chung, S.L., Lo, C.H., Ji, J., Lee, T.Y., Qian, Q., & Zhang, Q. (2009). Eocene Neotethyan slab breakoff in southern Tibet inferred from the Linzizong volcanic record. Tectonophysics, 477(1-2), 20-35. Doi: https://doi.org/10.1016/j.tecto.2009.02.031

Lee, J., Hager, C., Wallis, S.R., Stockli, D.F., Whitehouse, M.J., Aoya, M., & Wang, Y. (2011). Middle to late Miocene extremely rapid exhumation and thermal reequilibration in the Kung Co rift, southern Tibet, Tectonics, 30, TC2007, doi:10.1029/2010TC002745.

Lee, H.Y., Chung, S.L., Ji, J., Qian, Q., Gallet, S., Lo, C.H., ... & Zhang, Q. (2012). Geochemical and Sr–Nd isotopic constraints on the genesis of the Cenozoic Linzizong volcanic successions, southern Tibet. Journal of Asian Earth Sciences, 53, 96-114. Doi: https://doi.org/10.1016/j.jseaes.2011.08.019

Leier, A.L., DeCelles, P.G., Kapp, P., & Gehrels, G.E. (2007). Lower Cretaceous strata in the Lhasa Terrane, Tibet, with implications for understanding the early tectonic history of the Tibetan Plateau. Journal of Sedimentary Research, 77(10), 809-825. Doi: https://doi.org/10.2110/jsr.2007.078

Li, G., Kohn, B., Sandiford, M., Xu, Z., & Wei, L. (2015). Constraining the age of Liuqu Conglomerate, southern Tibet: Implications for evolution of the India–Asia collision zone. Earth and Planetary Science Letters, 426, 259-266. Doi: https://doi.org/10.1016/j.epsl.2015.06.010

Li, S., Guilmette, C., Ding, L., Xu, Q., Fu, J.J., & Yue, Y.H. (2017). Provenance of Mesozoic clastic rocks within the Bangong-Nujiang suture zone, central Tibet: implications for the age of the initial Lhasa-Qiangtang collision. J. Asian Earth Sci., 147, pp. 469-484

Liu, A.L., Wang, Q., Zhu, D.C., Zhao, Z.D., Liu, S.A., Wang, R., ... & Zhang, L.L. (2018). Origin of the ca. 50 Ma Linzizong shoshonitic volcanic rocks in the eastern Gangdese arc, southern Tibet. Lithos, 304, 374-387. Doi: https://doi.org/10.1016/j.lithos.2018.02.017

Long, S.P., Thomson, S.N. Reiners, P.W., & V. Di Fiori, R. (2015). Synorogenic extension localized by upper-crustal thickening: An example from the Late Cretaceous Nevadaplano. Geology; 43 (4): 351–354. doi:10.1130/G36431.1

Mahéo, G., Leloup, P. H., Valli, F., Lacassin, R., Arnaud, N., Paquette, J. L., ... & Tapponnier, P. 6. (2007). Post 4 Ma initiation of normal faulting in southern Tibet. Constraints from the Kung Co half graben. Earth and Planetary Science Letters, 256(1-2), 233-243. Doi:10.1016/j.epsl.2007.01.029

Marrett, R., & Strecker, M.R. (2000). Response of intracontinental deformation in the central Andes to late Cenozoic reorganization of South American Plate motions, Tectonics, 19(3), 452– 467, doi:10.1029/1999TC001102.

Maslin, M.A., Li, X.S., Loutre, M.F., & Berger, A. (1998). The contribution of orbital forcing to the progressive intensification of Northern Hemisphere glaciation. Quaternary Science Reviews, 17(4-5), 411-426. Doi: https://doi.org/10.1016/S0277-3791(97)00047-4

McCaffrey, R., & Nabelek J. (1998). Role of oblique convergence in the active deformation of the Himalayas and southern Tibet plateau. Geology; 26 (8): 691–694. doi: https://doi.org/10.1130/0091-7613(1998)026<0691:ROOCIT>2.3.CO;2

McCallister, A.T., Taylor, M.H., Murphy, M.A., Styron, R.H., & Stockli, D.F. (2014). Thermochronologic constraints on the late Cenozoic exhumation history of the Gurla Mandhata metamorphic core complex, Southwestern Tibet. Tectonics, 33(2), 27-52. Doi: https://doi.org/10.1002/2013TC003302

Mo, X., Niu, Y., Dong, G., Zhao, Z., Hou, Z., Zhou, S., & Ke, S. (2008). Contribution of syncollisional felsic magmatism to continental crust growth: a case study of the Paleogene Linzizong volcanic succession in southern Tibet. chemical Geology, 250(1-4), 49-67. Doi: https://doi.org/10.1016/j.chemgeo.2008.02.003

Molnar, P., & Qidong, D. (1984). Faulting associated with large earthquakes and the average rate of deformation in central and eastern Asia, J. Geophys. Res., 89(B7), 6203– 6227, doi:10.1029/JB089iB07p06203.

Molnar, P., & Tapponnier, P. (1978). Active tectonics of Tibet, J. Geophys. Res., 83(B11), 5361– 5375, doi:10.1029/JB083iB11p05361

.

Molnar, P., England, P., & Martinod, J. (1993), Mantle dynamics, uplift of the Tibetan Plateau, and the Indian Monsoon, Rev. Geophys., 31(4), 357– 396, doi:10.1029/93RG02030.

Murphy, M.A., Yin, A., Harrison, T.M., Duïrr, S.B., Chen, Z., Ryerson, F.J., Kidd, W.S.F., Wang, X., & Zhou, X. (1997). Did the Indo-Asian collision alone create the Tibetan plateau?. Geology; 25 (8): 719–722. doi: https://doi.org/10.1130/0091-7613(1997)025<0719:DTIACA>2.3.CO;2

Murphy, M.A., Yin, A., Kapp, P., Harrison, T.M., Manning, C.E., Ryerson, F.J., Ding, L., & Guo J. (2002). Structural evolution of the Gurla Mandhata detachment system, southwest Tibet: Implications for the eastward extent of the Karakoram fault system. GSA Bulletin; 114 (4): 428–447. doi: https://doi.org/10.1130/0016-7606(2002)114<0428:SEOTGM>2.0.CO;2

Murphy, M.A., & Yin, A. (2003). Structural evolution and sequence of thrusting in the Tethyan fold-thrust belt and Indus-Yalu suture zone, southwest Tibet. GSA Bulletin 2003; 115 (1): 21–34. doi: https://doi.org/10.1130/0016-7606(2003)115<0021:SEASOT>2.0.CO;2

Murphy, M.A., Sanchez, V., & Taylor, M.H. (2010). Syn-collisional extension along the India-Asia suture zone, south-central Tibet: Implications for crustal deformation of Tibet. Earth Planet. Sci. Lett., 290, pp. 233-243, 10.1016/j.epsl.2009.11.046

Nábelek, J., Hetényi, G., Vergne, J., Sapkota, S., Kafle, B., Jiang, M., Su, H., Chen, J., Huang, B.S. & Hi-CLIMB Team. (2009). Underplating in the Himalaya-Tibet collision zone revealed by the Hi-CLIMB experiment. Science. 2009 Sep 11;325(5946):1371-4. doi: 10.1126/science.1167719. PMID: 19745147.

Orme, D.A. (2019). Burial and exhumation history of the Xigaze forearc basin, Yarlung suture zone, Tibet. Geoscience Frontiers, 10(3), 895-908.doi: https://doi.org/10.1016/j.gsf.2017.11.011

Orme, D.A., Carrapa, B. & Kapp, P. (2015), Sedimentology, provenance and geochronology of the upper Cretaceous–lower Eocene western Xigaze forearc basin, southern Tibet. Basin Res, 27: 387-411. https://doi.org/10.1111/bre.12080

Orme, D.A., & Laskowski, A.K. (2016). Basin Analysis of the Albian–Santonian Xigaze Forearc, Lazi Region, South-Central Tibet. Journal of Sedimentary Research; 86 (8): 894–913. doi: https://doi.org/10.2110/jsr.2016.59

Owens, T., & Zandt, G. (1997). Implications of crustal property variations for models of Tibetan plateau evolution. Nature 387, 37–43. doi: 10.1038/387037a0

Paces, J.B., & Miller Jr, J.D. (1993). Precise U-Pb ages of Duluth complex and related mafic intrusions, northeastern Minnesota: Geochronological insights to physical, petrogenetic, paleomagnetic, and tectonomagmatic processes associated with the 1.1 Ga midcontinent rift system. Journal of Geophysical Research: Solid Earth, 98(B8), 13997-14013. Doi: https://doi.org/10.1029/93JB01159

Patriat, P., & Achache, J. (1984). India–Eurasia collision chronology has implications for crustal shortening and driving mechanism of plates. Nature 311, 615–621. https://doi.org/10.1038/311615a0

Pan, Y., & Kidd, W.S.F. (1992). Nyainqentanglha shear zone: A late Miocene extensional detachment in the southern Tibetan Plateau. Geology, 20(9), 775-778. Doi: https://doi.org/10.1130/0091-7613(1992)020%3C0775:NSZALM%3E2.3.CO;2

Pan, G.T., Ding, J., Yao, D.S., & Wang L.Q. (2004). Geological Map of the Tibetan Plateau and Adjacent Areas (1: 1,500,000) Chengdu Cartographic Publishing House, Chengdu

Platt, J.P., & England, P.C. (1994). Convective removal of lithosphere beneath mountain belts; thermal and mechanical consequences. American Journal of Science, 294(3), 307-336.

Pullen, A., Ibáñez-Mejia, M., Gehrels, G. E., Giesler, D., & Pecha, M. (2018). Optimization of a laser ablation-single collector-inductively coupled plasma-mass spectrometer (Thermo Element 2) for accurate, precise, and efficient zircon U-Th-Pb geochronology. Geochemistry, Geophysics, Geosystems, 19, 3689– 3705. https://doi.org/10.1029/2018GC007889

Ratschbacher, L., Frisch, W., Chen, C., & Pan, G. (1992). Deformation and motion along the southern margin of the Lhasa block (Tibet) prior to and during the India–Asia collision. Journal of Geodynamics , 16, 21–54. Doi:10.1016/0264-3707(92)90017-M

Ratschbacher, L., Frisch, W., Liu, G., & Chen, C. (1994). Distributed deformation in southern and western Tibet during and after the India-Asia collision. Journal of Geophysical Research , 99, 19,917–19,945. Doi:10.1029/94JB00932

Ratschbacher, L., Krumrei, I., Blumenwitz, M., Staiger, M., Gloaguen, R., Miller, B., Samson, S., & Appel, E. (2011). Rifting and strike-slip shear in central Tibet and the geometry, age and kinematics of upper crustal extension in Tibet. Geological Society London Special Publications. 353. 127-163. Doi:10.1144/SP353.8.

Reiners, P.W. (2005). Zircon (U-Th)/He thermochronometry. Reviews in Mineralogy and Geochemistry, 58(1), 151-179. Doi: https://doi.org/10.2138/rmg.2005.58.6

Reiners, P.W., & Farley, K.A. (2001). Influence of crystal size on apatite (U–Th)/He thermochronology: an example from the Bighorn Mountains, Wyoming. Earth and Planetary Science Letters, 188(3-4), 413-420. Doi: https://doi.org/10.1016/S0012-821X(01)00341-7

Reiners, P.W., Farley, K.A., & Hickes, H.J. (2002). He diffusion and (U–Th)/He thermochronometry of zircon: initial results from Fish Canyon Tuff and Gold Butte. Tectonophysics, 349(1-4), 297-308. Doi: https://doi.org/10.1016/S0040-1951(02)00058-6

Reiners, P.W., Spell, T.L., Nicolescu, S., & Zanetti, K.A. (2004). Zircon (U-Th)/He thermochronometry: He diffusion and comparisons with 40Ar/39Ar dating. Geochimica et cosmochimica acta, 68(8), 1857-1887. Doi: https://doi.org/10.1016/j.gca.2003.10.021

Richter, F.M., Lovera, O.M., Harrison, T.M., & Copeland, P. (1991). Tibetan tectonics from 40Ar/39Ar analysis of a single K-feldspar sample. Earth and Planetary Science Letters, 105(1-3), 266-278. Doi: https://doi.org/10.1016/0012-821X(91)90136-6

Sanchez, V.I., Murphy, M.A., Robinson, A.C., Lapen, T.J., & Heizler, M.T. (2013). Tectonic evolution of the India–Asia suture zone since Middle Eocene time, Lopukangri area, south-central Tibet. Journal of Asian Earth Sciences, 62, 205-220. Doi: https://doi.org/10.1016/j.jseaes.2012.09.004

Schärer, U., Xu, R.H., & Allègre, C.J. (1984). UPb geochronology of Gangdese (Transhimalaya) plutonism in the Lhasa-Xigaze region, Tibet. Earth and Planetary Science Letters, 69(2), 311-320. Doi: https://doi.org/10.1016/0012-821X(84)90190-0

Schmitz, M. D., & Bowring, S. A. (2001). U-Pb zircon and titanite systematics of the Fish Canyon Tuff: An assessment of high-precision U-Pb geochronology and its application to young volcanic rocks. Geochimica et Cosmochimica Acta, 65(15), 2571-2587. https://doi.org/10.1016/S0016-7037(01)00616-0

Schmitz, M.D., Bowring, S.A., & Ireland, T.R. (2003). Evaluation of Duluth Complex anorthositic series (AS3) zircon as a U-Pb geochronological standard: New high-precision isotope dilution thermal ionization mass spectrometry results. Geochimica et Cosmochimica Acta, 67(19), 3665-3672. Doi: https://doi.org/10.1016/S0016-7037(03)00200-X

Sobel, E.R., & Strecker, M.R. (2003). Uplift, exhumation and precipitation: tectonic and climatic control of Late Cenozoic landscape evolution in the northern Sierras Pampeanas, Argentina. Basin Research, 15(4), 431-451. Doi: https://doi.org/10.1046/j.1365-2117.2003.00214.x

Stockli, D.F., Taylor, M., Yin, A., Harrison, T.M., D'Andrea, J., Kapp, P., & Ding, L. (2002). Late Miocene-Pliocene inception of EW extension in Tibet as evidenced by apatite (U-Th)/He data. In Geological Society of America Abstracts with Programs (Vol. 34, No. 6, p. 411).

Styron, R., Taylor, M., & Okoronkwo, K. (2010). Database of Active Structures From the Indo-Asian Collision, Eos Trans. AGU, 91(20), 181– 182, doi:10.1029/2010EO200001.

Styron, R.H., Taylor, M.H., & Murphy, M.A. (2011). Oblique convergence, arc-parallel extension, and the role of strike-slip faulting in the High Himalaya. Geosphere; 7 (2): 582–596. doi: https://doi.org/10.1130/GES00606.1

Styron, R. H., Taylor, M. H., Sundell, K. E., Stockli, D. F., Oalmann, J. A. G., Möller, A., McCallister, A. T., Liu, D., & Ding, L. (2013). Miocene initiation and acceleration of extension in the South Lunggar rift, western Tibet: Evolution of an active detachment system from structural mapping and (U-Th)/He thermochronology, Tectonics, 32, 880– 907, Doi:10.1002/tect.20053.

Styron, R., Taylor, M. & Sundell, K. (2015). Accelerated extension of Tibet linked to the northward underthrusting of Indian crust. Nature Geosci 8, 131–134. Doi:10.1038/ngeo2336

Sundell, K. E., Taylor, M. H., Styron, R. H., Stockli, D. F., Kapp, P., Hager, C., Liu, D., & Ding, L. (2013). Evidence for constriction and Pliocene acceleration of east-west extension in the North Lunggar rift region of west central Tibet, Tectonics, 32, 1454– 1479, Doi:10.1002/tect.20086.

Sundell, K.E., Gehrels, G.E., Quinn, D.P., Pecha, M.E., Giesler, D.M., Pepper, M.B. George, S.W.M., and White, A.M. (2020), AgeCalcML: An open-source MATLAB-based data reduction platform for LA-ICP-MS geochronology and geochemistry data from the Arizona LaserChron Center, Geological Society of America Annual Meeting.

Sundell, K.E., Laskowski, A.K., Kapp, P.A., Ducea, M.N. & Chapman, J.B. (2021). Jurassic to Neogene Quantitative Crustal Thickness Estimates in Southern Tibet. GSA Today, 31(6), doi.org/10.1130/GSATG461A.1.

Taylor, M.H., & Yin, A. (2009). Active structures of the Himalayan-Tibetan orogen and their relationships to earthquake distribution, contemporary strain field, and Cenozoic volcanism. Geosphere; 5 (3): 199–214. doi: https://doi.org/10.1130/GES00217.1

Taylor, M., Yin, A., Ryerson, F.J., Kapp, P., & Ding, L. (2003). Conjugate strike-slip faulting along the Bangong-Nujiang suture zone accommodates coeval east-west extension and north-south shortening in the interior of the Tibetan Plateau. Tectonics, 22. Doi:10.1029/2002TC001383

Taylor, M. H., Forte, A.M., Laskowski, A. K., & Ding, L. (2021). Active Uplift of Southern Tibet Revealed. GSA Today. 31. Doi:10.1130/GSATG487A.1.

Thiede, R. C., Arrowsmith, J. R., Bookhagen, B., McWilliams, M., Sobel, E. R., & Strecker, M. R. (2006). Dome formation and extension in the Tethyan Himalaya, Leo Pargil, northwest India. Geological Society of America Bulletin, 118(5-6), 635-650. Doi: https://doi.org/10.1130/B25872.1

Tilmann, F., Ni, J., & Indepth Iii Seismic Team. (2003). Seismic imaging of the downwelling Indian lithosphere beneath central Tibet. Science, 300(5624), 1424-1427. Doi: https://doi.org/10.1126/science.1082777

Tremblay, M.M., Fox, M., Schmidt, J.L., Tripathy-Lang, A., Wielicki, M.M., Harrison, T.M., Zeitler, P.K., & Shuster, D.L., (2015). Erosion in southern Tibet shut down at ∼10 Ma due to enhanced rock uplift within the Himalaya. Proc. Natl. Acad. Sci. 112, 12030–12035. Doi:10.1073/pnas.1515652112

Turner, S., Hawkesworth, C., Liu, J., Rogers, N., Kelley, S., & Van Calsteren, P. (1993). Timing of Tibetan uplift constrained by analysis of volcanic rocks. Nature, 364, 50-54. doi: https://ui.adsabs.harvard.edu/link_gateway/1993Natur.364...50T/doi:10.1038/364050a0

Vermeesch, P., & Tian, Y. (2014). Thermal history modelling: HeFTy vs. QTQt. Earth-Science Reviews, 139, 279-290. Doi: https://doi.org/10.1016/j.earscirev.2014.09.010

Vermeesch, P. (2018). IsoplotR: A free and open toolbox for geochronology. Geoscience Frontiers, 9(5), 1479-1493. https://doi.org/10.1016/j.gsf.2018.04.001

Walker, J. D., Tikoff, B., Newman, J., Clark, R., Ash, J., Good, J., Bunse, E.G., Möller, A., Kahn, M., Williams, R.T., Michels, Z., Andrew, J.E., & Rufledt, C. (2019). StraboSpot data system for structural geology. Geosphere, 15(2), 533-547. Doi: https://doi.org/10.1130/GES02039.1

Wang, J.G., Hu, X.M., Wu, F.Y., & Jansa, L. (2010). Provenance of the Liuqu Conglomerate in southern Tibet: A Paleogene erosional record of the Himalayan–Tibetan orogen. Sedimentary Geology, 231(3-4), 74-84. Doi: https://doi.org/10.1016/j.sedgeo.2010.09.004

Wang, C., Li, X., Liu, Z., Li, Y., Jansa, L., Dai, J., & Wei, Y. (2012). Revision of the Cretaceous–Paleogene stratigraphic framework, facies architecture and provenance of the Xigaze forearc basin along the Yarlung Zangbo suture zone. Gondwana Research, 22(2), 415-433. Doi: https://doi.org/10.1016/j.gr.2011.09.014

Wang, J.G., Hu, X.M., Garzanti, E., & Wu, F.Y. (2013). Upper Oligocene–Lower Miocene Gangrinboche Conglomerate in the Xigaze area, southern Tibet: Implications for Himalayan uplift and paleo-Yarlung-Zangbo initiation. The Journal of Geology, 121(4), 425-444. Doi: 10.1086/670722

Wang E., Kamp P. J.J., Xu G., Hodges K.V., Meng K., Chen L., Wang G., & Luo H., (2015). Flexural bending of southern Tibet in a retro foreland setting: Scientific Reports, v. 5, article number 12076, doi: https://doi.org/10.1038/srep12076

Wang, C., Ding, L., Cai, F.L., Wang, H.Q., Zhang, L.Y., & Yue, Y.H. (2022). Evolution of the Sumdo Paleo-Tethyan Ocean: Constraints from Permian Luobadui Formation in Lhasa terrane, South Tibet. Palaeogeography, Palaeoclimatology, Palaeoecology, 595, 110974. Doi: https://doi.org/10.1016/j.palaeo.2022.110974

Wei, Z., Li, X., Laskowski, A.K., Reynolds, A.N., & Fan, X. (2021). Cretaceous forearc basin remnant sediments in the eastern Yarlung Zangbo suture zone, near the eastern Himalaya syntaxis. Palaeogeography, Palaeoclimatology, Palaeoecology, 580, art. no. 110620. Doi:10.1016/j.palaeo.2021.110620

Wells, M.L., & Hoisch, T.D. (2008). The role of mantle delamination in widespread Late Cretaceous extension and magmatism in the Cordilleran orogen, western United States. Geological Society of America Bulletin, 120(5-6), 515-530. Doi: https://doi.org/10.1130/B26006.1

Wells, M.L., Hoisch, T.D., Cruz-Uribe, A.M., & Vervoort, J.D. (2012). Geodynamics of synconvergent extension and tectonic mode switching: Constraints from the Sevier-Laramide orogen. Tectonics, 31(1). Doi: https://doi.org/10.1029/2011TC002913

Wernicke, B. (1992). Cenozoic extensional tectonics of the US Cordillera. The Geology of North America, 3, 553-582. Doi: https://doi.org/10.1130/DNAG-GNA-G3.553

Willett, S.D., McCoy, S.W., Perron, J.T., Goren, L., & Chen, C.Y. (2014). Dynamic reorganization of river basins. Science, 343(6175), 1248765. Doi: https://doi.org/10.1126/science.1248765

Williams, H., Turner, S., Kelley, S., & Harris, N. (2001). Age and composition of dikes in Southern Tibet: new constraints on the timing of east-west extension and its relationship to postcollisional volcanism. Geology, 29(4), 339-342. Doi:10.1130/0091-7613(2001)029<0339:AACODI>2.0.CO;2

Williams, H.M., Turner, S.P., Pearce, J.A., Kelley, S.P., & Harris, N.B.W. (2004). Nature of the source regions for post-collisional, potassic magmatism in southern and northern Tibet from geochemical variations and inverse trace element modelling. Journal of Petrololgy, 45(3), 555–607. Doi:10.1093/petrology/egg094

Wolff, R., Hetzel, R., Dunkl, I., Xu Q., Bröcker, M., & Anczkiewicz A.A., (2019). High-Angle Normal Faulting at the Tangra Yumco Graben (Southern Tibet) since ∼15 Ma. The Journal of Geology 2019 127:1, 15-36. Doi:10.1086/700406

Wolff, R., Hetzel, R., Hölzer, K., Dunkl, I., Xu, Q., Anczkiewicz, A.A., & Li, Z. (2023). Rift propagation in south Tibet controlled by under-thrusting of India: a case study of the Tangra Yumco graben (south Tibet). Journal of the Geological Society, jgs2022-090. Doi: https://doi.org/10.1144/jgs2022-090

Wu, H.R., Wang, D.A., & Wang, L.C. (1977). Cretaceous in Lhaze–Gyangze, southern Xizang: Scientia Geologica Sinica, v. 3, p. 250–261 (in Chinese with English abstract).

Wu, C., Nelson, K.D., Wortman, G., Samson, S.D., Yue, Y., Li, J., ... & Edwards, M. A. (1998). Yadong cross structure and South Tibetan Detachment in the east central Himalaya (89–90 E). Tectonics, 17(1), 28-45. Doi: https://doi.org/10.1029/97TC03386

Wu, F.Y., Ji, W.Q., Liu, C.Z., & Chung, S.L. (2010). Detrital zircon U–Pb and Hf isotopic data from the Xigaze fore-arc basin: constraints on Transhimalayan magmatic evolution in southern Tibet. Chemical Geology, 271(1-2), 13-25. Doi: https://doi.org/10.1016/j.chemgeo.2009.12.007

Wu, H., Li, C., Xu, M., & Li, X. (2015). Early Cretaceous adakitic magmatism in the Dachagou area, northern Lhasa terrane, Tibet: Implications for slab roll-back and subsequent slab break-off of the lithosphere of the Bangong–Nujiang Ocean. Journal of Asian Earth Sciences, 97, 51-66. Doi: https://doi.org/10.1016/j.jseaes.2014.10.014

Yin, A. (2000). Mode of Cenozoic east-west extension in Tibet suggesting a common origin of rifts in Asia during the Indo-Asian collision, J. Geophys. Res., 105 (B9), 21745– 21759. Doi:10.1029/2000JB900168.

Yin, A. (2006) Cenozoic tectonic evolution of the Himalayan orogen as constrained by along-strike variation of structural geometry, exhumation history, and foreland sedimentation. Earth-Science Reviews, Volume 76, Issues 1–2, 1-131. Doi: 10.1016/j.earscirev.2005.05.004

Yin, A., & Harrison, T.M. (2000). Geologic evolution of the Himalayan-Tibetan orogen. Annual review of earth and planetary sciences, 28(1), 211-280. Doi: https://doi.org/10.1146/annurev.earth.28.1.211

Yin, A., & Taylor, M.H. (2011), Mechanics of V-shaped conjugate strike-slip faults and the corresponding continuum mode of continental deformation. Bulletin, 123, 1798–1821. doi: https://doi.org/10.1130/B30159.1

Yin, A., Harrison, T.M., Ryerson, F.J., Chen, W., Kidd, W.S.F., & Copeland, P. (1994). Tertiary structural evolution of the Gangdese thrust system, southeastern Tibet. Journal of Geophysical Research , 99, 18,175–18,201. Doi: 10.1029/94JB00504

Yin, A., Harrison, T.M., Murphy, M.A., Grove, M., Nie, S., Ryerson, F., Feng, W., & Le, C. (1999). Tertiary deformation history of southeastern and southwestern Tibet during the Indo-Asian collision. GSA Bulletin; 111 (11): 1644–1664. doi:10.1130/0016-7606(1999)111<1644:TDHOSA>2.3.CO;2

Zhang, P., Shen, Z., Wang, M., Gan, W., Bürgmann, R., & Molnar, P. (2004). Continuous deformation of the Tibetan Plateau from global positioning system data. Geology, 32, 809–812. Doi:10.1130/G20554.1

Zhang K., Zhang Y., Tang X., & Xia, B., (2012). Late Mesozoic tectonic evolution and growth of the Tibetan plateau prior to the Indo-Asian collision Earth-Science Reviews. Vol. 114, Iss. 3–4, 236-249. https://doi.org/10.1016/j.earscirev.2012.06.001

Zhang, L.Y., Ducea, M.N., Ding, L., Pullen, A., Kapp, P., & Hoffman, D. (2014). Southern Tibetan Oligocene–Miocene adakites: A record of Indian slab tearing. Lithos, 210, 209-223. Doi: https://doi.org/10.1016/j.lithos.2014.09.029

Zhang, J., Dai, J., Qian, X., Ge, Y., & Wang, C. (2017). Sedimentology, provenance and geochronology of the Miocene Qiuwu Formation: Implication for the uplift history of Southern Tibet. Geoscience Frontiers, 8(4), 823-839.doi: https://doi.org/10.1016/j.gsf.2016.05.010

Zhang, Y., Huang, F., Xu, J., Zeng, Y., Wang, B., Lv, M., ... & Zhang, L. (2023). Origin of the volcanic rocks in Dianzhong Formation, central Lhasa Terrane, Tibet: implication for the genesis of syn-collisional magmatism and Neo-Tethyan slab roll-back. International Geology Review, 65(1), 21-39. Doi: https://doi.org/10.1080/00206814.2022.2031314

Zhu, B., Kidd, W. S., Rowley, D. B., Currie, B. S., & Shafique, N. (2005). Age of initiation of the India-Asia collision in the east-central Himalaya. The Journal of Geology, 113(3), 265-285. Doi: https://doi.org/10.1086/428805

Zhu, D.C., Zhao, Z.D., Niu, Y., Mo, X.X., Chung, S.L., Hou, Z.Q., ... & Wu, F.Y. (2011). The Lhasa Terrane: Record of a microcontinent and its histories of drift and growth. Earth and Planetary Science Letters, 301(1-2), 241-255. Doi: https://doi.org/10.1016/j.epsl.2010.11.005

Zhu, D.C., Zhao, Z.D., Niu, Y., Dilek, Y., Wang, Q., Ji, W.H., ... & Mo, X.X. (2012). Cambrian bimodal volcanism in the Lhasa Terrane, southern Tibet: record of an early Paleozoic Andean-type magmatic arc in the Australian proto-Tethyan margin. Chemical Geology, 328, 290-308. Doi: https://doi.org/10.1016/j.chemgeo.2011.12.024

Zhu, D.C., Wang, Q., Zhao, Z.D., Chung, S.L., Cawood, P.A., Niu, Y., ... & Mo, X.X. (2015). Magmatic record of India-Asia collision. Scientific reports, 5(, 14289. Doi: https://doi.org/10.1038/srep14289

CHAPTER THREE

DYNAMICS OF RIFTING IN SOUTH-CENTRAL TIBET

Contribution of Authors and Co-Authors

Manuscript in Chapter 3

Author: Aislin N. Reynolds

Contributions: Conception of study, performed analyses, interpreted results, created figures, and wrote the manuscript.

Co-Author: Andrew K. Laskowski

Contributions: Conception of study, discussed implications, and writing review.

Manuscript Information

Aislin N. Reynolds[1], Andrew K. Laskowski[1]

[1]Department of Earth Sciences, Montana State University, Bozeman, MT, USA

Geology

Status of Manuscript:

_x__ Prepared for submission to a peer-reviewed journal

____ Officially submitted to a peer-reviewed journal

____ Accepted by a peer-reviewed journal

____ Published in a peer-reviewed journal

<u>Abstract</u>

Evaluating spatial and temporal patterns of rifting during plate convergence is an essential step towards disentangling the complex tectonic evolution of southern Tibet from Oligocene to Miocene time. Here, we examine spatial trends in thermochronology data for two classes of rifts: Tibetan rifts that are generally >150 km in length and crosscut the Lhasa Terrane, and Gangdese rifts that are typically <50 km long and isolated within the high topography of the Gangdese Range. Analysis of compiled zircon (U-Th)/He (ZHe) data from two Tibetan rifts and three Gangdese rifts reveals all samples from Gangdese rifts and Tibetan rifts that spatially overlap the Gangdese Range yield ages between ~28-16 Ma, whereas samples north of the Gangdese Range yield ages between ~12-4 Ma. We interpret these results to reflect Gangdese rift initiation by ~28 Ma, prior to the recent episode of India underthrusting beginning at ~20 Ma, while young ages from Tibetan rift portions North of the Gangdese Range (~12-4 Ma) are likely to reflect extension timing along Tibetan rifts driven by India Underthrusting. We suggest Gangdese rift initiation was driven by surface uplift of the Gangdese Range, with ZHe ages conspicuously overlapping timing estimates for contraction along the Gangdese Thrust and Great Counter Thrust until ~16-12 Ma. Our results suggest potentially new interactions and feedbacks between contractional and extensional structures in southern Tibet that are more complex than previously demonstrated.

Introduction

Evaluating spatial and temporal patterns of rifting is an essential step towards disentangling the complex and multifaceted interactions characterizing the active deformation of southern Tibet (Molnar and Tapponnier, 1978). We examine two classes of rifts: Tibetan rifts that are generally >150 km in length and crosscut the Lhasa Terrane, and Gangdese rifts that are typically <50 km long and isolated within the high topography of the Gangdese Range (Fig. 1). Studies motivated by the novelty of active extension along Tibetan rifts during continental collision have revealed systematic spatial distributions and orientations of normal faults across Tibet, suggesting a common mechanism of origin (e.g., Kapp and Guynn, 2004). Timing estimates from thermochronology studies indicate either synchronous or diachronous extension onset during Miocene time followed by an acceleration of rift rates in the Pliocene (Sundell et al., 2013; Styron et al., 2013, 2015; Wolff et al., 2019, 2023; Bian et al., 2022). These observations require a greater level of complexity in our interpretations of the tectonic systems that drive or influence rift initiation and evolution.

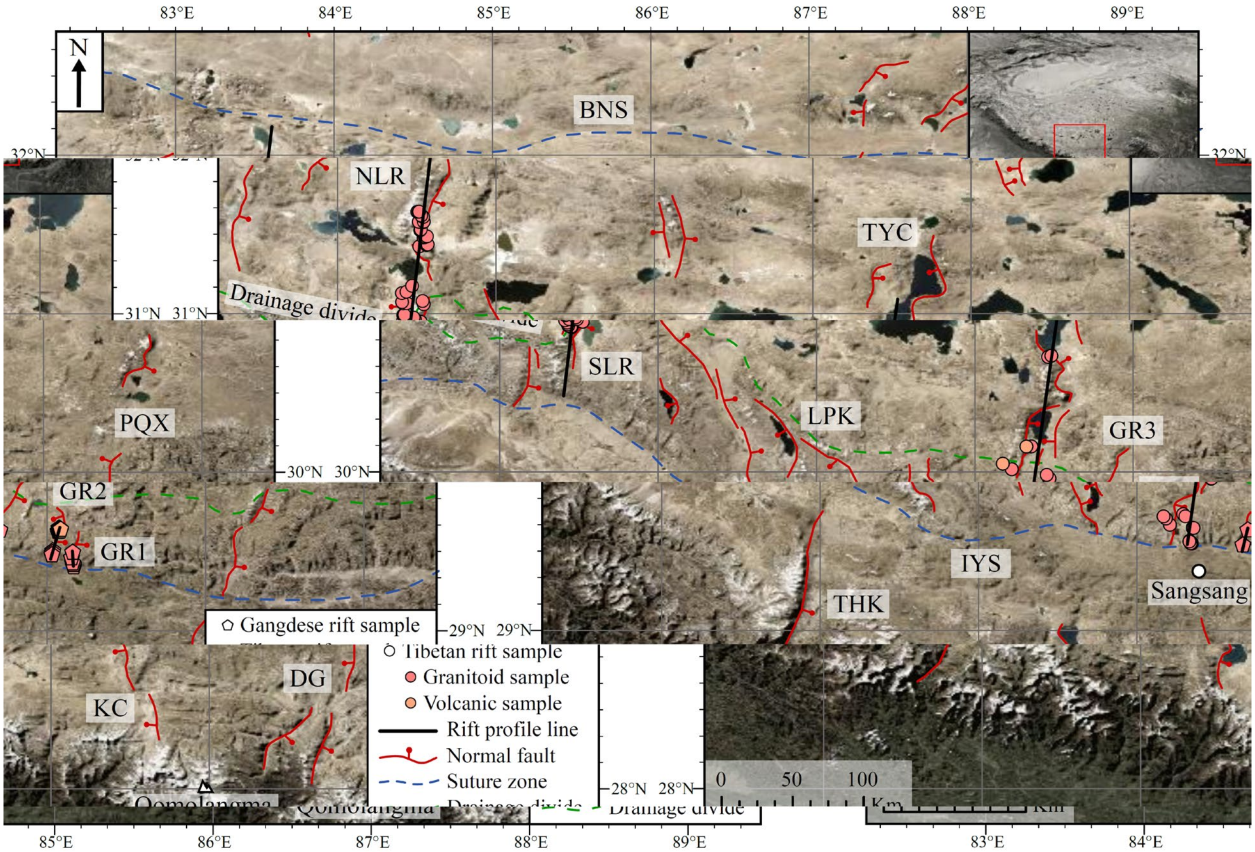

Figure 1. Overview map showing active extensional structures (red) and compiled zircon (U-Th)/He sample locations for ages used in this study. Blue dashed lines indicate the approximate northern extent of the Indus-Yarlung Suture (IYS) zone and southern extent of the Bangong-Nujiang Suture (BNS) zone. Green dashed line indicates the approximate location of the Gangdese drainage divide. NLR = North Lunggar Rift; SLR = South Lunggar Rift; LPK = Lopu-Kangri; TYC = Tangra Yumco; PQX = Pum Qu-Xainza; THK = Thakkhola; DG = Dinggye; KC = Kung Co; GR1 = Gangdese Rift 1; GR2 = Gangdese Rift 2; GR3 = Gangdese Rift 3. Full information for compiled data including positional information for all samples, reasoning for exclusion of specific ages or sample groups (e.g., published samples from Lopu Kangri are excluded), and references cited are included in supplementary materials (Table S5).

We investigate trends in the timing of extension onset by utilizing a compilation of zircon (U-Th)/He (ZHe) thermochronology data (Dixon et al., in review) for two Tibetan rift systems, including the Tangra Yumco rift (TYC), North Lunggar rift (NLR) and South Lunggar rift (SLR), and three Gangdese rifts (GR1, GR2, GR3; Fig. 1) and compare observed age trends to three distinct tectonic hypotheses. We report key distinctions between Tibetan and Gangdese rifts and discuss implications for the mechanisms that influence rift initiation and evolution at different scales across southern Tibet.

Potential Tectonic Models

Researchers have endeavored to explain the mechanisms or forces which drive rifting in Tibet through a variety of tectonic models, with India underthrusting constituting a leading model among recent studies of Tibetan rifts (DeCelles et al., 2002; Copley et al., 2011; Sundell et al., 2013; Styron et al., 2013, 2015; Wolff et al., 2019, 2023; Bian et al., 2022). However, investigations of Gangdese rifts are considerably less prevalent in the literature (Yin, 2000; Burke et al., 2021). Despite limited prior exploration, we suspect the mechanisms driving Gangdese rifts may differ from those proposed for Tibetan rifts (i.e., India underthrusting) based on distinctions in the timing of extension onset and fault kinematics from previous studies (e.g., Burke et al., 2021). While studies of Tibetan rifts indicate extension onset between ~16-12 Ma (or even as old as 19 Ma; Wolff et al., 2023), Gangdese rifts yield surprisingly older timing estimates for extension onset, with compiled ZHe ages falling between ~28-16 Ma for all Gangdese rift samples (this study).

These timing estimates for Gangdese rifts conspicuously overlap with the development of other first-order physiographic features and structures in Tibet, including: (1) the Gangdese drainage divide demarcated by the crest of the Gangdese Range which separates the internally and externally drained portions of the plateau (Fielding et al., 1994; Tapponnier et al., 2001); (2) a structural culmination beneath the Gangdese Range, supported by evidence from structural mapping, geochronology, and thermochronology data (Laskowski et al., 2018) and seismic reflection profiles from project INDEPTH showing folded and truncated reflectors at depth (Alsdorf et al., 1998); and (3) the Gangdese Thrust and Great Counter Thrust systems. Although debated, the timing of GCT activity is estimated to be between ca. 23-16 Ma, constrained by Kailas Formation deposition (26-23 Ma; Leary et al., 2016) and the initiation of N-S striking normal faults that crosscut the GCT (e.g., Sundell et al., 2013). Clear evidence of the GT has not yet been observed in south-central Tibet, but if the GT or an equivalent structure were present at the surface or at depth in this region, it would likely have been active between ca. 23-13 Ma, overlapping the estimated timing of Great Counter thrust system activity and exhumation in southern Tibet (e.g., Tremblay et al., 2015; Laskowski et al., 2018). We consider the configuration, timing estimates, and tectonic interactions of these structures because together they could accommodate ongoing north-south contraction and surface uplift, perhaps balanced by east-west extension along Gangdese rifts (Burke et al., 2021).

We do not attempt to replicate the efforts of studies that proposing dynamic models for Tibetan rifts here as our results are in broad agreement with published work, but instead we discuss the implications of our results with respect to tectonic hypotheses that incorporate timing constraints from published work. Figure 2 outlines three tectonic models based on hypotheses (H1, H2, H3) from studies of Tibetan rifts and four kinematic models (A, B, C, D) based on studies exploring fault growth mechanisms (e.g., Curry et al., 2016). Kinematic models are considered alongside tectonic models here to develop a holistic interpretation of rift development, with the observed fault kinematics in each rift system likely influenced by or significantly related to the tectonic forces that drive rift initiation and evolution.

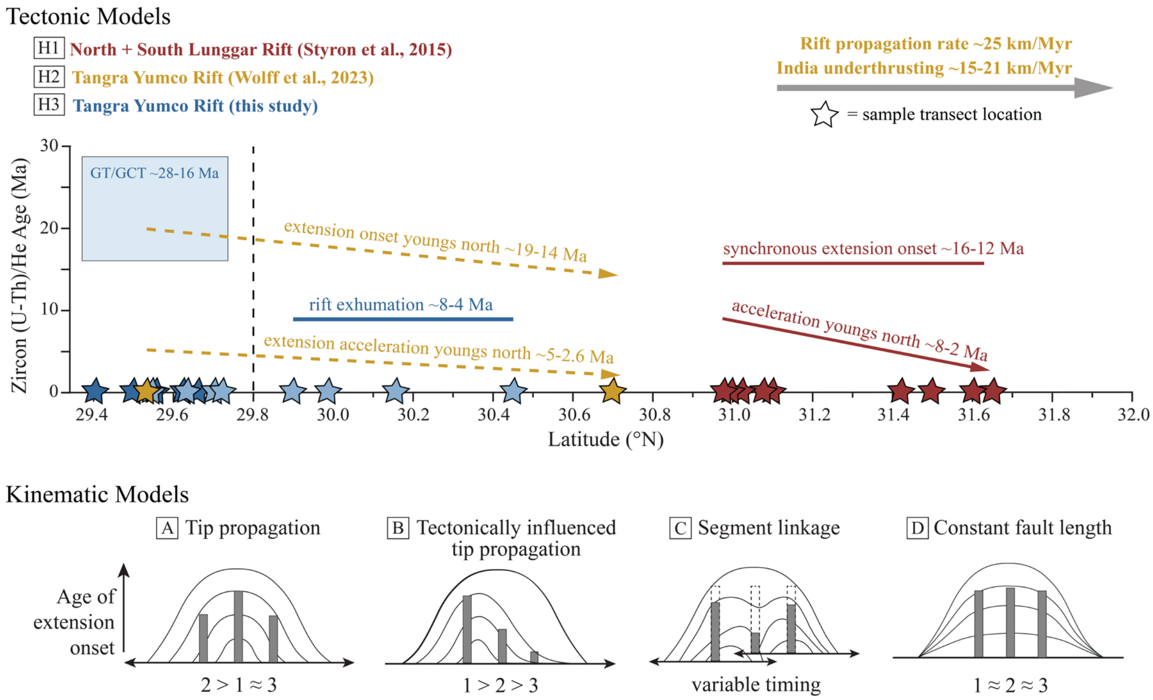

Figure 2. Proposed tectonic models (H1 = red; H2 = yellow; H3 = blue) and kinematic models (A, B, C, D) for the evolution of rifting in Tibet, with observed zircon (U-Th)/He age relationships plotted against latitude to evaluate N-S trends in rift timing. Stars represent locations of sample transects and are color coded by hypothesis; for H3 light blue stars = Tangra Yumco rift transects and dark blue stars = Gangdese rift transects. Gray arrow indicates approximate direction and rate of India underthrusting. Colored arrows indicate direction of younging in trends of extension onset or rates for each study. Age trendlines for H2 are dashed due to the existence of only two sample transects with a straight line inferred between them where no data are available. Black dashed line indicates approximate northern extent of Gangdese Range. Kinematic models show predicted map patterns of fault displacement and age of extension onset along rift strike (gray blocks 1, 2, and 3, where taller blocks = older ages). Models reflect different mechanisms for fault growth, including (A) tip propagation, (B) tectonically influenced tip propagation, (C) segment linkage, and (D) constant fault length.

Tectonic hypothesis one (**H1**) is based on results from samples in the North Lunggar rift (Sundell et al., 2013) and South Lunggar rift (Styron et al., 2013, 2015) indicating synchronous extension onset between ~16-12 Ma followed by a northward sweeping acceleration of extension rates which track the leading edge of the underthrusting Indian plate, causing rapid footwall exhumation between ~8-2 Ma (8 Ma in the SLR from Styron et al., 2013 and between ~5-2 Ma in the NLR from Sundell et al., 2013). Hypothesis two (**H2**) is based on results from two sample transects in the Tangra Yumco rift (Wolff et al., 2019, 2023) that suggest extension onset as early as ~19 Ma in south TYC, ~14 Ma in northern TYC, and accelerated extension beginning at ~5 Ma, with both the timing of extension onset and rift acceleration younging to the north at a rate of ~25 km/Myr which is plausibly consistent with rates of India underthrusting (~15-21 km/Myr; see Wolff et al., 2023 for full discussion). Here we propose hypothesis three (**H3**) based on additional thermochronology results (this study) from eight sample transects in the southern Tangra Yumco rift (light blue stars) and five sample transects from Gangdese rifts (dark blue stars). **H3** suggests older ages (~28-16 Ma) observed at Gangdese latitudes (~29.4-29.8°N) are related to contraction, surface uplift, and exhumation along the Gangdese Thrust (GT) and Great Counter Thrust (GCT) systems during uplift of the Gangdese Range, whereas samples north of ~29.8°N yielding younger ages (~8-4 Ma) likely reflect the timing of rift-related exhumation along TYC. Kinematic models include: (A) tip propagation, (B) tectonically influenced tip propagation, (C) segment linkage, and (D) constant fault length, with each model depicting different predictions for patterns of fault displacement and trends in thermochronologic ages along rift strike. Each model describes a different mechanism for normal fault growth to be considered together with tectonic models in interpretations of rift development.

The crucial parameters for testing of tectonic and kinematic models are (1) patterns of fault displacement, (2) spatial distributions in the timing of extension onset, and (3) trends in the rates of extension through time. Here, we focus on comparing trends in thermochronologic data along strike of Tibetan and Gangdese rifts, conducting a broad comparison of regional trends in rift timing to provide expanded interpretations for the mechanisms driving and/or influencing rift evolution in southern Tibet.

Spatial and Temporal Analysis of Tibetan and Gangdese Rifts

To analyze spatial patterns of extension onset for Tibetan and Gangdese rifts, we plotted compiled ZHe cooling ages against sample distance from the Indus Yarlung Suture (IYS) zone (Fig. 3). We constructed smooth trendlines by first creating an interpolated age surface in ArcGIS Pro, calculating ages based on the nearest available ZHe data point for each rift system using an inverse distance weighted (IDW) method. We then sampled the interpolated age surface at 1 km intervals along linear profiles (Fig. 1) oriented approximately parallel to the strike of each rift, reflecting the nearest actual ZHe age value which the polynomial trendlines shown in Figure 3 were applied. Trendlines from interpolated ages appear to indicate a general pattern of older in the south and younger in the north timing of extension onset for Tibetan rifts, particularly evident in the Lunggar rift system. Yet during evaluation of distributions of actual ZHe ages, we notice a distinct break in sample age for the Tangra Yumco rift between ~25-45 km distance from the IYS which roughly corresponds to latitudes of ~29.7-29.9°N marking the approximate northern extent of the Gangdese Range in the TYC rift region. Samples from the TYC rift located south of this break overlap the Gangdese Range and yield distinctly older ages between ~21-13 Ma compared to samples north of the break, which yield ages predominantly between ~12-4 Ma. For Gangdese rifts, trends in the along-strike timing of extension onset are more difficult to interpret due to large intra-sample variability in ZHe ages, especially in rifts GR1 and GR2. The wide spread of ages between ~28-16 Ma suggests an older and more protracted cooling history for Gangdese rifts, with exhumation potentially occurring at a slower rate over time.

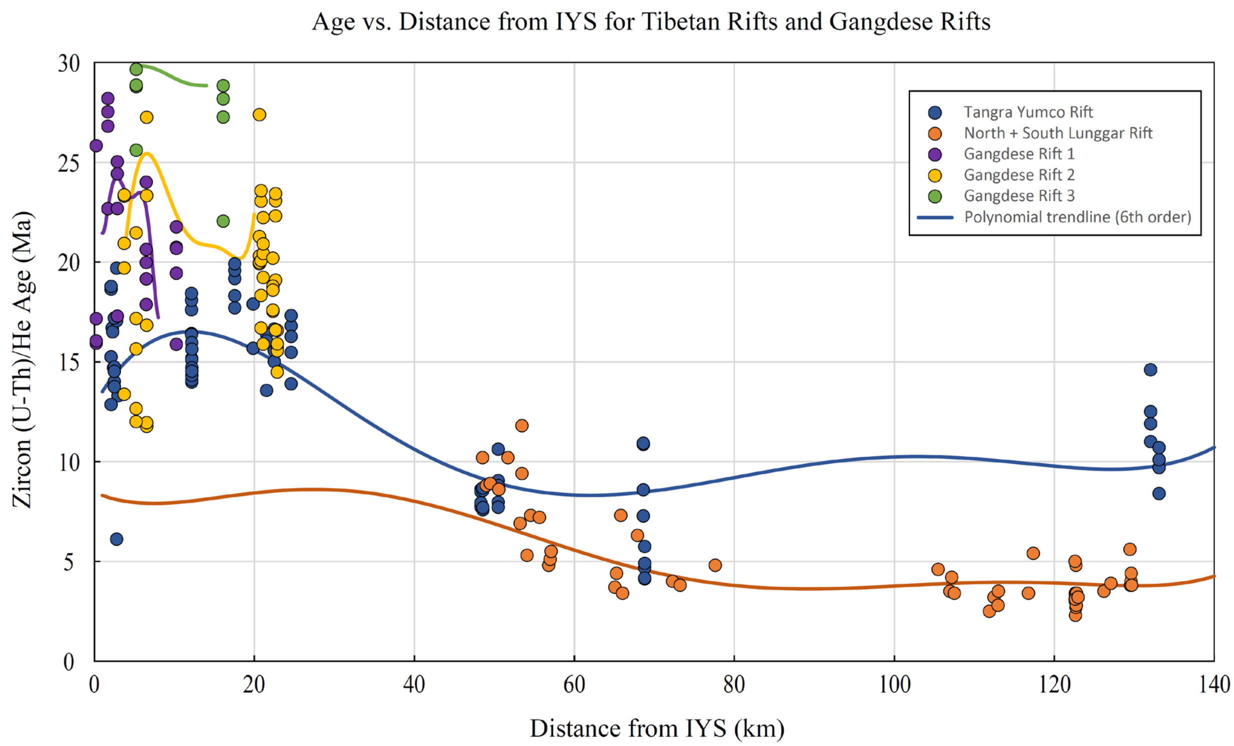

Figure 3. Zircon (U-Th)/He cooling ages (points) plotted against sample distance from the Indus Yarlung Suture (IYS) zone to evaluate trends in the along-strike timing of extension onset for the North Lunggar Rift and South Lunggar Rift (orange), the Tangra Yumco Rift (blue), and three Gangdese Rifts (GR1 = purple; GR2 = yellow; GR3 = green). Polynomial trendlines (6th order) were plotted as smoothed curves using the Inverse Distance Weighted (IDW) geoprocessing tool in ArcGIS Pro which interpolates a raster surface (i.e., age values) from points using an inverse distance weighted (IDW) technique. Representative age values were then selected from the raster surface at one-km increments along rift profiles (a full description of methods and data tables are included in supplementary materials).

Drivers of Extension in Southern Tibet

Trends in the timing of extension onset in Tibetan rifts indicate a northward younging of extension onset, consistent with previous studies citing India underthrusting as a leading model.

However, spatial distributions of ZHe ages reveal distinctly different thermal histories for Tibetan rifts and Gangdese rifts, or rather, differing thermal histories for samples collected from portions of rifts that overlap the Gangdese Range (southern TYC, GR1, GR2, GR3) as opposed to samples that do not overlap the Gangdese Range (northern TYC, NLR, SLR). These results suggest differing rift kinematics and tectonic drivers for Tibetan rifts and Gangdese rifts and support the idea that tectonic activity driving uplift of the Gangdese Range may have exerted some influence on the initiation and evolution of Gangdese rifts (Fig. 4). We suggest the following interpretations for the tectonic evolution of rifts in southern Tibet:

(1) Surface uplift of the Gangdese Range is driven by localized crustal thickening above a deep-seated structural culmination which accommodates north-south contraction, possibly similar to the lesser Himalayan duplex. Surface uplift elevates Gangdese Range topography to a critical thickness or gravitational potential energy, driving initiation of extension along Gangdese rifts by ~28 Ma to balance continued uplift.

(2) Rollback (~26 Ma) and breakoff (~21 Ma) of the India slab (Fig. 4A) drives deposition of the Kailas Formation at low elevations and a southward sweep of potassic–adakitic magmatism across the Lhasa terrane (DeCelles et al., 2011; Leary et al., 2016; Chapman and Kapp, 2017; Kapp and DeCelles, 2019), followed by a return to shallow northward underthrusting of the Indian plate. A reduction in slab-pull forces following breakoff and potential mechanical coupling between the underthrusting Indian lithosphere and Asian lower crust (Copley et al., 2011) likely reduces rates of underthrusting between ~20-10 Ma (Molnar and Stock, 2009).

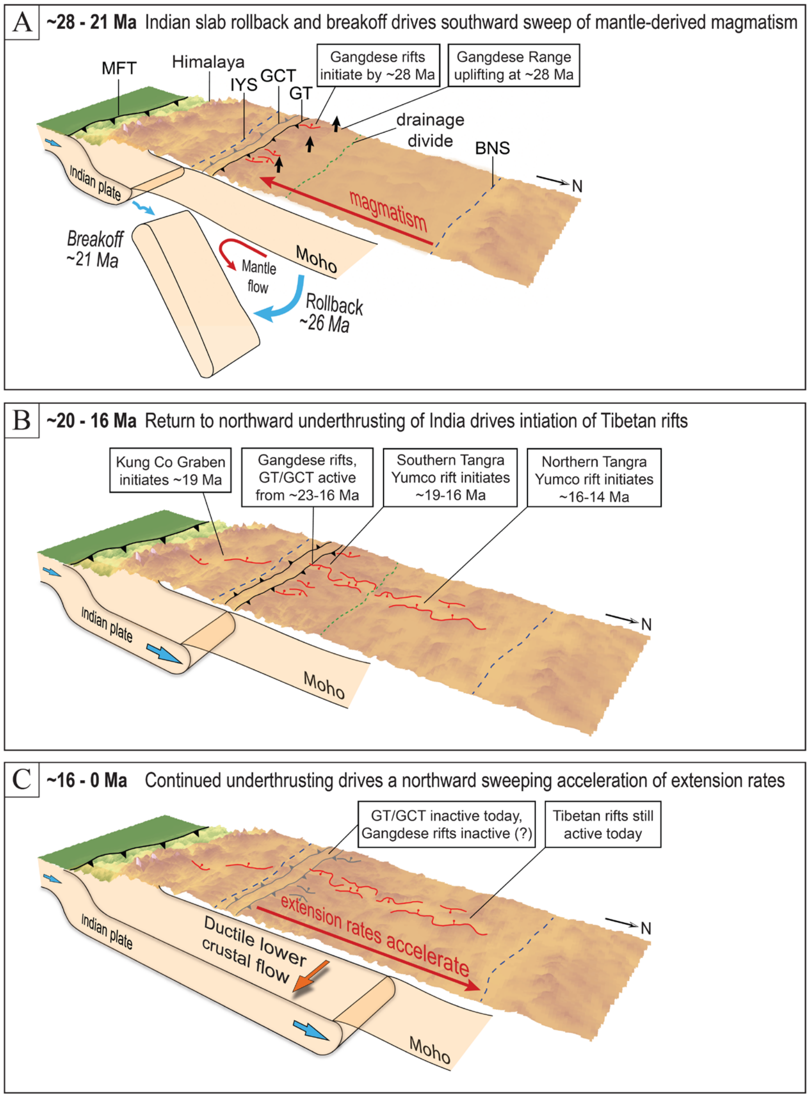

Figure 4. Three-dimensional conceptual model showing the tectonic evolution of the Tangra Yumco rift region of south-central Tibet and timing of activity for extensional structures (red) and contractional structures (black). Structures shown in gray are inactive. MFT = Main Frontal Thrust; GT = Gangdese Thrust; GCT = Great Counter Thrust; IYS = Indus-Yarlung Suture; BNS = Bangong-Nujiang Suture. (A) Uplift of the Gangdese Range and Gangdese rift initiation by ~28 Ma, followed by rollback (~26 Ma) and breakoff (~21 Ma) of the Indian slab. (B) A return to northwards underthrusting of India at ~20 Ma drives the onset of E-W extension along Tibetan rifts between ~19-16 Ma in the southern Lhasa terrane and around ~14 Ma in the northern Lhasa terrane, with the GT, GCT, and Gangdese rifts active until at least ~16 Ma. (C) Continued northwards underthrusting of India beneath Tibet drives a northward sweeping acceleration of extension rates, potentially related to an intensification of eastward ductile flow or extrusion of the mid-lower crust and mantle (orange arrows). Gangdese rifts may be active to balance continued uplift of the Gangdese Range or may be inactive today. Figure inspired by Styron et al. (2015). Vertical exaggeration of topography = 5:1.

(3) Continued crustal thickening and uplift of the Tibetan plateau drives initiation of Tibetan rifts between ~19-16 Ma in the southern Lhasa terrane and ~14 Ma in the northern Lhasa terrane (Fig. 4B), with the timing of rift initiation sweeping northward at a rate similar to the northward convergence of India (e.g., Wolff et al., 2023). Variations in initiation timing between different Tibetan rifts may relate to the northern edge of the Indian plate being irregular in shape (Chen et al., 2017; Wolff et al., 2023). Continued north-south contraction persists surface uplift of the Gangdese Range balanced by rifting until at least ~16 Ma, with the possibility that the structural culmination beneath the Gangdese Range is inactive today.

(4) Underthrusting of the Indian plate continues from ~16-0 Ma (Fig. 4C), causing a northward sweeping termination of mantle derived magmatism in the Lhasa terrane between ~13-10 Ma and a northward sweeping acceleration of extension rates due to additional crustal thickening and rapid eastward flow of the ductile lower crust of Asia during the Pliocene at ~5 Ma, tracking the leading edge of India (Styron et al., 2015; Wolff et al., 2023).

Conclusions

Spatial trends in thermochronology data from Tibetan and Gangdese rifts allow testing of models for rift initiation and evolution, and implications for the tectonic development of southern Tibet from Oligocene to Miocene time. We reveal different thermal histories for Tibetan and Gangdese rifts, and specifically, distinct timing estimates for extension onset in rift portions that spatially overlap the Gangdese Range (~28-16 Ma) in comparison to rift portions that do not overlap Gangdese Range (~14 Ma). ZHe data suggests initiation along Gangdese rifts occurred by ~28 Ma, prior to the recent episode of northward underthrusting of the Indian plate which is thought to have begun at ~20 Ma and is cited as a driving mechanism for Tibetan rifts (Fig. 4). Therefore, we interpret Gangdese rift initiation was driven by surface uplift of the Gangdese Range which is constrained by timing estimates for activity along the GT and GCT. These results suggest interactions and feedbacks between contractional and extensional structures in southern Tibet which are more complex than previously demonstrated. Further investigation is needed to determine if E-W extension along Gangdese rifts is active today and balancing ongoing uplift of the Gangdese Range (e.g., Burke et al., 2021), or if extension along Gangdese rifts ceased at ~16-12 Ma overlapping with the suggested timing of GCT cessation (e.g., Laskowski et al., 2018) and youngest ZHe ages from Gangdese rifts in this study. Although not reflected through ZHe thermochronology data compiled here, if recent extension at lower rates or magnitudes along Gangdese rifts has occurred, it may be recorded by other thermochronometers reflecting lower-temperature thermal histories of Gangdese rift footwall rocks, and thus could be examined in future studies by utilizing methods such as apatite fission track dating.

Acknowledgements

This work was funded by NSF Tectonics Awards to Dr. Andrew K. Laskowski (#1917685), Dr. Michael H. Taylor (#1917706), and Dr. Adam M. Forte (#1917695), and a GSA Graduate Student Research Grant award to PhD Candidate Aislin N. Reynolds.

References Cited

Alsdorf, D., Brown, L., Nelson, K. D., Makovsky, Y., Klemperer, S., & Zhao, W. (1998). Crustal deformation of the Lhasa terrane, Tibet plateau from Project INDEPTH deep seismic reflection profiles. Tectonics, 17(4), 501-519. https://doi.org/10.1029/98TC01315

Bian, S., Gong, J., Zuza, A.V., Yang, R., Chen, L., Ji, J., et al. (2022). Along-strike variation in the initiation timing of the north-trending rifts in southern Tibet as revealed from the Yadong-Gulu rift. Tectonics, 41, e2021TC007091. https://doi.org/10.1029/2021TC007091

Burke, W.B., Laskowski, A.K., Orme, D.A., Sundell, K.E., Taylor, M.H., Guo, X., & Ding, L. (2021). Record of Crustal Thickening and Synconvergent Extension from the Dajiamang Tso Rift, Southern Tibet. Geosciences, 11, 209. https://doi.org/10.3390/geosciences11050209

Chapman, J. B., & Kapp, P. (2017). Tibetan magmatism database. Geochemistry, Geophysics, Geosystems, 18, 4229– 4234. https://doi.org/10.1002/2017GC007217

Chen, M., Niu, F., Tromp, J., Lenardic, A., Lee, C. T. A., Cao, W., & Ribeiro, J. (2017). Lithospheric foundering and underthrusting imaged beneath Tibet. Nature communications, 8(1), 15659. https://doi.org/10.1038/ncomms15659

Copley, A., Avouac, J.P., & Wernicke, B.P. (2011). Evidence for mechanical coupling and strong Indian lower crust beneath southern Tibet. Nature, 472(7341), 79–81. https://doi.org/10.1038/nature09926

Curry, M. A. E., Barnes, J. B., and Colgan, J. P. (2016). Testing fault growth models with low-temperature thermochronology in the northwest Basin and Range, USA, Tectonics, 35, 2467– 2492, doi:10.1002/2016TC004211.

DeCelles, P.G., Robinson, D.M., & Zandt, G. (2002). Implications of shortening in the Himalayan fold-thrust belt for uplift of the Tibetan Plateau, Tectonics, 21, 1062, doi:10.1029/2001TC001322.

DeCelles, P.G., Kapp, P., Quade, J., & Gehrels, G.E. (2011). Oligocene–Miocene Kailas basin, southwestern Tibet: Record of postcollisional upper-plate extension in the Indus-Yarlung suture zone. GSA Bulletin; 123 (7-8): 1337–1362. doi: https://doi.org/10.1130/B30258.1

Fielding, E., Isacks, B., Barazangi, M., & Duncan, C. (1994). How flat is Tibet? Geology, 22(2), 163– 167. https://doi.org/10.1130/0091-7613(1994)022<0163:HFIT>2.3.CO;2

Kapp, P., & DeCelles, P.G. (2019). Mesozoic–Cenozoic geological evolution of the Himalayan-Tibetan orogen and working tectonic hypotheses. Am. J. Sci., 319, 159–254. DOI: 10.2475/03.2019.01

Kapp, P., & Guynn J.H. (2004). Indian punch rifts Tibet. Geology (2004); 32 (11): 993–996. doi:/10.1130/G20689.1

Laskowski A.K., Kapp, P., & Cai, F. (2018). Gangdese culmination model: Oligocene–Miocene duplexing along the India-Asia suture zone, Lazi region, southern Tibet. GSA Bulletin; 130 (7-8): 1355–1376. doi: https://doi.org/10.1130/B31834.1

Leary, R., Orme, D.A., Laskowski, A.K., DeCelles, P.G., Kapp, P., Carrapa, B., & Dettinger, M. (2016). Along-strike diachroneity in deposition of the Kailas Formation in central southern Tibet: Implications for Indian slab dynamics. Geosphere; 12 (4): 1198–1223. doi: https://doi.org/10.1130/GES01325.1

Molnar, P., & Stock, J. M. (2009). Slowing of India's convergence with Eurasia since 20 Ma and its implications for Tibetan mantle dynamics. Tectonics, 28(3). https://doi.org/10.1029/2008TC002271

Molnar, P., & Tapponnier, P. (1978). Active tectonics of Tibet, J. Geophys. Res., 83(B11), 5361– 5375, doi:10.1029/JB083iB11p05361.

Styron, R. H., Taylor, M. H., Sundell, K. E., Stockli, D. F., Oalmann, J. A. G., Möller, A., McCallister, A. T., Liu, D., & Ding, L. (2013). Miocene initiation and acceleration of extension in the South Lunggar rift, western Tibet: Evolution of an active detachment system from structural mapping and (U-Th)/He thermochronology, Tectonics, 32, 880– 907, Doi:10.1002/tect.20053.

Styron, R., Taylor, M. & Sundell, K. (2015). Accelerated extension of Tibet linked to the northward underthrusting of Indian crust. Nature Geosci 8, 131–134. Doi:10.1038/ngeo2336

Sundell, K. E., Taylor, M. H., Styron, R. H., Stockli, D. F., Kapp, P., Hager, C., Liu, D., & Ding, L. (2013). Evidence for constriction and Pliocene acceleration of east-west extension in the North Lunggar rift region of west central Tibet, Tectonics, 32, 1454– 1479, Doi:10.1002/tect.20086.

Tapponnier, P., Zhiqin, X., Roger, F., Meyer, B., Arnaud, N., Wittlinger, G., & Jingsui, Y. (2001). Oblique stepwise rise and growth of the Tibet Plateau. science, 294(5547), 1671-1677. https://doi.org/10.1126/science.105978

Wolff, R., Hetzel, R., Dunkl, I., Xu Q., Bröcker, M., & Anczkiewicz A.A., (2019). High-Angle Normal Faulting at the Tangra Yumco Graben (Southern Tibet) since ∼15 Ma. The Journal of Geology 2019 127:1, 15-36. Doi:10.1086/700406

Wolff, R., Hetzel, R., Hölzer, K., Dunkl, I., Xu, Q., Anczkiewicz, A.A., & Li, Z. (2023). Rift propagation in south Tibet controlled by under-thrusting of India: a case study of the Tangra

Yumco graben (south Tibet). Journal of the Geological Society, jgs2022-090. Doi: https://doi.org/10.1144/jgs2022-090

Yin, A. (2000). Mode of Cenozoic east-west extension in Tibet suggesting a common origin of rifts in Asia during the Indo-Asian collision, J. Geophys. Res., 105 (B9), 21745– 21759. Doi:10.1029/2000JB900168.

CHAPTER FOUR

GENERAL CONCLUSIONS

New geologic mapping, structural measurements, zircon (U-Th)/He thermochronology results, igneous zircon U-Pb results, and HeFTy thermal models from the Tangra Yumco (TYC) rift suggest differing rift dynamics for Tibetan rifts and Gangdese rifts. These results provide new insights into rift development in a collisional tectonic setting, and can potentially inform future research in such settings. Highlights of this work include:

(1) Enhanced understanding of synconvergent extension related to continental collision. Our results inform the mechanics of rift initiation and evolution and provide a detailed account of the geometry and kinematics of the TYC rift, which are critical steps towards understanding the processes that drive rifting in contractional settings and more broadly, inform our understanding of the behavior and morphological expression of early stage continental rifts.

(2) Application of zircon (U-Th)/He thermochronology to evaluate spatial trends in the timing of extension onset in the southern TYC rift and nearby Gangdese rifts reveal extension timing correlates strongly with latitude. Interpretation of these data reveal relationships between contractional and extensional structures in southern Tibet and provide tests for kinematic and tectonic models that seek to explain how the Himalayan-Tibetan orogenic system operates. Our findings suggest rift processes in southern Tibet may be more complex than previously thought, and that current tectonic models suggesting India underthrusting as a driver for rifting in Tibet (e.g., DeCelles et al., 2002; Kapp and Guynn, 2004; Styron et al., 2013, 2015; Sundell et al., 2013, 2021; Wolff et al., 2019, 2023) that cannot fully explain the complexity of spatiotemporal

patterns in extension timing, highlighting the importance of considering the impact of normal fault growth processes on rift evolution (e.g., Curry et al., 2016).

(3) Contribution of a high resolution and spatially robust thermochronology dataset including ~245 single-grain ZHe ages (49 mean ages) as well as 18 U-Pb mean ages from the southern TYC rift and neighboring Gangdese rifts and kinematic interpretations from this study establish an unprecedented thermochronologic dataset for this region. These data build a strong foundation upon which future generation of researchers can build and provide an important framework for the investigation of extensional structures in other settings where synconvergent extension is documented.

Based on our results and the conclusions made in this contribution, several possibilities exist for future research directions towards the goal of evaluating spatial trends in the timing of rift onset and progressing comparisons between Tibetan rifts and Gangdese rifts. Further detailed mapping and structural analysis of thus far unexplored portions of Tibetan rifts (e.g., northern Tangra Yumco) and Gangdese rifts would provide better spatial and temporal constraints for interactions between contractional and extensional structures in southern Tibet, particularly in the region overlapping and directly north of the Indus Yarlung Suture zone and Gangdese Range where contractional structures such as the Great Counter Thrust and Tibetan rift systems are known to interactions (e.g., South Lunggar rift, Sundell et al., 2013).

Results from this work are timely, as there is currently a high level of interest in the tectonics community in investigating rift processes in extensional settings around the world (e.g., Bian et al., 2021; Brune et al., 2023). Our results independently support and expand on models of upper crustal extension from recent studies of Tibetan rifts (e.g., Wolff et al., 2023) and a synthesis of the tectonic development of southern Tibet (Kapp and DeCelles, 2019).

References Cited

Bian, S., Gong, J., Zuza, A.V., Yang, R., Chen, L., Ji, J., et al. (2022). Along-strike variation in the initiation timing of the north-trending rifts in southern Tibet as revealed from the Yadong-Gulu rift. Tectonics, 41, e2021TC007091. https://doi.org/10.1029/2021TC007091

Brune, S., Kolawole, F., Olive, JA. *et al.* Geodynamics of continental rift initiation and evolution. *Nat Rev Earth Environ* (2023). https://doi.org/10.1038/s43017-023-00391-3

Curry, M. A. E., Barnes, J. B., and Colgan, J. P. (2016). Testing fault growth models with low-temperature thermochronology in the northwest Basin and Range, USA, Tectonics, 35, 2467– 2492, doi:10.1002/2016TC004211.

DeCelles, P.G., Robinson, D.M., & Zandt, G. (2002). Implications of shortening in the Himalayan fold-thrust belt for uplift of the Tibetan Plateau, Tectonics, 21, 1062, doi:10.1029/2001TC001322.

Kapp, P., & DeCelles, P.G. (2019). Mesozoic–Cenozoic geological evolution of the Himalayan-Tibetan orogen and working tectonic hypotheses. Am. J. Sci., 319, 159–254. DOI: 10.2475/03.2019.01

Kapp, P., & Guynn J.H. (2004). Indian punch rifts Tibet. Geology (2004); 32 (11): 993–996. doi:/10.1130/G20689.1

Styron, R. H., Taylor, M. H., Sundell, K. E., Stockli, D. F., Oalmann, J. A. G., Möller, A., McCallister, A. T., Liu, D., & Ding, L. (2013). Miocene initiation and acceleration of extension in the South Lunggar rift, western Tibet: Evolution of an active detachment system from structural mapping and (U-Th)/He thermochronology, Tectonics, 32, 880– 907, Doi:10.1002/tect.20053.

Styron, R., Taylor, M. & Sundell, K. (2015). Accelerated extension of Tibet linked to the northward underthrusting of Indian crust. Nature Geosci 8, 131–134. Doi:10.1038/ngeo2336

Sundell, K. E., Taylor, M. H., Styron, R. H., Stockli, D. F., Kapp, P., Hager, C., Liu, D., & Ding, L. (2013). Evidence for constriction and Pliocene acceleration of east-west extension in the North Lunggar rift region of west central Tibet, Tectonics, 32, 1454– 1479, Doi:10.1002/tect.20086.

Sundell, K.E., Laskowski, A.K., Kapp, P.A., Ducea, M.N. & Chapman, J.B. (2021). Jurassic to Neogene Quantitative Crustal Thickness Estimates in Southern Tibet. GSA Today, 31(6), doi.org/10.1130/GSATG461A.1.

Tremblay, M.M., Fox, M., Schmidt, J.L., Tripathy-Lang, A., Wielicki, M.M., Harrison, T.M., Zeitler, P.K., & Shuster, D.L., (2015). Erosion in southern Tibet shut down at ∼10 Ma due to enhanced rock uplift within the Himalaya. Proc. Natl. Acad. Sci. 112, 12030–12035. Doi:10.1073/pnas.1515652112

Wolff, R., Hetzel, R., Dunkl, I., Xu Q., Bröcker, M., & Anczkiewicz A.A., (2019). High-Angle Normal Faulting at the Tangra Yumco Graben (Southern Tibet) since ∼15 Ma. The Journal of Geology 2019 127:1, 15-36. Doi:10.1086/700406

Wolff, R., Hetzel, R., Hölzer, K., Dunkl, I., Xu, Q., Anczkiewicz, A.A., & Li, Z. (2023). Rift propagation in south Tibet controlled by under-thrusting of India: a case study of the Tangra Yumco graben (south Tibet). Journal of the Geological Society, jgs2022-090. Doi: https://doi.org/10.1144/jgs2022-090

CUMULATIVE REFERENCES CITED

Ai, K., Zhang, K., Song, B., Shen, T., & Ji, J. (2022). Upper Oligocene–Lower Miocene Gangdese Conglomerate Along the Yarlung-Zangbo Suture Zone and its Implications for Palaeo-Yarlung-Zangbo Initiation. Front. Earth Sci. 10:808843. doi: 10.3389/feart.2022.808843

Aitchison, J.C., Davis, A.M., Zhu, B.D., & Luo, H. (2002). New constraints on the India-Asia collision: the Lower Miocene Gangrinboche conglomerates, Yarlung Tsangpo suture zone, SE Tibet. J. Asian Earth Sci., 21 (3), pp. 251-263. Doi:10.1016/S1367-9120(02)00037-8

Allmendinger, R.W. (1986). Tectonic development, southeastern border of the Puna Plateau, northwestern Argentine Andes. GSA Bulletin 1986;; 97 (9): 1070–1082. doi: https://doi.org/10.1130/0016-7606(1986)97<1070:TDSBOT>2.0.CO;2

Alsdorf, D., Brown, L., Nelson, K. D., Makovsky, Y., Klemperer, S., & Zhao, W. (1998). Crustal deformation of the Lhasa terrane, Tibet plateau from Project INDEPTH deep seismic reflection profiles. Tectonics, 17(4), 501-519. https://doi.org/10.1029/98TC01315

An, W., Hu, X., Garzanti, E., BouDagher-Fadel, M.K., Wang, J., & Sun, G. (2014) Xigaze forearc basin revisited (South Tibet): Provenance changes and origin of the Xigaze Ophiolite. GSA Bulletin; 126 (11-12): 1595–1613. doi: https://doi.org/10.1130/B31020.1

Anders, M.H., & Schlische, R.W. (1994). Overlapping Faults, Intrabasin Highs, and the Growth of Normal Faults. The Journal of Geology, 102, 165 - 179. Doi:10.1086/629661

Armijo, R., Tapponnier, P., Mercier, J. L., & Han, T.L. (1986). Quaternary extension in southern Tibet: Field observations and tectonic implications, J. Geophys. Res., 91(B14), 13803–13872, doi:10.1029/JB091iB14p13803.

Ault, A.K., Gautheron, C., & King, G.E. (2019). Innovations in (U–Th)/He, fission track, and trapped charge thermochronometry with applications to earthquakes, weathering, surface-mantle connections, and the growth and decay of mountains. Tectonics, 38, 3705– 3739. https://doi.org/10.1029/2018TC005312

Avouac, J.P., & Tapponnier, P. (1993). Kinematic model of active deformation in central Asia. Geophysical Research Letters, 20(10), 895– 898. Doi:10.1029/93gl00128

Axen, G.J., Fletcher, J.M., Cowgill, E., Murphy, M., Kapp, P., MacMillan, I., Ramos-Velázquez, E., & Aranda-Gómez, J. (1999). Range-front fault scarps of the Sierra El Mayor, Baja

California: Formed above an active low-angle normal fault?. Geology; 27 (3): 247–250. doi: https://doi.org/10.1130/0091-7613(1999)027<0247:RFFSOT>2.3.CO;2

Bian, S., Gong, J., Zuza, A.V., Yang, R., Chen, L., Ji, J., et al. (2022). Along-strike variation in the initiation timing of the north-trending rifts in southern Tibet as revealed from the Yadong-Gulu rift. Tectonics, 41, e2021TC007091. https://doi.org/10.1029/2021TC007091

Bischoff, S.H., & Flesch, L.M. (2018). Normal faulting and viscous buckling in the Tibetan Plateau induced by a weak lower crust. Nature Communications, 9, 4952. https://doi.org/10.1038/s41467-018-07312-9

Black, L.P., Kamo, S.L., Allen, C.M., Davis, D.W., Aleinikoff, J.N., Valley, J.W., & Foudoulis, C. (2004). Improved 206Pb/238U microprobe geochronology by the monitoring of a trace-element-related matrix effect; SHRIMP, ID–TIMS, ELA–ICP–MS and oxygen isotope documentation for a series of zircon standards. Chemical Geology, 205(1-2), 115-140. Doi: https://doi.org/10.1016/j.chemgeo.2004.01.003

Blisniuk, P., Hacker, B., Glodny, J. et al. Normal faulting in central Tibet since at least 13.5 Myr ago. Nature 412, 628–632 (2001). https://doi.org/10.1038/35088045

Braun, J. (2003). Pecube: A new finite-element code to solve the 3-D heat transport equation including the effects of a time-varying, finite amplitude surface topography. Computers and Geosciences, 29(6), 787–794. https://doi.org/10.1016/S0098-3004(03)00052-9

Braun, J., van der Beek, P., Valla, P., Robert, X., Herman, F., Glotzbach, C., et al. (2012). Quantifying rates of landscape evolution and tectonic processes by thermochronology and numerical modeling of crustal heat transport using PECUBE. Tectonophysics, 524–525(1), 1–28. https://doi.org/10.1016/j.tecto.2011.12.035

Brune, S., Kolawole, F., Olive, JA. *et al.* Geodynamics of continental rift initiation and evolution. *Nat Rev Earth Environ* (2023). https://doi.org/10.1038/s43017-023-00391-3

Buck, W.R. (1988). Flexural rotation of normal faults: Tectonics,v. 7, p. 959–973, doi:10.1029/TC007i005p00959.

Buck, W.R. (1991). Modes of continental lithospheric extension, J. Geophys. Res., 96, 20161, https://doi.org/10.1029/91JB01485.

Buck, W.R. (1993). Effect of lithospheric thickness on the formation of high- and low-angle normal faults. Geology; 21 (10): 933–936. doi: https://doi.org/10.1130/0091-7613(1993)021<0933:EOLTOT>2.3.CO;2

Burchfiel, B.C. & Royden, L.H. (1985). North-south extension within the convergent Himalayan region: Geology, v. 13, p. 679–682, doi:10.1130/0091-7613(1985)13<679:NEWTCH>2.0.CO;2.

Burchfiel, B.C., Chen, Z., Hodges, K.V., Liu, Y., Royden, L.H., Deng, C., & Jiene, X. (1992). The South Tibetan detachment system, Himalayan orogen: Extension contemporaneous with and parallel to shortening in a collisional mountain belt. Geological Society of America, Special Papers, 269, 1–41. https://doi.org/10.1130/SPE269-p1

Burg, J. P., Proust, F., Tapponnier, P., & Ming, C. G. (1983). Deformation phases and tectonic evolution of the Lhasa block (southern Tibet, China). Eclogae Geologicae Helvetiae, 76(3), 643-665.

Burke, W.B., Laskowski, A.K., Orme, D.A., Sundell, K.E., Taylor, M.H., Guo, X., & Ding, L. (2021). Record of Crustal Thickening and Synconvergent Extension from the Dajiamang Tso Rift, Southern Tibet. Geosciences, 11, 209. https://doi.org/10.3390/geosciences11050209

Carrapa, B., Orme, D.A., DeCelles, P.G., Kapp, P., Cosca, M.A., & Waldrip R. (2014). Miocene burial and exhumation of the India-Asia collision zone in southern Tibet: Response to slab dynamics and erosion. Geology; 42 (5): 443–446. doi: https://doi.org/10.1130/G35350.1

Chapman, J. B., & Kapp, P. (2017). Tibetan magmatism database. Geochemistry, Geophysics, Geosystems, 18, 4229– 4234. https://doi.org/10.1002/2017GC007217

Chen, M., Niu, F., Tromp, J., Lenardic, A., Lee, C. T. A., Cao, W., & Ribeiro, J. (2017). Lithospheric foundering and underthrusting imaged beneath Tibet. Nature communications, 8(1), 15659. https://doi.org/10.1038/ncomms15659

Chevalier, M.L., Tapponnier, P., van der Woerd, J., Leloup, P.H., Wang, S., Pan, J., et al. (2020). Late Quaternary extension rates across the northern half of the Yadong-Gulu rift: Implication for east-west extension in southern Tibet. Journal of Geophysical Research: Solid Earth, 125, e2019JB019106. https://doi.org/10.1029/2019JB019106

Cogan, M.J., Nelson, K.D., Kidd, W.S.F., & Wu, C., (1998), Shallow structure of the Yadong-Gulu rift, southern Tibet, from refraction analysis of Project INDEPTH common midpoint data, Tectonics, 17(1), 46– 61, doi:10.1029/97TC03025.

Coleman, M., & Hodges, K. (1995). Evidence for Tibetan plateau uplift before 14 Myr ago from a new minimum age for east-west extension. Nature, 374, 49–52. https://doi.org/10.1038/374049a0

Cooperdock, E. H. G., Ketcham, R. A., and Stockli, D. F.: Resolving the effects of 2-D versus 3-D grain measurements on apatite (U–Th)/He age data and reproducibility, Geochronology, 1, 17–41, https://doi.org/10.5194/gchron-1-17-2019, 2019.

Copeland, P., Harrison, T.M., Kidd, W.E.A., Ronghua, X., & Yuquan, Z. (1987). Rapid early Miocene acceleration of uplift in the Gangdese Belt, Xizang (southern Tibet), and its bearing on accommodation mechanisms of the India-Asia collision. Earth and Planetary Science Letters, 86(2-4), 240-252. Doi: https://doi.org/10.1016/0012-821X(87)90224-X

Copeland, P., Harrison, T.M., Pan, Y., Kidd, W. S.F., Roden, M., & Zhang, Y. (1995). Thermal evolution of the Gangdese batholith, southern Tibet: A history of episodic unroofing. Tectonics, 14(2), 223-236. Doi: https://doi.org/10.1029/94TC01676

Copley, A., Avouac, J.P., & Wernicke, B.P. (2011). Evidence for mechanical coupling and strong Indian lower crust beneath southern Tibet. Nature, 472(7341), 79–81. https://doi.org/10.1038/nature09926

Corfu, F., Hanchar, J. M., Hoskin, P., & Kinny P., (2003). Atlas of Zircon Textures. Reviews in Mineralogy and Geochemistry; 53 (1): 469–500. doi: https://doi.org/10.2113/0530469

Crameri, F., G.E. Shephard, and P.J. Heron (2020). The misuse of colour in science communication, Nature Communications, 11, 5444. https://doi.org/10.1038/s41467-020-19160-7

Crameri, F. (2018). Geodynamic diagnostics, scientific visualisation and StagLab 3.0, Geosci. Model Dev. Discuss. https://doi.org/10.5194/gmd-2017-328

Curry, M. A. E., Barnes, J. B., and Colgan, J. P. (2016). Testing fault growth models with low-temperature thermochronology in the northwest Basin and Range, USA, Tectonics, 35, 2467– 2492, doi:10.1002/2016TC004211.

DeCelles, P.G., Robinson, D.M., & Zandt, G. (2002). Implications of shortening in the Himalayan fold-thrust belt for uplift of the Tibetan Plateau, Tectonics, 21, 1062, doi:10.1029/2001TC001322.

DeCelles, P.G., Kapp, P., Quade, J., & Gehrels, G.E. (2011). Oligocene–Miocene Kailas basin, southwestern Tibet: Record of postcollisional upper-plate extension in the Indus-Yarlung suture zone. GSA Bulletin; 123 (7-8): 1337–1362. doi: https://doi.org/10.1130/B30258.1

DeCelles, P.G., Carrapa, B., Gehrels, G.E., Chakraborty, T., & Ghosh, P. (2016), Along-strike continuity of structure, stratigraphy, and kinematic history in the Himalayan thrust belt: The view from Northeastern India, Tectonics, 35, 2995– 3027, doi:10.1002/2016TC004298.

Dodson, M.H. (1973), Closure temperature in cooling geochronological and petrological systems, Contrib. Mineral. Petrol., 40(3), 259– 274, doi:10.1007/BF00373790.

Dürr, S.B. (1996). Provenance of Xigaze fore-arc basin clastic rocks (Cretaceous, south Tibet). Geological Society of America Bulletin, 108(6), 669-684. Doi: https://doi.org/10.1130/0016-7606(1996)108%3C0669:POXFAB%3E2.3.CO;2

Einsele, G., Liu, B., Dürr, S., Frisch, W., Liu, G., Luterbacher, H.P., Ratschbacher, L., Ricken. W., Wendt, J., Wetzel, A., Yu, G., & Zheng H. (1994). The Xigaze forearc basin: evolution and facies architecture (Cretaceous, Tibet) Sediment. Geol., 90 (1–2), pp. 1-32

England P.C. & Houseman G.A., (1989). Extension during continental convergence, with application to the Tibetan Plateau: Journal of Geophysical Research, v. 94, p. 17,561–17,579, doi:10.1029/JB094iB12p17561.

England, P., & Searle, M. (1986), The Cretaceous-tertiary deformation of the Lhasa Block and its implications for crustal thickening in Tibet, Tectonics, 5(1), 1– 14, doi:10.1029/TC005i001p00001.

Farley, K.A., Wolf, R.A., & Silver, L.T. (1996). The effects of long alpha-stopping distances on (U-Th)/He ages. Geochimica et cosmochimica acta, 60(21), 4223-4229. https://doi.org/10.1016/S0016-7037(96)00193-7

Faulds, J.E., & Varga, R.J. (1998). The role of accommodation zones and transfer zones in the regional segmentation of extended terranes. Geological Society of America Special Papers, 323, 1-45. https://doi.org/10.1130/0-8137-2323-X.1

Fielding, E., Isacks, B., Barazangi, M., & Duncan, C. (1994). How flat is Tibet? Geology, 22(2), 163– 167. https://doi.org/10.1130/0091-7613(1994)022<0163:HFIT>2.3.CO;2

Gan, W., Zhang, P. et al. (2007). Present-day crustal motion within the Tibetan Plateau inferred from GPS measurements. Journal of Geophysical Research, 112, B08416. https://doi.org/10.1029/2005JB004120

Gansser, A. (1964), Geology of the Himalayas, pp. 289, Wiley Interscience, London.

Gao, R., Chen, C., Lu, Z.W., Brown, L.D., Xiong, X.S., Li, W.H., & Deng, G. (2013). New constraints on crustal structure and Moho topography in Central Tibet revealed by SinoProbe deep seismic reflection profiling. Tectonophysics, 606, 160– 170. https://doi.org/10.1016/j.tecto.2013.08.006

Gao, T., Ding, Z., Wang, X., & Jiang, L. (2021). Joint inversion of receiver functions, Rayleigh wave dispersion and ZH ratio for crustal structure in Southeast Tibetan Plateau and its implications for dynamics. Chinese Journal of Geophysics, 64(6), 1885-1906. Doi: 10.6038/cjg2021O0282

Garzione, C.N., DeCelles, P.G., Hodkinson, D.G., Ojha, T.P., & Upreti, B.N. (2003). East–west extension and Miocene environmental change in the southern Tibetan Plateau: Thakkhola graben, central Nepal. Geological Society of American Bulletin , 115, 3–20. Doi: https://doi.org/10.1130/0016-7606(2003)115%3C0003:EWEAME%3E2.0.CO;2

Gehrels, G., Valencia, V., & Pullen, A. (2006). Detrital Zircon Geochronology by Laser-Ablation Multicollector ICPMS at the Arizona LaserChron Center. The Paleontological Society Papers, 12, 67-76. doi:10.1017/S1089332600001352

Gehrels, G.E., Valencia, V.A., & Ruiz, J. (2008), Enhanced precision, accuracy, efficiency, and spatial resolution of U-Pb ages by laser ablation–multicollector–inductively coupled plasma–mass spectrometry, Geochem. Geophys. Geosyst., 9, Q03017, doi:10.1029/2007GC001805.

Gehrels G.E., (2009), Arizona LaserChron Center analysis tools for U-Th-Pb geochronologic data: Homepage: https://sites.google.com/laserchron.org/arizonalaserchroncenter/home; Document:https://drive.google.com/file/d/1ju5B_h4kHvbK7PR2WHM9DJQELByqdJP_/view?pli=1 (accessed February 2023).

Gehrels, G., Rusmore, M., Woodsworth, G., Crawford, M., Andronicos, C., Hollister, L., ... & Girardi, J. (2009). U-Th-Pb geochronology of the Coast Mountains batholith in north-coastal British Columbia: Constraints on age and tectonic evolution. Geological Society of America Bulletin, 121(9-10), 1341-1361. doi: https://doi.org/10.1130/B26404.1

Geng, Q.R., Sun, Z.M., Pan, G.T., Zhu, D.C., & Wang, L.Q. (2009). Origin of the Gangdise (Transhimalaya) Permian arc in southern Tibet: Stratigraphic and volcanic geochemical constraints. Island Arc, 18(3), 467-487. Doi: https://doi.org/10.1111/j.1440-1738.2009.00664.x

Giovanni, M. K., Horton, B. K., Garzione, C. N., McNulty, B., & Grove, M. (2010). Extensional basin evolution in the Cordillera Blanca, Peru: Stratigraphic and isotopic records of detachment faulting and orogenic collapse in the Andean hinterland. Tectonics, 29(6).

Guenthner, W.R., Reiners, P.W., Ketcham, R.A., Nasdala, L., & Giester, G. (2013). Helium diffusion in natural zircon: Radiation damage, anisotropy, and the interpretation of zircon (U-Th)/He thermochronology. American Journal of Science, 313(3), 145-198. DOI: https://doi.org/10.2475/03.2013.01

Ha, G., Wu, Z., & Liu, F. (2019). Late quaternary vertical slip rates along the southern Yadong–Gulu rift, southern Tibetan plateau. Tectonophysics, 755, 75-90. Doi: https://doi.org/10.1016/j.tecto.2019.02.014

Han, Z., Sinclair, H.D., Li, Y., Wang, C., Tao, Z., Qian, X., et al (2019). Internal drainage has sustained low-relief Tibetan landscapes since the early Miocene. Geophysical Research Letters, 46, 8741– 8752. https://doi.org/10.1029/2019GL083019

Harrison, T.M., Copeland, P., Kidd, W.S.F., & Yin, A.N. (1992). Raising tibet. Science, 255(5052), 1663-1670. Doi: https://doi.org/10.1126/science.255.5052.1663

Harrison, T.M., Copeland, P., Kidd, W.S.F., & Lovera, O.M. (1995). Activation of the Nyainqentanghla Shear Zone: Implications for uplift of the southern Tibetan Plateau, Tectonics, 14(3), 658– 676, doi:10.1029/95TC00608.

Harrison, T.M., Yin, A., Grove, M., Lovera, O.M., Ryerson, F.J., & Zhou, X. (2000). The Zedong Window: A record of superposed Tertiary convergence in southeastern Tibet. Journal of Geophysical Research: Solid Earth, 105(B8), 19211-19230. Doi: https://doi.org/10.1029/2000JB900078

Harley, S.L., Kelly, N.M., & Möller, A. (2007). Zircon behaviour and the thermal histories of mountain chains. Elements, 3(1), 25-30. Doi: https://doi.org/10.2113/gselements.3.1.25

He, S., Kapp, P., DeCelles, P.G., Gehrels, G.E., & Heizler, M. (2007). Cretaceous–Tertiary geology of the Gangdese Arc in the Linzhou area, southern Tibet. Tectonophysics, 433(1-4), 15-37. Doi: https://doi.org/10.1016/j.tecto.2007.01.005

Heim, A., & Gansser, A., 1939, Central Himalaya, geological observations of the Swiss expeditions 1936: Memoires de la Société Helvetiques des Sciences Naturelles , 73. 1-245.

Hoskin, P.W., & Schaltegger, U. (2003). The composition of zircon and igneous and metamorphic petrogenesis. Reviews in mineralogy and geochemistry, 53(1), 27-62. Doi: https://doi.org/10.2113/0530027

Hou, Z.Q., Gao, Y.F., Qu, X.M., Rui, Z.Y., & Mo, X.X. (2004). Origin of adakitic intrusives generated during mid-Miocene east-west extension in southern Tibet. Earth Planet. Sci. Lett., 220, pp. 139-155. Doi: https://doi.org/10.1016/S0012-821X(04)00007-X

Hourigan, J.K., Reiners, P.W., & Brandon, M.T. (2005). U-Th zonation-dependent alpha-ejection in (U-Th)/He chronometry. Geochimica et Cosmochimica Acta, 69(13), 3349-3365. Doi: https://doi.org/10.1016/j.gca.2005.01.024

Houseman, G.A., McKenzie, D.P., & Molnar, P. (1981). Convective instability of a thickened boundary layer and its relevance for the thermal evolution of continental convergent belts. Journal of Geophysical Research: Solid Earth, 86(B7), 6115-6132. Doi: https://doi.org/10.1029/JB086iB07p06115

Huang, W., Dupont-Nivet, G., Lippert, P.C., van Hinsbergen, D.J., & Hallot, E. (2013). Inclination shallowing in Eocene Linzizong sedimentary rocks from Southern Tibet: correction, possible causes and implications for reconstructing the India–Asia collision. Geophysical Journal International, 194(3), 1390-1411. Doi: https://doi.org/10.1093/gji/ggt188

Huang, F., Li, M., Xu, J., Zeng, Y., Chen, J., Wang, B., ... & Zhang, Z. (2019). Geodynamic transition from subduction to extension: evidence from the geochronology and geochemistry of granitoids in the Sangsang area, southern Lhasa Terrane, Tibet. International Journal of Earth Sciences, 108, 1663-1681. Doi: https://doi.org/10.1007/s00531-019-01729-3

Hughes, C.A., Jessup, M.J., Shaw, C.A., & Newell, D.L. (2019). Deformation conditions during syn-convergent extension along the Cordillera Blanca shear zone, Peru. Geosphere, 15(4), 1342-1367. Doi: https://doi.org/10.1130/GES02040.1

Huntington, K.W., & Klepeis, K.A. (2018). Challenges and opportunities for research in tectonics: Understanding deformation and the processes that link Earth systems, from geologic time to human time. A community vision document submitted to the US National Science Foundation. URI: http://hdl.handle.net/1773/40754

Jessup, M.J., Newell, D.L., Cottle, J. M., Berger, A. L., & Spotila, J. A. (2008). Orogen-parallel extension and exhumation enhanced by denudation in the trans-Himalayan Arun River gorge, Ama Drime Massif, Tibet-Nepal. Geology; 36 (7): 587–590. doi: https://doi.org/10.1130/G24722A.1

Ji, W.Q., Wu, F.Y., Chung, S.L., Li, J.X., & Liu, C.Z. (2009). Zircon U–Pb geochronology and Hf isotopic constraints on petrogenesis of the Gangdese batholith, southern Tibet. Chemical Geology, 262(3-4), 229-245. Doi: https://doi.org/10.1016/j.chemgeo.2009.01.020

Kali, E., Leloup, P.H., Arnaud, N., Mahéo, G., Liu, D., Boutonnet, E., Van der Woerd, J., Liu, X., Liu-Zeng, J., & Li, H. (2010). Exhumation history of the deepest central Himalayan rocks, Ama Drime range: Key pressure-temperature-deformation-time constraints on orogenic models, Tectonics, 29, TC2014, doi:10.1029/2009TC002551.

Kapp, P., & DeCelles, P.G. (2019). Mesozoic–Cenozoic geological evolution of the Himalayan-Tibetan orogen and working tectonic hypotheses. Am. J. Sci., 319, 159–254. DOI: 10.2475/03.2019.01

Kapp, P., & Guynn J.H. (2004). Indian punch rifts Tibet. Geology (2004); 32 (11): 993–996. doi:/10.1130/G20689.1

Kapp, P., Yin, A., Manning, C.E., Harrison, T.M., Taylor, M.H., & Ding, L. (2003). Tectonic evolution of the early Mesozoic blueschist-bearing Qiangtang metamorphic belt, central Tibet, Tectonics, 22, 1043, doi:10.1029/2002TC001383, 4.

Kapp, J. L.D., Harrison, T.M., Kapp, P., Grove, M., Lovera, O.M., & Lin, D. (2005), Nyainqentanglha Shan: A window into the tectonic, thermal, and geochemical evolution of the Lhasa block, southern Tibet, J. Geophys. Res., 110, B08413, doi:10.1029/2004JB003330.

Kapp, P., DeCelles, P.G., Leier, A., Fabijanic, J.M., He, S., Pullen, A., Gehrels G.E., & Ding, L. (2007). The Gangdese retroarc thrust belt revealed. GSA Today. 17. 4-9. doi: 10.1130/GSAT01707A.1.

Kapp, P., Taylor, M., Stockli, D., & Ding, L. (2008). Development of active low-angle normal fault systems during orogenic collapse. Geology 36, 7–10. doi: https://doi.org/10.1130/G24054A.1

Kay, R.W., & Kay, S.M. (1993). Delamination and delamination magmatism. Tectonophysics, 219(1-3), 177-189. Doi: https://doi.org/10.1016/0040-1951(93)90295-U

Ketcham, R.A. (2005). Forward and inverse modeling of low-temperature thermochronometry data. Reviews in mineralogy and geochemistry, 58(1), 275-314. Doi: https://doi.org/10.2138/rmg.2005.58.11

Ketcham, R.A., Gautheron, C., & Tassan-Got, L. (2011). Accounting for long alpha-particle stopping distances in (U–Th–Sm)/He geochronology: Refinement of the baseline case. Geochimica et Cosmochimica Acta, 75(24), 7779-7791. Doi: https://doi.org/10.1016/j.gca.2011.10.011

Kind, R., Yuan, X., Saul, J., Nelson, D., Sobolev, S., Mechie, J., & Achauer, U. (2002). Seismic images of crust and upper mantle beneath Tibet: Evidence for Eurasian plate subduction. Science, 298, 1219–1221. Doi: 10.1126/science.1078115

Klemperer, S.L., Zhao, P., Whyte, C.J., Darrah, T.H., Crossey, L.J., Karlstrom, K.E., ... & Ding, L. (2022). Limited underthrusting of India below Tibet: 3He/4He analysis of thermal springs locates the mantle suture in continental collision. Proceedings of the National Academy of Sciences, 119(12), e2113877119. Doi: https://doi.org/10.1073/pnas.2113877119

Labrousse, L., Huet, B., Le Pourhiet, L., Jolivet, L., & Burov, E. (2016). Rheological implications of extensional detachments: Mediterranean and numerical insights. Earth-Science Reviews, 161, 233-258. Doi: https://doi.org/10.1016/j.earscirev.2016.09.003

Lang, K.A., & Huntington, K.W. (2014). Antecedence of the Yarlung–Siang–Brahmaputra River, eastern Himalaya. Earth and Planetary Science Letters, 397, 145-158. Doi: https://doi.org/10.1016/j.epsl.2014.04.026

Laskowski, A.K., Kapp, P., Ding, L., Campbell, C., & Liu, X.H. (2017). Tectonic evolution of the Yarlung suture zone, Lopu Range region, southern Tibet, Tectonics, 36, 108– 136, doi:10.1002/2016TC004334.

Laskowski A.K., Kapp, P., & Cai, F. (2018). Gangdese culmination model: Oligocene–Miocene duplexing along the India-Asia suture zone, Lazi region, southern Tibet. GSA Bulletin; 130 (7-8): 1355–1376. doi: https://doi.org/10.1130/B31834.1

Leary, R., Orme, D.A., Laskowski, A.K., DeCelles, P.G., Kapp, P., Carrapa, B., & Dettinger, M. (2016). Along-strike diachroneity in deposition of the Kailas Formation in central southern Tibet: Implications for Indian slab dynamics. Geosphere; 12 (4): 1198–1223. doi: https://doi.org/10.1130/GES01325.1

Lee, H.Y., Chung, S.L., Lo, C.H., Ji, J., Wen, D.J., Qian, Q., ... & Zhang, Q. (2007). On the age and geodynamic significance of the Linzizong volcanic successions, southern Tibet: Neo-Tethyan slab breakoff in the early stage of the India-Asia collision.

Lee, H.Y., Chung, S.L., Lo, C.H., Ji, J., Lee, T.Y., Qian, Q., & Zhang, Q. (2009). Eocene Neotethyan slab breakoff in southern Tibet inferred from the Linzizong volcanic record. Tectonophysics, 477(1-2), 20-35. Doi: https://doi.org/10.1016/j.tecto.2009.02.031

Lee, J., Hager, C., Wallis, S.R., Stockli, D.F., Whitehouse, M.J., Aoya, M., & Wang, Y. (2011). Middle to late Miocene extremely rapid exhumation and thermal reequilibration in the Kung Co rift, southern Tibet, Tectonics, 30, TC2007, doi:10.1029/2010TC002745.

Lee, H.Y., Chung, S.L., Ji, J., Qian, Q., Gallet, S., Lo, C.H., ... & Zhang, Q. (2012). Geochemical and Sr–Nd isotopic constraints on the genesis of the Cenozoic Linzizong volcanic successions, southern Tibet. Journal of Asian Earth Sciences, 53, 96-114. Doi: https://doi.org/10.1016/j.jseaes.2011.08.019

Leier, A.L., DeCelles, P.G., Kapp, P., & Gehrels, G.E. (2007). Lower Cretaceous strata in the Lhasa Terrane, Tibet, with implications for understanding the early tectonic history of the Tibetan Plateau. Journal of Sedimentary Research, 77(10), 809-825. Doi: https://doi.org/10.2110/jsr.2007.078

Li, G., Kohn, B., Sandiford, M., Xu, Z., & Wei, L. (2015). Constraining the age of Liuqu Conglomerate, southern Tibet: Implications for evolution of the India–Asia collision zone. Earth and Planetary Science Letters, 426, 259-266. Doi: https://doi.org/10.1016/j.epsl.2015.06.010

Li, S., Guilmette, C., Ding, L., Xu, Q., Fu, J.J., & Yue, Y.H. (2017). Provenance of Mesozoic clastic rocks within the Bangong-Nujiang suture zone, central Tibet: implications for the age of the initial Lhasa-Qiangtang collision. J. Asian Earth Sci., 147, pp. 469-484

Liu, A.L., Wang, Q., Zhu, D.C., Zhao, Z.D., Liu, S.A., Wang, R., ... & Zhang, L.L. (2018). Origin of the ca. 50 Ma Linzizong shoshonitic volcanic rocks in the eastern Gangdese arc, southern Tibet. Lithos, 304, 374-387. Doi: https://doi.org/10.1016/j.lithos.2018.02.017

Long, S.P., Thomson, S.N. Reiners, P.W., & V. Di Fiori, R. (2015). Synorogenic extension localized by upper-crustal thickening: An example from the Late Cretaceous Nevadaplano. Geology; 43 (4): 351–354. doi:10.1130/G36431.1

Mahéo, G., Leloup, P. H., Valli, F., Lacassin, R., Arnaud, N., Paquette, J. L., ... & Tapponnier, P. 6. (2007). Post 4 Ma initiation of normal faulting in southern Tibet. Constraints from the Kung Co half graben. Earth and Planetary Science Letters, 256(1-2), 233-243. Doi:10.1016/j.epsl.2007.01.029

Marrett, R., & Strecker, M.R. (2000). Response of intracontinental deformation in the central Andes to late Cenozoic reorganization of South American Plate motions, Tectonics, 19(3), 452– 467, doi:10.1029/1999TC001102.

Maslin, M.A., Li, X.S., Loutre, M.F., & Berger, A. (1998). The contribution of orbital forcing to the progressive intensification of Northern Hemisphere glaciation. Quaternary Science Reviews, 17(4-5), 411-426. Doi: https://doi.org/10.1016/S0277-3791(97)00047-4

McCaffrey, R., & Nabelek J. (1998). Role of oblique convergence in the active deformation of the Himalayas and southern Tibet plateau. Geology; 26 (8): 691–694. doi: https://doi.org/10.1130/0091-7613(1998)026<0691:ROOCIT>2.3.CO;2

McCallister, A.T., Taylor, M.H., Murphy, M.A., Styron, R.H., & Stockli, D.F. (2014). Thermochronologic constraints on the late Cenozoic exhumation history of the Gurla Mandhata metamorphic core complex, Southwestern Tibet. Tectonics, 33(2), 27-52. Doi: https://doi.org/10.1002/2013TC003302

Mo, X., Niu, Y., Dong, G., Zhao, Z., Hou, Z., Zhou, S., & Ke, S. (2008). Contribution of syncollisional felsic magmatism to continental crust growth: a case study of the Paleogene Linzizong volcanic succession in southern Tibet. chemical Geology, 250(1-4), 49-67. Doi: https://doi.org/10.1016/j.chemgeo.2008.02.003

Molnar, P., & Qidong, D. (1984). Faulting associated with large earthquakes and the average rate of deformation in central and eastern Asia, J. Geophys. Res., 89(B7), 6203– 6227, doi:10.1029/JB089iB07p06203.

Molnar, P., & Stock, J. M. (2009). Slowing of India's convergence with Eurasia since 20 Ma and its implications for Tibetan mantle dynamics. Tectonics, 28(3). https://doi.org/10.1029/2008TC002271

Molnar, P., & Tapponnier, P. (1978). Active tectonics of Tibet, J. Geophys. Res., 83(B11), 5361– 5375, doi:10.1029/JB083iB11p05361.

Molnar, P., England, P., & Martinod, J. (1993), Mantle dynamics, uplift of the Tibetan Plateau, and the Indian Monsoon, Rev. Geophys., 31(4), 357– 396, doi:10.1029/93RG02030.

Murphy, M.A., Yin, A., Harrison, T.M., Dürr, S.B., Chen, Z., Ryerson, F.J., Kidd, W.S.F., Wang, X., & Zhou, X. (1997). Did the Indo-Asian collision alone create the Tibetan plateau?. Geology; 25 (8): 719–722. doi: https://doi.org/10.1130/0091-7613(1997)025<0719:DTIACA>2.3.CO;2

Murphy, M.A., Yin, A., Kapp, P., Harrison, T.M., Manning, C.E., Ryerson, F.J., Ding, L., & Guo J. (2002). Structural evolution of the Gurla Mandhata detachment system, southwest Tibet: Implications for the eastward extent of the Karakoram fault system. GSA Bulletin; 114 (4): 428–447. doi: https://doi.org/10.1130/0016-7606(2002)114<0428:SEOTGM>2.0.CO;2

Murphy, M.A., & Yin, A. (2003). Structural evolution and sequence of thrusting in the Tethyan fold-thrust belt and Indus-Yalu suture zone, southwest Tibet. GSA Bulletin 2003; 115 (1): 21–34. doi: https://doi.org/10.1130/0016-7606(2003)115<0021:SEASOT>2.0.CO;2

Murphy, M.A., Sanchez, V., & Taylor, M.H. (2010). Syn-collisional extension along the India-Asia suture zone, south-central Tibet: Implications for crustal deformation of Tibet. Earth Planet. Sci. Lett., 290, pp. 233-243, 10.1016/j.epsl.2009.11.046

Nábelek, J., Hetényi, G., Vergne, J., Sapkota, S., Kafle, B., Jiang, M., Su, H., Chen, J., Huang, B.S. & Hi-CLIMB Team. (2009). Underplating in the Himalaya-Tibet collision zone revealed by the Hi-CLIMB experiment. Science. 2009 Sep 11;325(5946):1371-4. doi: 10.1126/science.1167719. PMID: 19745147.

Orme, D.A. (2019). Burial and exhumation history of the Xigaze forearc basin, Yarlung suture zone, Tibet. Geoscience Frontiers, 10(3), 895-908.doi: https://doi.org/10.1016/j.gsf.2017.11.011

Orme, D.A., Carrapa, B. & Kapp, P. (2015), Sedimentology, provenance and geochronology of the upper Cretaceous–lower Eocene western Xigaze forearc basin, southern Tibet. Basin Res, 27: 387-411. https://doi.org/10.1111/bre.12080

Orme, D.A., & Laskowski, A.K. (2016). Basin Analysis of the Albian–Santonian Xigaze Forearc, Lazi Region, South-Central Tibet. Journal of Sedimentary Research; 86 (8): 894–913. doi: https://doi.org/10.2110/jsr.2016.59

Owens, T., & Zandt, G. (1997). Implications of crustal property variations for models of Tibetan plateau evolution. Nature 387, 37–43. doi: 10.1038/387037a0

Paces, J.B., & Miller Jr, J.D. (1993). Precise U-Pb ages of Duluth complex and related mafic intrusions, northeastern Minnesota: Geochronological insights to physical, petrogenetic, paleomagnetic, and tectonomagmatic processes associated with the 1.1 Ga midcontinent rift system. Journal of Geophysical Research: Solid Earth, 98(B8), 13997-14013. Doi: https://doi.org/10.1029/93JB01159

Patriat, P., & Achache, J. (1984). India–Eurasia collision chronology has implications for crustal shortening and driving mechanism of plates. Nature 311, 615–621. https://doi.org/10.1038/311615a0

Pan, Y., & Kidd, W.S.F. (1992). Nyainqentanglha shear zone: A late Miocene extensional detachment in the southern Tibetan Plateau. Geology, 20(9), 775-778. Doi: https://doi.org/10.1130/0091-7613(1992)020%3C0775:NSZALM%3E2.3.CO;2

Pan, G.T., Ding, J., Yao, D.S., & Wang L.Q. (2004). Geological Map of the Tibetan Plateau and Adjacent Areas (1: 1,500,000) Chengdu Cartographic Publishing House, Chengdu

Platt, J.P., & England, P.C. (1994). Convective removal of lithosphere beneath mountain belts; thermal and mechanical consequences. American Journal of Science, 294(3), 307-336.

Pullen, A., Ibáñez-Mejia, M., Gehrels, G. E., Giesler, D., & Pecha, M. (2018). Optimization of a laser ablation-single collector-inductively coupled plasma-mass spectrometer (Thermo Element 2) for accurate, precise, and efficient zircon U-Th-Pb geochronology. Geochemistry, Geophysics, Geosystems, 19, 3689– 3705. https://doi.org/10.1029/2018GC007889

Ratschbacher, L., Frisch, W., Chen, C., & Pan, G. (1992). Deformation and motion along the southern margin of the Lhasa block (Tibet) prior to and during the India–Asia collision. Journal of Geodynamics , 16, 21–54. Doi:10.1016/0264-3707(92)90017-M

Ratschbacher, L., Frisch, W., Liu, G., & Chen, C. (1994). Distributed deformation in southern and western Tibet during and after the India-Asia collision. Journal of Geophysical Research , 99, 19,917–19,945. Doi:10.1029/94JB00932

Ratschbacher, L., Krumrei, I., Blumenwitz, M., Staiger, M., Gloaguen, R., Miller, B., Samson, S., & Appel, E. (2011). Rifting and strike-slip shear in central Tibet and the geometry, age and kinematics of upper crustal extension in Tibet. Geological Society London Special Publications. 353. 127-163. Doi:10.1144/SP353.8.

Reiners, P.W. (2005). Zircon (U-Th)/He thermochronometry. Reviews in Mineralogy and Geochemistry, 58(1), 151-179. Doi: https://doi.org/10.2138/rmg.2005.58.6

Reiners, P.W., & Farley, K.A. (2001). Influence of crystal size on apatite (U–Th)/He thermochronology: an example from the Bighorn Mountains, Wyoming. Earth and Planetary Science Letters, 188(3-4), 413-420. Doi: https://doi.org/10.1016/S0012-821X(01)00341-7

Reiners, P.W., Farley, K.A., & Hickes, H.J. (2002). He diffusion and (U–Th)/He thermochronometry of zircon: initial results from Fish Canyon Tuff and Gold Butte. Tectonophysics, 349(1-4), 297-308. Doi: https://doi.org/10.1016/S0040-1951(02)00058-6

Reiners, P.W., Spell, T.L., Nicolescu, S., & Zanetti, K.A. (2004). Zircon (U-Th)/He thermochronometry: He diffusion and comparisons with 40Ar/39Ar dating. Geochimica et cosmochimica acta, 68(8), 1857-1887. Doi: https://doi.org/10.1016/j.gca.2003.10.021

Richter, F.M., Lovera, O.M., Harrison, T.M., & Copeland, P. (1991). Tibetan tectonics from 40Ar/39Ar analysis of a single K-feldspar sample. Earth and Planetary Science Letters, 105(1-3), 266-278. Doi: https://doi.org/10.1016/0012-821X(91)90136-6

Sanchez, V.I., Murphy, M.A., Robinson, A.C., Lapen, T.J., & Heizler, M.T. (2013). Tectonic evolution of the India–Asia suture zone since Middle Eocene time, Lopukangri area, south-central Tibet. Journal of Asian Earth Sciences, 62, 205-220. Doi: https://doi.org/10.1016/j.jseaes.2012.09.004

Schärer, U., Xu, R.H., & Allègre, C.J. (1984). UPb geochronology of Gangdese (Transhimalaya) plutonism in the Lhasa-Xigaze region, Tibet. Earth and Planetary Science Letters, 69(2), 311-320. Doi: https://doi.org/10.1016/0012-821X(84)90190-0

Schmitz, M. D., & Bowring, S. A. (2001). U-Pb zircon and titanite systematics of the Fish Canyon Tuff: An assessment of high-precision U-Pb geochronology and its application to young volcanic rocks. Geochimica et Cosmochimica Acta, 65(15), 2571-2587. https://doi.org/10.1016/S0016-7037(01)00616-0

Schmitz, M.D., Bowring, S.A., & Ireland, T.R. (2003). Evaluation of Duluth Complex anorthositic series (AS3) zircon as a U-Pb geochronological standard: New high-precision isotope dilution thermal ionization mass spectrometry results. Geochimica et Cosmochimica Acta, 67(19), 3665-3672. Doi: https://doi.org/10.1016/S0016-7037(03)00200-X

Sobel, E.R., & Strecker, M.R. (2003). Uplift, exhumation and precipitation: tectonic and climatic control of Late Cenozoic landscape evolution in the northern Sierras Pampeanas, Argentina. Basin Research, 15(4), 431-451. Doi: https://doi.org/10.1046/j.1365-2117.2003.00214.x

Stockli, D.F., Taylor, M., Yin, A., Harrison, T.M., D'Andrea, J., Kapp, P., & Ding, L. (2002). Late Miocene-Pliocene inception of EW extension in Tibet as evidenced by apatite (U-Th)/He data. In Geological Society of America Abstracts with Programs (Vol. 34, No. 6, p. 411).

Styron, R., Taylor, M., & Okoronkwo, K. (2010). Database of Active Structures From the Indo-Asian Collision, Eos Trans. AGU, 91(20), 181– 182, doi:10.1029/2010EO200001.

Styron, R.H., Taylor, M.H., & Murphy, M.A. (2011). Oblique convergence, arc-parallel extension, and the role of strike-slip faulting in the High Himalaya. Geosphere; 7 (2): 582–596. doi: https://doi.org/10.1130/GES00606.1

Styron, R. H., Taylor, M. H., Sundell, K. E., Stockli, D. F., Oalmann, J. A. G., Möller, A., McCallister, A. T., Liu, D., & Ding, L. (2013). Miocene initiation and acceleration of extension in the South Lunggar rift, western Tibet: Evolution of an active detachment system from structural mapping and (U-Th)/He thermochronology, Tectonics, 32, 880– 907, Doi:10.1002/tect.20053.

Styron, R., Taylor, M. & Sundell, K. (2015). Accelerated extension of Tibet linked to the northward underthrusting of Indian crust. Nature Geosci 8, 131–134. Doi:10.1038/ngeo2336

Sundell, K. E., Taylor, M. H., Styron, R. H., Stockli, D. F., Kapp, P., Hager, C., Liu, D., & Ding, L. (2013). Evidence for constriction and Pliocene acceleration of east-west extension in the North Lunggar rift region of west central Tibet, Tectonics, 32, 1454– 1479, Doi:10.1002/tect.20086.

Sundell, K.E., Gehrels, G.E., Quinn, D.P., Pecha, M.E., Giesler, D.M., Pepper, M.B. George, S.W.M., and White, A.M. (2020), AgeCalcML: An open-source MATLAB-based data reduction platform for LA-ICP-MS geochronology and geochemistry data from the Arizona LaserChron Center, Geological Society of America Annual Meeting.

Sundell, K.E., Laskowski, A.K., Kapp, P.A., Ducea, M.N. & Chapman, J.B. (2021). Jurassic to Neogene Quantitative Crustal Thickness Estimates in Southern Tibet. GSA Today, 31(6), doi.org/10.1130/GSATG461A.1.

Tapponnier, P., Zhiqin, X., Roger, F., Meyer, B., Arnaud, N., Wittlinger, G., & Jingsui, Y. (2001). Oblique stepwise rise and growth of the Tibet Plateau. science, 294(5547), 1671-1677. https://doi.org/10.1126/science.105978

Taylor, M.H., & Yin, A. (2009). Active structures of the Himalayan-Tibetan orogen and their relationships to earthquake distribution, contemporary strain field, and Cenozoic volcanism. Geosphere; 5 (3): 199–214. doi: https://doi.org/10.1130/GES00217.1

Taylor, M., Yin, A., Ryerson, F.J., Kapp, P., & Ding, L. (2003). Conjugate strike-slip faulting along the Bangong-Nujiang suture zone accommodates coeval east-west extension and north-south shortening in the interior of the Tibetan Plateau. Tectonics, 22. Doi:10.1029/2002TC001383

Taylor, M. H., Forte, A.M., Laskowski, A. K., & Ding, L. (2021). Active Uplift of Southern Tibet Revealed. GSA Today. 31. Doi:10.1130/GSATG487A.1.

Thiede, R. C., Arrowsmith, J. R., Bookhagen, B., McWilliams, M., Sobel, E. R., & Strecker, M. R. (2006). Dome formation and extension in the Tethyan Himalaya, Leo Pargil, northwest India. Geological Society of America Bulletin, 118(5-6), 635-650. Doi: https://doi.org/10.1130/B25872.1

Tilmann, F., Ni, J., & Indepth Iii Seismic Team. (2003). Seismic imaging of the downwelling Indian lithosphere beneath central Tibet. Science, 300(5624), 1424-1427. Doi: https://doi.org/10.1126/science.1082777

Tremblay, M.M., Fox, M., Schmidt, J.L., Tripathy-Lang, A., Wielicki, M.M., Harrison, T.M., Zeitler, P.K., & Shuster, D.L., (2015). Erosion in southern Tibet shut down at ∼10 Ma due to enhanced rock uplift within the Himalaya. Proc. Natl. Acad. Sci. 112, 12030–12035. Doi:10.1073/pnas.1515652112

Turner, S., Hawkesworth, C., Liu, J., Rogers, N., Kelley, S., & Van Calsteren, P. (1993). Timing of Tibetan uplift constrained by analysis of volcanic rocks. Nature, 364, 50-54. doi: https://ui.adsabs.harvard.edu/link_gateway/1993Natur.364...50T/doi:10.1038/364050a0

Vermeesch, P., & Tian, Y. (2014). Thermal history modelling: HeFTy vs. QTQt. Earth-Science Reviews, 139, 279-290. Doi: https://doi.org/10.1016/j.earscirev.2014.09.010

Vermeesch, P. (2018). IsoplotR: A free and open toolbox for geochronology. Geoscience Frontiers, 9(5), 1479-1493. https://doi.org/10.1016/j.gsf.2018.04.001

Walker, J. D., Tikoff, B., Newman, J., Clark, R., Ash, J., Good, J., Bunse, E.G., Möller, A., Kahn, M., Williams, R.T., Michels, Z., Andrew, J.E., & Rufledt, C. (2019). StraboSpot data system for structural geology. Geosphere, 15(2), 533-547. Doi: https://doi.org/10.1130/GES02039.1

Wang, J.G., Hu, X.M., Wu, F.Y., & Jansa, L. (2010). Provenance of the Liuqu Conglomerate in southern Tibet: A Paleogene erosional record of the Himalayan–Tibetan orogen. Sedimentary Geology, 231(3-4), 74-84. Doi: https://doi.org/10.1016/j.sedgeo.2010.09.004

Wang, C., Li, X., Liu, Z., Li, Y., Jansa, L., Dai, J., & Wei, Y. (2012). Revision of the Cretaceous–Paleogene stratigraphic framework, facies architecture and provenance of the Xigaze forearc basin along the Yarlung Zangbo suture zone. Gondwana Research, 22(2), 415-433. Doi: https://doi.org/10.1016/j.gr.2011.09.014

Wang, J.G., Hu, X.M., Garzanti, E., & Wu, F.Y. (2013). Upper Oligocene–Lower Miocene Gangrinboche Conglomerate in the Xigaze area, southern Tibet: Implications for Himalayan uplift and paleo-Yarlung-Zangbo initiation. The Journal of Geology, 121(4), 425-444. Doi: 10.1086/670722

Wang E., Kamp P. J.J., Xu G., Hodges K.V., Meng K., Chen L., Wang G., & Luo H., (2015). Flexural bending of southern Tibet in a retro foreland setting: Scientific Reports, v. 5, article number 12076, doi: https://doi.org/10.1038/srep12076

Wang, C., Ding, L., Cai, F.L., Wang, H.Q., Zhang, L.Y., & Yue, Y.H. (2022). Evolution of the Sumdo Paleo-Tethyan Ocean: Constraints from Permian Luobadui Formation in Lhasa terrane, South Tibet. Palaeogeography, Palaeoclimatology, Palaeoecology, 595, 110974. Doi: https://doi.org/10.1016/j.palaeo.2022.110974

Wei, Z., Li, X., Laskowski, A.K., Reynolds, A.N., & Fan, X. (2021). Cretaceous forearc basin remnant sediments in the eastern Yarlung Zangbo suture zone, near the eastern Himalaya syntaxis. Palaeogeography, Palaeoclimatology, Palaeoecology, 580, art. no. 110620. Doi:10.1016/j.palaeo.2021.110620

Wells, M.L., & Hoisch, T.D. (2008). The role of mantle delamination in widespread Late Cretaceous extension and magmatism in the Cordilleran orogen, western United States. Geological Society of America Bulletin, 120(5-6), 515-530. Doi: https://doi.org/10.1130/B26006.1

Wells, M.L., Hoisch, T.D., Cruz-Uribe, A.M., & Vervoort, J.D. (2012). Geodynamics of synconvergent extension and tectonic mode switching: Constraints from the Sevier-Laramide orogen. Tectonics, 31(1). Doi: https://doi.org/10.1029/2011TC002913

Wernicke, B. (1992). Cenozoic extensional tectonics of the US Cordillera. The Geology of North America, 3, 553-582. Doi: https://doi.org/10.1130/DNAG-GNA-G3.553

Willett, S.D., McCoy, S.W., Perron, J.T., Goren, L., & Chen, C.Y. (2014). Dynamic reorganization of river basins. Science, 343(6175), 1248765. Doi: https://doi.org/10.1126/science.1248765

Williams, H., Turner, S., Kelley, S., & Harris, N. (2001). Age and composition of dikes in Southern Tibet: new constraints on the timing of east-west extension and its relationship to postcollisional volcanism. Geology, 29(4), 339-342. Doi:10.1130/0091-7613(2001)029<0339:AACODI>2.0.CO;2

Williams, H.M., Turner, S.P., Pearce, J.A., Kelley, S.P., & Harris, N.B.W. (2004). Nature of the source regions for post-collisional, potassic magmatism in southern and northern Tibet from geochemical variations and inverse trace element modelling. Journal of Petrololgy, 45(3), 555–607. Doi:10.1093/petrology/egg094

Wolff, R., Hetzel, R., Dunkl, I., Xu Q., Bröcker, M., & Anczkiewicz A.A., (2019). High-Angle Normal Faulting at the Tangra Yumco Graben (Southern Tibet) since ∼15 Ma. The Journal of Geology 2019 127:1, 15-36. Doi:10.1086/700406

Wolff, R., Hetzel, R., Hölzer, K., Dunkl, I., Xu, Q., Anczkiewicz, A.A., & Li, Z. (2023). Rift propagation in south Tibet controlled by under-thrusting of India: a case study of the Tangra

Yumco graben (south Tibet). Journal of the Geological Society, jgs2022-090. Doi: https://doi.org/10.1144/jgs2022-090

Wu, H.R., Wang, D.A., & Wang, L.C. (1977). Cretaceous in Lhaze–Gyangze, southern Xizang: Scientia Geologica Sinica, v. 3, p. 250–261 (in Chinese with English abstract).

Wu, C., Nelson, K.D., Wortman, G., Samson, S.D., Yue, Y., Li, J., ... & Edwards, M. A. (1998). Yadong cross structure and South Tibetan Detachment in the east central Himalaya (89–90 E). Tectonics, 17(1), 28-45. Doi: https://doi.org/10.1029/97TC03386

Wu, F.Y., Ji, W.Q., Liu, C.Z., & Chung, S.L. (2010). Detrital zircon U–Pb and Hf isotopic data from the Xigaze fore-arc basin: constraints on Transhimalayan magmatic evolution in southern Tibet. Chemical Geology, 271(1-2), 13-25. Doi: https://doi.org/10.1016/j.chemgeo.2009.12.007

Wu, H., Li, C., Xu, M., & Li, X. (2015). Early Cretaceous adakitic magmatism in the Dachagou area, northern Lhasa terrane, Tibet: Implications for slab roll-back and subsequent slab break-off of the lithosphere of the Bangong–Nujiang Ocean. Journal of Asian Earth Sciences, 97, 51-66. Doi: https://doi.org/10.1016/j.jseaes.2014.10.014

Yin, A. (2000). Mode of Cenozoic east-west extension in Tibet suggesting a common origin of rifts in Asia during the Indo-Asian collision, J. Geophys. Res., 105 (B9), 21745– 21759. Doi:10.1029/2000JB900168.

Yin, A. (2006) Cenozoic tectonic evolution of the Himalayan orogen as constrained by along-strike variation of structural geometry, exhumation history, and foreland sedimentation. Earth-Science Reviews, Volume 76, Issues 1–2, 1-131. Doi: 10.1016/j.earscirev.2005.05.004

Yin, A., & Harrison, T.M. (2000). Geologic evolution of the Himalayan-Tibetan orogen. Annual review of earth and planetary sciences, 28(1), 211-280. Doi: https://doi.org/10.1146/annurev.earth.28.1.211

Yin, A., & Taylor, M.H. (2011), Mechanics of V-shaped conjugate strike-slip faults and the corresponding continuum mode of continental deformation. Bulletin, 123, 1798–1821. doi: https://doi.org/10.1130/B30159.1

Yin, A., Harrison, T.M., Ryerson, F.J., Chen, W., Kidd, W.S.F., & Copeland, P. (1994). Tertiary structural evolution of the Gangdese thrust system, southeastern Tibet. Journal of Geophysical Research , 99, 18,175–18,201. Doi: 10.1029/94JB00504

Yin, A., Harrison, T.M., Murphy, M.A., Grove, M., Nie, S., Ryerson, F., Feng, W., & Le, C. (1999). Tertiary deformation history of southeastern and southwestern Tibet during the Indo-Asian collision. GSA Bulletin; 111 (11): 1644–1664. doi:10.1130/0016-7606(1999)111<1644:TDHOSA>2.3.CO;2

Zhang, P., Shen, Z., Wang, M., Gan, W., Bürgmann, R., & Molnar, P. (2004). Continuous deformation of the Tibetan Plateau from global positioning system data. Geology, 32, 809–812. Doi:10.1130/G20554.1

Zhang K., Zhang Y., Tang X., & Xia, B., (2012). Late Mesozoic tectonic evolution and growth of the Tibetan plateau prior to the Indo-Asian collision Earth-Science Reviews. Vol. 114, Iss. 3–4, 236-249. https://doi.org/10.1016/j.earscirev.2012.06.001

Zhang, L.Y., Ducea, M.N., Ding, L., Pullen, A., Kapp, P., & Hoffman, D. (2014). Southern Tibetan Oligocene–Miocene adakites: A record of Indian slab tearing. Lithos, 210, 209-223. Doi: https://doi.org/10.1016/j.lithos.2014.09.029

Zhang, J., Dai, J., Qian, X., Ge, Y., & Wang, C. (2017). Sedimentology, provenance and geochronology of the Miocene Qiuwu Formation: Implication for the uplift history of Southern Tibet. Geoscience Frontiers, 8(4), 823-839.doi: https://doi.org/10.1016/j.gsf.2016.05.010

Zhang, Y., Huang, F., Xu, J., Zeng, Y., Wang, B., Lv, M., ... & Zhang, L. (2023). Origin of the volcanic rocks in Dianzhong Formation, central Lhasa Terrane, Tibet: implication for the genesis of syn-collisional magmatism and Neo-Tethyan slab roll-back. International Geology Review, 65(1), 21-39. Doi: https://doi.org/10.1080/00206814.2022.2031314

Zhu, B., Kidd, W. S., Rowley, D. B., Currie, B. S., & Shafique, N. (2005). Age of initiation of the India-Asia collision in the east-central Himalaya. The Journal of Geology, 113(3), 265-285. Doi: https://doi.org/10.1086/428805

Zhu, D.C., Zhao, Z.D., Niu, Y., Mo, X.X., Chung, S.L., Hou, Z.Q., ... & Wu, F.Y. (2011). The Lhasa Terrane: Record of a microcontinent and its histories of drift and growth. Earth and Planetary Science Letters, 301(1-2), 241-255. Doi: https://doi.org/10.1016/j.epsl.2010.11.005

Zhu, D.C., Zhao, Z.D., Niu, Y., Dilek, Y., Wang, Q., Ji, W.H., ... & Mo, X.X. (2012). Cambrian bimodal volcanism in the Lhasa Terrane, southern Tibet: record of an early Paleozoic Andean-type magmatic arc in the Australian proto-Tethyan margin. Chemical Geology, 328, 290-308. Doi: https://doi.org/10.1016/j.chemgeo.2011.12.024

Zhu, D.C., Wang, Q., Zhao, Z.D., Chung, S.L., Cawood, P.A., Niu, Y., ... & Mo, X.X. (2015). Magmatic record of India-Asia collision. Scientific reports, 5(, 14289. Doi: https://doi.org/10.1038/srep14289